Role of lipopolysaccharide in membrane-active-peptide interactions with cells as probed by whole-cell deuterium NMR

By

©Sarika Kumari

A thesis submitted to the school of graduate studies in partial fulfillment of requirements for the degree of Doctor of Philosophy

Department of Biochemistry, Faculty of Science

Memorial University of Newfoundland,

October 2022

St. John's, Newfoundland, and Labrador

Abstract

The increasing appearance of multidrug-resistant pathogens has created an urgent need for suitable alternatives to current antibiotics. Antimicrobial peptides (AMPs), which act as defensive weapons against microbes, have shown great promise because bacteria develop no or low resistance to AMPs. However, only a few antimicrobial peptides are clinically available for clinical use.

Understanding how non-phospholipid components of bacteria affect antimicrobial peptide-induced membrane disruption is important for a comprehensive understanding of AMP mechanisms and informing AMP-based drug development. Therefore, the main aim of this thesis was to investigate how lipopolysaccharide (LPS) affects membrane disruption by the AMP MSI-78 and compare the results to the effect of TP2, a cell-penetrating peptide that crosses membrane bilayers without permeabilizing them. We destabilize the LPS layer of *Escherichia coli* (*E. coli*) cells via chelation of the stabilizing divalent cations. ^{2}H NMR observations of membrane-deuterated *E. coli* demonstrate that an ethylenediaminetetraacetic acid (EDTA) concentration of 9.0 mM alone has a minor effect on lipid acyl chain order. Interestingly, we find that *E. coli* pretreated with 9.0 mM EDTA are more sensitive to AMP-induced acyl chain disruption resulting from subsequent treatment with the AMP MSI-78. This indicates that LPS protects *E. coli* from membrane disruption caused by MSI-78. Surprisingly, we also found that at the level of ^{2}H-NMR, the peptide-induced acyl chain disruptions are similar for MSI-78 and CPP-TP2, although MSI-78 permeabilizes the bilayer and TP2 does not. Furthermore, having intact LPS appears to sensitize the bacteria to TP2, in contrast to intact LPS' ability to protect bacteria from MSI-78.

I also provide some information about AMP selectivity by examining whether non-bacterial cells, i.e., mammalian cells, can compete with bacteria for AMP binding in a mixture of

bacteria and mammalian cells. Interestingly, our preliminary data shows that when the MSI-78 was added to the mixture of cells, i.e., membrane-deuterated *E. coli* and Ramos cells, the presence of Ramos cells slightly reduced the amount of MSI-78 available to interact with the *E. coli*. Presumably due to some binding of MSI-78 by the Ramos cells.

Overall, we show here that LPS, present in bacteria but not model membranes, protects bacteria to some extent from the AMP MSI-78. LPS protection from AMP membrane permeabilization would explain why model lipid bilayers are more prone to permeabilization by AMP than are bilayers in whole bacteria. In addition, since efforts to optimize AMPs as drugs often rely solely on optimizing the AMP's lipid-permeabilizing activities, consideration of other interactions like AMP-LPS interactions may prove helpful in AMP-based drug design.

Co-authorship Statement

Much of the work presented in this thesis has been published in the peer-reviewed journal article:

1) Wijesinghe, A., Kumari, S., & Booth, V. (2022). Conjugates for use in peptide therapeutics: A systematic review and meta-analysis. PloS one, 17(3), e0255753.
2) Kumari, S., & Booth, V. (2022). Antimicrobial peptide mechanisms studied by whole-cell deuterium NMR. International Journal of Molecular Sciences, 23(5), 2740.
3) Kumari, S., Morrow, M., Booth, V. (2022). Role of lipopolysaccharide in antimicrobial and cell-penetrating peptide membrane interactions probed by deuterium NMR of whole-cell, Biomembrane. 22, 184053.

My contributions to the above published work were.

1) Wijesinghe, Kumari and Booth, 2022: I screened half the papers for the systematic review and made suggestions on the first draft written by Ashan Wijesinghe.
2) Kumari and Booth, 2022, were invited to review. I performed the literature review, wrote the first draft and revised the papers with help from my supervisor.
3) Kumari, Morrow and Booth, 2022: I carried out all the experiments, performed all the data analysis, wrote the first draft and revised the paper with help from my supervisors.

The parts of this work not adopted from the above published work and solely authored by me (with help from supervisors) were:

Chapter 1 sections 1.1 (1.1.1-1.1.4), 1.2 (1.2.5, 1.2.6, 1.2.8,1.2.9), 1.3 (1.3.1,1.3.3) 1.4.

Chapter 2 sections (2.10,2.11,2.12).

Chapter 3 section MAS moments analysis 3.1 and 3.1.2.

Chapter 7 and Chapter 8, section 8.1.

COVID Statement

The COVID-19 year (2020-2021) was challenging for everyone. A major challenge for me was that I had a 3-year-old at home when the covid lockdowns in 2020 were implemented, so the daycare was closed. I was stuck inside my house with an energetic 3-year-old and preparing for my comprehensive exam. Even when the restriction was released and the daycare opened, many limitations kept her on and off from daycare during 2020-2021.

The original intention of my thesis was to expand chapter 7 more. The time when research labs were closed, and I had many childcare responsibilities during the data collection phase of the project. I could thus only carry out a limited number of experiments for the final objective of my thesis.

Acknowledgments

First and foremost, I am very grateful to my supervisor Dr. Valerie Booth for allowing me to join her lab. Even knowing that I had an 8-month-old baby in my hand, she trusted me that I was capable of starting this degree. Thank you to Dr. Booth for being an excellent supervisor who has given her constant support and guidance through the ups and downs of research and kept me motivated. I have learned a lot through the level of detail while designing the experiment and writing. Her constant motivations have helped me to come over from the mental stress that covid has given to all of us. Even while we were locked inside our house during the covid lockdown, she always found a way to motivate her student, whether writing journal papers or analyzing the data.

I would also like to give my deepest thanks to my co-supervisor, Dr. Michael Morrow, for teaching me the concepts of ^{2}H NMR. I genuinely appreciate his warm welcome, endless patience, and wide overview, which equipped me with a wide horizon over this subject.

I would like to thank my advisory committee members, Dr. Sherri Christian and Dr. Kapil Tahlan, for their valuable suggestions and encouragement throughout the supervisory committee meetings. Thank Dr. Sherri Christian, who agreed to be my mentor for the Teaching Skills Enhancement Program (TSEP) course. I am grateful to all my course instructors, Dr. Valerie Booth, Dr. Michael Morrow and Dr. Anand Yethiraj.

Dr. Celine Schneider assisted in the NMR experiment and Chris Cockrum for his valuable feedback for flow cytometry experiments.

I am grateful to the Biochemistry staff and faculty for providing support through my research.

I am thankful to my funding agencies, the School of Graduate Studies, and the Memorial University of Newfoundland. I am grateful to the National Science and Engineering Research Council and the Department of Biochemistry.

I am pleased to acknowledge my gratitude to several current and former lab members: Dr. Nury Paula Santisteban, Dr. Gagandeep Sandhu, Dr. Tadiwos Gatachew, Liam Gregory, Yantiza Trosel and Sina Abdolrahim Poor Heravi.

My academic thank would be incomplete without thanking Dr. P. K. Madhu (Professor at Tata Institute of Fundamental Research), from whom my passion for research started.

Last but not least, my acknowledgment would be incomplete without thanking the biggest source of my strength, my family. I must express my high thanks to my little daughter, who was eight months old when I started my Ph.D., this little girl has taught us many things, her patience, her wait for mommy to be at home and feed her, playing with her. My husband, Sanjay Dubey, who always stood for me, took the initiative to stay home and care for our daughter while I got familiar with my Ph.D. program.

My deep indebtedness to my respected parents, whose blessing and inspiration have always encouraged me to move forward. I would like to thank them for trusting in me and encouraging me to follow my dreams.

Last but not least, I would like to thank MUN daycare, who kept my daughter happy and safe while I was busy with my Ph.D. work.

Table of Contents

List of Abbreviations and symbols

AMP	Antimicrobial peptide
Ca^{2+}	Calcium divalent ion
CDTA	1,2-cyclohexanediamine tetraacetic acid
CFU	Colony-forming unit
CL	Cardiolipin
CPP	Cell-penetrating peptide
DNA	Deoxyribonucleic acid
DPC	n-dodecyl phosphocholine
DPPC-d_{62}	1,2-dipalmitoyl-sn-glycero-3-phosphocholine
DSC	Differential scanning calorimetry
EDTA	Ethylenediaminetetraacetic acid
^2H	Deuterium
HDTA	N-(2-Hydroxyethyl) ethylenediamine-N, N', N'-triacetic acid
	Trisodium salt
Kdo	3-Deoxy-d-manno-octulosonic acid
LPS	Lipopolysaccharide
MAS	Magic-angle spinning
MBC	Minimum bactericidal concentration
MD	Molecular dynamics
Mg^{2+}	Magnesium divalent ion
MIC	Minimal inhibitory concentration

MTT	(3-(4, 5-dimethylthiazolyl-2)-2, 5-diphenyltetrazolium bromide)
NaCl	Sodium chloride
NMR	Nuclear magnetic resonance
OA	Oleic acid
OM	Outer membrane
PA-d_{31}	Deuterated palmitic acid
PBS	Phosphate buffer saline
PE	Phosphatidylethanolamine
PG	Phosphatidylglycerol
PGN	Peptidoglycan
PI	Propidium iodide
ppm	Parts per million
RBCs	Red blood cells
siRNA	Small interfering RNA
SMTP	Spontaneous membrane translocation peptide
TA	Teichoic acid
WHO	World health Organization

List of Units

µl	Unit of volume (microlitre)
h	Unit of time (hour)
Hz	Unit of frequency (cycles per second)
min	Unit of time (minutes)
ml	Unit of volume (millilitre)
mM	Unit of concentration (millimolar)
nm	Unit of length (nanometer)
^{o}C	Unit of temperature (degree Celsius)
rpm	Unit of rotational speed (rotation per minute)
s	Unit of time (second)

List of Tables

List of Figures

Chapter 1. Introduction

1.1 Conventional antibiotics and bacteria

1.1.1 History of antibiotics

Antibiotics are defined as therapeutic agents used to treat and prevent bacterial and fungal infections. The classical definition of antibiotic is a small molecule that are made by microorganisms, and which are antagonistic to other microorganisms. The antibiotic can either kill microbes or prevent microbial growth. Antibiotics as therapeutic agents date back to at least as early as AD 350 when they were used by the Nubians,[1] who used what were later shown to be tetracycline-based compounds to treat infections like pneumonia.

Microorganisms produce antibiotics to protect their environmental niche and inhibit the growth of competing microorganisms. In 1928 Sir Alexander Fleming noticed that the zone immediately around a *Penicillium* mold (fungi) inhibited *Staphylococcus* growth. Fleming hypothesized that the mold secreted an active compound to inhibit bacterial growth. The active compound secreted by the mold was penicillin which was further developed and purified by Ernst Chain and Howard Florey. It was initially used in 1942 during World War II [2].

The antibiotics field then experienced a "golden" era as many families of antibiotics, such as sulfonamides, aminoglycosides, fluoroquinolones and cephalosporins, were discovered in the next 20 years. These novel discoveries led to large-scale therapeutic research, and the commercial industry focused on treating bacterial infections. Interestingly, different families of antibiotics target different components of the bacteria, which will be described in detail in section 1.1.3.

1.1.2 Structure of Bacterial Cell and Membrane

It is important to understand the basic structure and components of the bacterial cell envelope before looking into the mechanism of action of certain antibiotics. Bacteria are divided into two broad classes, i.e., Gram-positive and Gram-negative. The morphology and molecular components of membranes from Gram-positive bacteria (**Fig. 1.1A**) are structurally different from those of Gram-negative bacteria (**Fig. 1.1B**).

Gram-negative bacteria are generally characterized by their cell wall consisting of a thin peptidoglycan layer and an outer membrane. The outer layer of the outer membrane contains lipopolysaccharide as the major lipid component, a lipid species unique to Gram-negative bacteria [3]. Gram-positive bacteria lack the outer membrane layer that Gram-negative bacteria [4]. In addition, the cell wall of Gram-positive bacteria contains teichoic acids. The major lipid components of the inner monolayer of the outer membrane of Gram-negative bacteria and the monolayers of the cell membrane of both types of bacteria include zwitterionic and negative phospholipid, mainly phosphatidylethanolamine, phosphatidylglycerol, and cardiolipin [5].

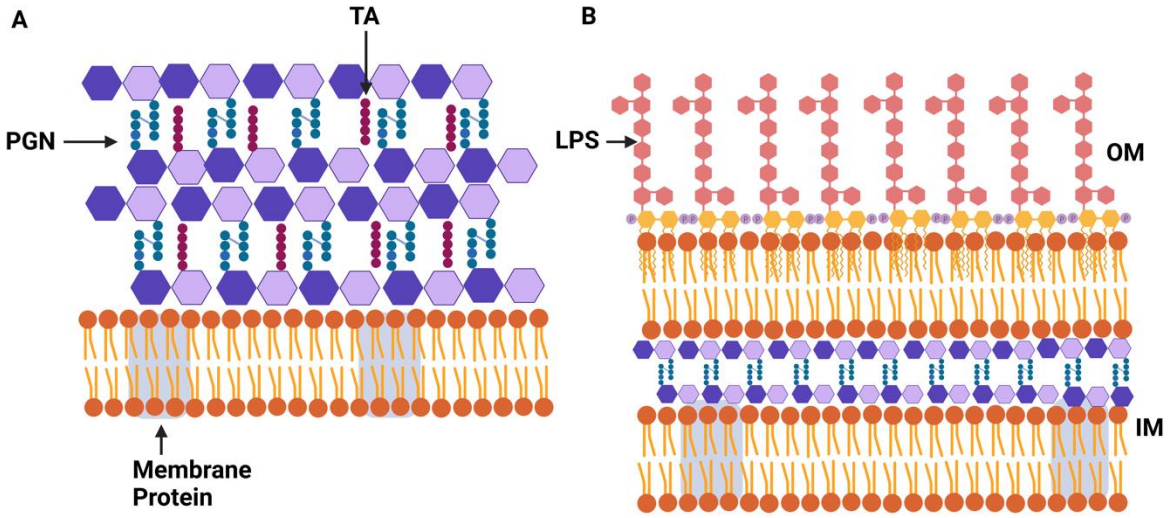

Fig. 1.1 A: Gram-positive bacteria, PGN: peptidoglycan layer, TA: Teichoic Acid and **B**: Gram-negative bacteria, LPS: Lipopolysaccharide layer, OM: the outer membrane, IM: inner membrane. The purple "P" is phosphate (Created in Biorender.com)

Gram-negative bacteria's outer membrane (OM) is a highly asymmetric bilayer membrane. It serves as a barrier to prevent the entry of noxious compounds and simultaneously allows the influx of nutrient molecules [6]. The LPS layer is an excellent barrier to foreign molecules that are harmful to the bacteria, such as antibiotics and lysozyme. It contains a negative surface charge that helps stabilize the overall membrane structure [7].

LPS typically comprises three distinct regions: lipid A, a core oligosaccharide, and an O-antigenic polysaccharide [8]. The basic structure of LPS, a covalently linked lipid and heteropolysaccharide (**Fig. 1.2**), is common to all LPS molecules in Gram-negative bacteria, but otherwise, there are extensive variations in the chemical structures of LPS depending on bacterial strain and species [9].

1.1.2.1 Lipid A

The lipid A domain anchors the LPS in the outer membrane and is the most conserved part of LPS [6]. A common type of lipid A occurs in *E. coli,* in which the hydrophilic backbone consists of a β-(1→6)-linked 2-amino 2-deoxyglucopyranose (GlcN) disaccharide, carrying two phosphate groups at positions 1 and 4 ' and four moieties of (R)3-hydroxymyristic acid in ester and amide linkages [10]. The negatively charged phosphate groups are important for reinforcing the LPS monolayer by linking molecules via ionic bridges with divalent cations [6].

Lipid A is generally required for bacterial growth as it is needed to maintain the integrity of the outer membrane barrier [11]. Therefore, several inhibitory agents targeting its synthesis have been investigated to produce novel antimicrobials [12].

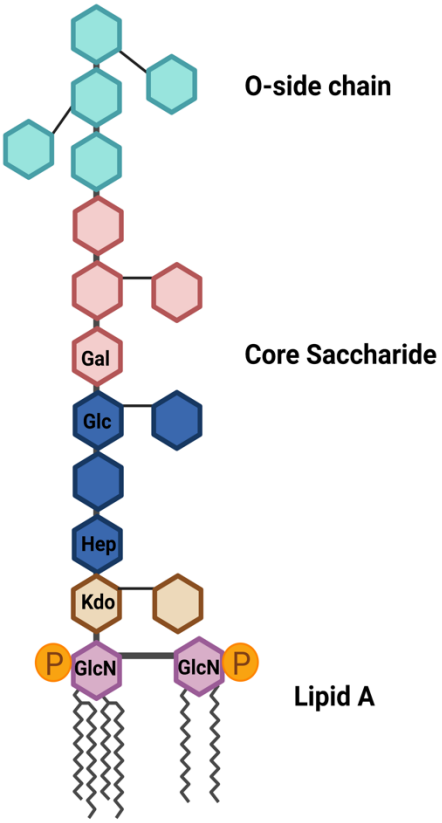

Fig. 1.2: Chemical structure of wild-type lipopolysaccharides (LPSs) from *E. coli,* Gal, (brown) galactose; Glc, (blue) glucose; GlcN, (purple) N-acetylglucosamine; Hep, L-glycero-D-manno-heptoseketo-deoxyoctulosonate; Kdo, 3-deoxy-D-manno-2-octulosonic acid; P, (yellow) phosphate. (Created in Biorender.com)

1.1.2.2 The core oligosaccharide

The complex heteropolysaccharide (core oligosaccharide and O-specific chain) is covalently linked to position 6' of lipid A [10]. The core region can be subdivided based on structural features into the inner (ReLPS) and outer core regions (RaLPS). The inner core region is composed of at least one molecule of 3-deoxy-α-D-*manno*-oct-2-ulopyranosonic acid (also called 2-keto-3-deoxyoctulosonic acid, Kdo) and two or more residues of L-*glycero*-α-D-*manno*-heptopyranose (L, D-Hep) [8]. The outer core typically consists of common hexose sugars, such as glucose, galactose, *N*-acetyl galactosamine and *N*-acetyl glucosamine and is generally more variable than the inner core region [12]. The composition of the core has an essential role in the biological activity of LPS. The core also has a negative charge conferred by the phosphorylated groups [8, 12].

The 2-keto-3-deoxyoctulosonic acid (Kdo) is the most conserved part of the LPS having a negatively charged substituent [6]. The negative charges provided by the phosphate groups in the Hep region of *E. coli* are essential in maintaining the barrier function of the OM by offering sites for cross-linking adjacent LPS molecules with divalent cations [11,13]. These negative charges, provided by residues Kdo and phosphate, allow neighbouring LPS molecules to be crosslinked by divalent cations (Mg^{2+} and Ca^{2+}), structurally reinforcing the OM [14]. Likewise, the negative charges play an important role in creating interaction between LPS and positive charges of OM proteins. This part of the LPS is selectively targeted by several cationic antibiotics and positively charged host defence peptides [8].

1.1.2.3 The O-specific chain

The third component of LPS, the O-specific chain (O-antigen), is a highly variable polysaccharide [15,16]. It consists of repeating oligosaccharide subunits made up of three to five

sugars. The individual chains can vary in length, extending up to 40 repeat units. The O-polysaccharide is much longer than the core oligosaccharide, and, it contains the hydrophilic part of the LPS [10,15]. The O-antigen is generally not essential for the survival of bacteria; however, several studies have shown that O-antigen plays an important role in the effective colonization of host cells, resistance to complement-mediated killing and resistance to cationic antimicrobial peptides that are key elements of the immune system [17].

1.1.3 Categories of antibiotics

Antibiotics can be categorized according to their mechanism of action. There are hundreds of antibiotics [13], which can be natural, synthetic, or semi-synthetic, making classification important. Antibiotics commonly kill or inhibit the growth of bacteria by hindering a major pathway or interacting with a specific structural component. The common classes of antibiotics and their mechanisms of action are summarized in **Table 1.1**.

Penicillin is the name given to a group of antibiotics, including penicillin G, penicillin V, and ampicillin. The structural similarity is the β lactam ring necessary to inhibit the cell wall synthesis in bacteria. The β lactam moiety binds to D- alanyl-D-alanine-transpeptidase, an enzyme that normally facilitates the peptidoglycan cross-linking. This binding interaction leads to the weakening of the cell wall, which can result in bacterial cell lysis due to the osmotic pressure [18]. Interestingly, tetracycline-based antibiotics such as methacyclin work synergistically with penicillin as penicillin weakens the peptidoglycan and facilitates the entry of methacyclin into the bacterial cells to inhibit protein synthesis [19]. Sulfonamides are a class of synthetic antimicrobial drugs used broadly to treat human and animal bacterial infections. Sulfonamides are competitive antagonists and structural analogs of p-aminobenzoic acid (PABA) in folic acid synthesis, which is essential for further DNA production in bacteria [20,21]. Nalidixic acid is considered the first

generation of quinolones, and it was introduced in 1962. It was initially for Gram-negative urinary tract infections in humans and animals. Ciprofloxacin was one of the most used fluoroquinolones and was introduced in the market in 1987 [22]. Rifampin is an antibacterial agent that targets Gram-positive and Gram-negative bacteria, for example, *Mycobacteria*, *Clostridium difficile*, *Neisseria meningitides* and Hemophilus influenza [23]. Its mechanism of action is by specifically inhibiting bacterial RNA polymerase, RNA polymerase is responsible for DNA transcription by forming a stable drug-enzyme complex with a binding constant of 10^{-9} M (at 37°C). Bacterial resistance to rifampin is caused by a mutation in that changes the structure of the beta subunits of RNA polymerase [23].

Table 1.1: Classes of antibiotics, mechanism of actions and acquired resistance.

Antibiotic class (example)	Mechanism of action	Mechanism of acquired resistance
β lactams [24] • Penicillin (penicillin, ampicillin) • Cephalosporins (cefotaxime) • Carbapenems (imipenem) • Monobactams (aztreonam) • Tetracyclines (methacycline)	Interference of cell wall synthesis [24] Inhibition of protein synthesis [21, 25]	• β lactamases produced by bacteria that cleave the β lactam ring • Modified or low-affinity DD-transpeptidase • Removal by efflux pump • Modification of targets such as ribosomes
Tetracyclines (methacycline)	Inhibition of protein synthesis [21,25]	• Modification of targets such as ribosomes
Sulfonamide (sulfamethoxazole)	Inhibition of folic acid synthesis [21]	• New enzymes via the acquisition of foreign genes
Fluoroquinolones	Inhibition of DNA replications [21]	• Modification of the target enzymes involved in DNA replication
Rifampin	Inhibition of RNA synthesis [21]	• A point mutation in the gene encoding for RNA polymerase
Polypeptides (polymyxin) Ionophores (gramicidin)	Disrupting bacterial membrane [21]	• Altered membrane structure • Enzymatic degradation

1.1.4 Antibiotic resistance

Antibiotics have not only saved patients lives, but they have also played an important role in achieving advances in medicine and surgery. Many people will suffer from infectious diseases without antibiotic drugs[26]. But sadly, after antibiotics were introduced clinically to treat infections, it was noted that antibiotics began to lose efficacy due to the growing number of antibiotic-resistant pathogens [27]. Some bacterial species have chromosomal DNA that also encodes for an efflux pump, enabling them to remove the antibiotic from the cell [22]. Non-lethal mutations in the chromosomal DNA can arise by mistakes made by the DNA polymerase during DNA replication which might be beneficial for the bacterium. This might be beneficial for the bacteria if the mutation modifies the antibiotic target, thus preventing the antibiotic from interacting with the target and rendering the organism resistant. This leads to an urgent need for new antibiotics to reduce the death rates associated with infectious diseases.

The search for and discovery of novel antibiotic classes has involved many outstanding achievements. Regardless of the successes, investigations, and production of different antibiotics, it has become imperative in modern medicine to solve the challenges related to antibiotic resistance.

The emergence of multidrug-resistant pathogens is one of the most critical recent threats to public health, and there is an urgent need for novel alternatives to current antibiotics. In 2021 and 2014, WHO report on the worldwide observation of antimicrobial-resistant pathogens showed that many resistant bacteria still threaten global public health and result in significant health and economic burden [28,29]. The increasing number of infections resulting from human pathogens, such as *Staphylococcus aureus*, and *Mycobacterium tuberculosis*, have shown the consequences of increased resistance against conventional antibiotics [30]. In some cases, the pathogen could

not be killed by any antibiotics. To overcome this problem, a potential alternative to conventional antibiotics, called antimicrobial peptides (AMPs), is investigated as a class of novel antibiotics.

1.2 Antimicrobial peptides (AMPs)

1.2.1 Classification of antimicrobial peptides

Antimicrobial peptides are a distinct and diverse class of molecules. There are thousands of AMP sequences reported to date, so it is important to categorize AMPs. AMPs can be categorized into many different groups, which can be based on structure, amino acid sequence and biological functions [31,32]. Often, AMPs are classified into three major antimicrobial groups according to the amino acid composition and peptide structures [31].

The α-helical AMPs were the first AMP structure class to be characterized [33] and are extensively studied. One good example of an α-helical AMP class is the magainins isolated from the African clawed frog *Xenopus laevis* and active against Gram-positive and Gram-negative bacteria, fungi, yeast, and viruses [34]. The structure and function relationship of the magainins has been well studied [35]. Magainin was the first AMP tested in the clinic but failed in clinical trials because it was not better than standard treatment [36]. However, the C-terminally modified MSI-78 (pexiganan) peptide, an analog of magainin 2 with a more positive charge, is currently in clinical trials as a topical antimicrobial treatment for mild-to-moderate foot ulcers in diabetic patients [37,38].

The second group of AMPs has a secondary structure characterized by β-strands. These peptides adopt a β-sheet structure when in contact with a lipid membrane. In contrast to α-helical AMPs, the structure of these β-sheet peptides is less flexible because of the structural restraints introduced by the disulfide bonds between the β-strands. This is the case, for example, with

tachyplesin, protegrin, and human α-defensins [36,39]. Defensins are a large group of AMPs involved in antibacterial, antifungal, antiviral, immune, and inflammatory responses [40].

The third group of AMPs are those with extended coil structure for example, the cathelicidin family [41] is rich in proline, an amino acid known to break α-helical and β-sheet secondary structures. The cathelicidin LL-37 is named for its 37 amino acids and N-terminal di-Leucine (Leu) (LL) motif. LL-37 is active against Gram-negative and Gram-positive bacteria, including *E. coli*, *S. aureus*, and *P. aeruginosa* [42]. Another example is indolicidin from bovine neutrophils, which is rich in tryptophan and has only 13 amino acids [43,44]. Nuclear magnetic resonance (NMR) and circular dichroism (CD) studies reveal that indolicidin forms a well-defined extended structure in the presence of membrane-mimicking micelles [44,45].

1.2.2 Common properties of antimicrobial peptides

AMPs often share several common properties regarding sequence, structure, and sources. Cationic AMPs display a net positive charge from +2 to +13 and may contain a specific cationic domain. The cationic nature can be allocated to the presence of lysine and arginine residues [46]. Many studies have demonstrated a correlation between the charge and antimicrobial activity of AMPs. Dathe et al. showed that increasing the charge of magainin 2 from +3 to +5 improved the antibacterial activity against Gram-positive and Gram-negative bacteria [47]. However, an increase to +6 or +7 led to a dramatic rise in hemolytic activity and loss of antimicrobial activity [47]. One possible explanation for the loss of antimicrobial activity with increasing charge may be that a strong interaction between the peptide and the phospholipid head group would prevent the translocation of the peptide into the inner leaflet of the membrane [48].

Most AMPs form amphipathic structures upon interaction with target membranes, but some of the best-known examples of amphipathicity in AMP structures are those with α-helices. The α-helix allows the peptide to form two faces, namely the polar and nonpolar faces referring to the arrangement of the hydrophobic and hydrophilic sidechains of the residues in the helix. While the degree of amphipathic helicity influences peptide activity against negatively charged biomembranes, it also provides AMPs with the capacity for hemolytic activity against zwitterionic or neutral membranes [48,49].

The last feature shared by all antimicrobial peptides is hydrophobicity. This is defined as the percent of hydrophobic residues, such as leucine, isoleucine, alanine, phenylalanine, methionine, tyrosine, valine, and tryptophan, in the peptide sequence. Hydrophobicity and amphipathicity are important parameters for those peptides whose sole target is the cytoplasmic membrane [50]. Hydrophobicity controls the extent to which the water-soluble AMPs can partition into the membrane lipid bilayer [51]. It is required for membrane permeabilization. Excessive levels of hydrophobicity can lead to mammalian cell toxicity and loss of antimicrobial selectivity [52,53]. Chen et al. studied the influence of hydrophobicity in a synthetic α-helical AMP (V13KL) on antimicrobial activity and hemolysis of human red blood cells (RBCs) [53]. The results showed an optimal hydrophobicity needed for good antimicrobial activity. Sequences with hydrophobicities below and very much above this threshold made the peptides inactive. The decrease in activity when the hydrophobicity is high may be due to the increased possibility of dimerization, thereby preventing access of the peptide to the bacterial membrane [53]. Furthermore, increasing the hydrophobicity of the non-polar face of the amphipathic α-helix also enhances the lysis of RBCs. This may be due to the membrane discrimination mechanism, as

peptides with higher hydrophobicity penetrate deeper into the hydrophobic core of the RBC membrane [53].

1.2.3 Mechanism of antimicrobial peptide action

Several models (**Fig. 1.3**) describe how most AMPs are thought to permeabilize microbial cytoplasmic membranes, which are often primary targets for AMPs. AMPs can be divided into groups based on whether they target the membrane or non-membrane cell components. For AMPs that target membranes, it is suggested that electrostatic interaction plays a prominent role in attraction between mainly cationic AMPs and negatively charged bacterial membrane components such as the anionic LPS of Gram-negative bacteria or lipoteichoic acid in the case of Gram-positive bacteria. [54,55]. AMPs that do not target the membrane must then act on intracellular targets.

In one mechanism, the barrel-stave model (**Fig. 1.3A**), peptides organize into a barrel-like ring around an aqueous pore [52,53]. The AMPs are initially oriented parallel to the membrane but eventually insert perpendicularly into the lipid bilayer [53-55]. Only a few AMPs, for example, alamethicin [54], pardaxin [57], and protegrins [58], have been shown to form barrel-stave channels.

Another suggested structure, the toroidal pore model (**Fig. 1.3B**), is one of the most well-characterized peptide-membrane interactions. In this model, AMPs bind in the polar head group region of the lipids, pushing the headgroups apart and inducing a positive curvature strain [59–61]. Specific properties of the toroidal pore include ion selectivity and discrete size [48]. Several AMPs, such as aurein 2.2 [62] and melittin [54], have formed toroidal pores. Both pore-forming models (toroidal pore and barrel stave) lead to membrane depolarization and cell death.

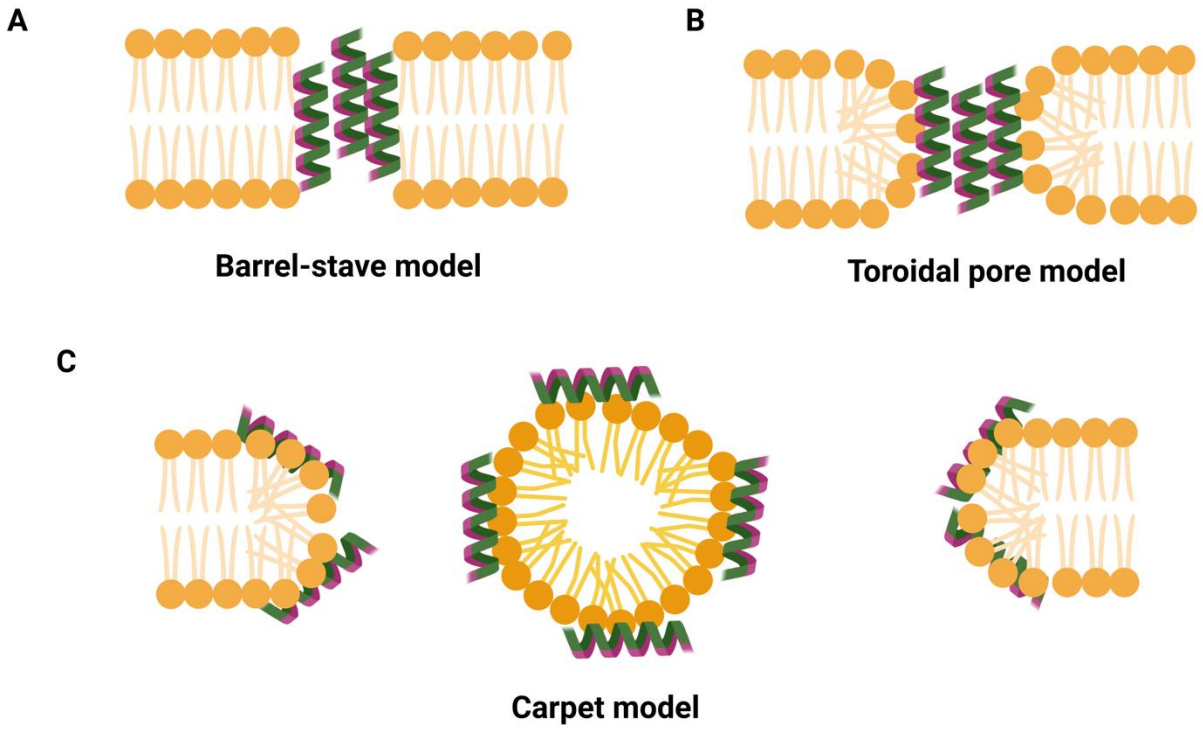

Fig. 1.3: Showing AMPs mechanism of actions models **A**: Barrel-stave model. **B**: Toroidal pore model. **C**: Carpet model. (Created in Biorender.com)

Recently, the disordered toroidal pore model has been proposed as an alternative to this traditional toroidal pore model. In this model, the inside of the pore is not well organized and has an irregular arrangement [60,63].

The carpet model (**Fig. 1.3C**) arises from a suggestion that AMPs can also act without forming specific pores in the membrane [48] [64]. In this case, the AMPs accumulate parallel to the lipid bilayer and reach a maximum concentration at which they envelop the surface of the membrane, thereby forming a "carpet." This leads to unfavourable interactions on the membrane surface [48]. Laadhari et.al. has shown that changes in phospholipid interactions increase the membrane lipid disorder, leading to membrane disruption and loss of membrane integrity [137].

The direct targeting of the bacterial membrane, through membrane permeabilization and lipid bilayer disruption, is widely accepted as an important mode of AMP activity [65]. The suggested mechanism for such activity is that, after initial electrostatic and hydrophobic interactions, the AMPs aggregate at the surface and then self-assemble into some form of peptide aggregate on the bacterial membrane after reaching a threshold concentration [66,67].

Almost all AMPs have a high affinity toward the cytoplasmic membrane, which leads to at least a certain amount of membrane perturbation. That said, a growing list of AMPs has been shown to harm bacteria without disrupting the membrane enough to cause substantial permeabilization. Such peptides generally cross the membrane and reach one or more intracellular targets [63,64,65,66]. These AMPs interact with the cytoplasmic membrane first and then accumulate intracellularly to block cellular processes [70].

Potential intracellular targets of AMPs include many fundamental processes, such as DNA and protein synthesis, the disruption of which could be effective in killing bacteria [58]. Friedrich

et al. showed that one of the indolicidin variants, CP10A inhibits the incorporation of amino acid precursors in *S. aureus* at twice the minimum inhibitory concentration (MIC) [71]. Some studies with buforin variants have shown the *in vitro* binding of buforin to duplex DNA. For example, Lan et al. showed that buforin adopted an extended conformation bound to DNA and reported that α-helix conformation is unnecessary for DNA binding [72].

1.2.4 AMP vs CPP

AMPs are commonly referred to as 'host defence peptides' (HDPs), a term that captures the more general mechanisms of some AMPs/HDPs, for example, in modulating the host's immune response [73]. Cell-penetrating peptides (CPPs) are another class of membrane-active peptides that share similar physiochemical properties with AMPs. Like AMPs, CPPs interact with membranes, but in contrast to AMPs, CPPs do not permeabilize the membrane [74]. Instead, CPPs translocate from one side of the bilayer to the other without bilayer permeabilization [75]. CPPs and AMPs have attracted attention due to their potential in novel drug delivery systems [76]. Cell-penetrating peptides are found in nature, are typically relatively short peptide sequences, and can be linked to cargo for transport into cells [76]. CPPs can deliver a variety of molecules into cells, including proteins, peptides, siRNA, DNA, liposomes, and nanoparticles [77], leading to much interest in their potential clinical uses [78]. CPPs enter cells by one of two modes, either by endocytosis, which is energy-dependent or by energy-independent passive uptake [78]. In both modes, peptides adsorb at the membrane surface, where they interact with negatively charged lipids and some, perhaps with glycoconjugates or membrane proteins [79]. One challenge in developing CPPs as delivery systems is that they often toxically permeabilize cells beyond a safe-threshold concentration [74]. Although CPPs have the potential for use in drug delivery, their

ability to enter cells of almost any kind still confers significant toxicity concerns that must be addressed.

1.2.5 Challenges with antimicrobial peptides

Over recent years, more than 300 AMPs have been made in an effort to integrate novel broad-spectrum antimicrobial peptides into clinical use, with minimal success [80,81]. There are several reasons for this failure, but the main unsettled issues involve poor oral bioavailability and short half-life in bloodstream stability [82].

Peptide drugs, like dietary peptides, are susceptible to digestive enzymes in the gastrointestinal tract. Even when peptides make it past the stomach, intestinal impermeability to molecules of their size limits entry to the systemic circulation [82,83]. Peptide therapeutics are often utilized to treat bacterial skin infections, pink eye, or wounds [84,85]. This administration route is still well suited to the management of acute diseases. For example, a few AMPs like Vacocin, Cubicin, Orbactiv, Dalvance and Coly-mycins have been approved for direct injection because of their long elimination half-life [86–89]. Therefore, much research is being carried out to optimize the residence time of such therapeutics in the bloodstream [90]. Once in the bloodstream, studies have shown that peptides without special modifications often only last minutes to a couple of hours before they are cleared by proteolysis or renal filtration [91]. Plasma clearance generally depends on two main peptide characteristics: size and surface charge. Strategies employed to increase plasma half-life typically manipulate one or both of these properties [89-92]. Furthermore, alamethicin and melittin, two extensively studied AMPs, are hemolytic and cytotoxic [93–97]; therefore, no clinical study has been performed.

1.2.6 Strategies to improve antimicrobial peptides

Many efforts have been made to make AMPs less toxic to humans while improving their potency to eliminate bacteria. Some methods, such as chemical strategies, enhance peptide specificity and stability. These methods are now being targeted to develop new antibiotics for AMPs. To improve AMP stability, researchers can try to modify and optimize the cyclization of peptides by linking C and N termini to improve serum stability and microbicidal activity [96].

Replacing natural amino acids with non-natural amino acids or D amino acids is another approach to protect the AMPs from proteolytic enzyme degradation since host proteases can identify and hydrolyze natural L-amino acids. In a recent study, the Zhao group isolated a lysine-rich AMP from the venom of the social wasp MPI, which has shown activity against Gram-positive and Gram-negative bacteria [97]. To test the proteolytic activity of trypsin, Zhao et al. designed two peptides, one with all amino acids substituted with D-amino acids (D-MPI) and the second peptide sequence with only the lysine residues replaced with D-amino acids (D-lys-MPI). This is because trypsin cleaves after positively charged amino acids, such as lysine [97]. Interestingly results showed that both the peptides, D-MPI and D-lys-MPI, were resistant to trypsin digestion. However, only D-MPI was equal in terms of activity compared to MPI. D-lys-MPI was inert because the secondary structure was destabilized by the introduction of single D-amino acids [97].

Another approach to improving AMP function is conjugating peptides to other active molecules. Incorporating peptides into non-biological molecules, for example, polyethylene glycol (PEG) or biological molecules like lipids, sugar, and proteins, allows the advantage of both types of biological molecules to be combined and overcome their weakness [83,92,98–100]. The advantages of PEGylation include reduced non-specific uptake in tissue, reduced cell toxicity, increased blood half-life and reduced proteolytic degradation [97].

1.2.7 AMP interactions with non-lipid cell envelope components of bacteria

Knowing the structure of the non-lipid components of the cell envelope is important for understanding how AMPs traverse them to reach the target cell membrane. In addition to the lipid bilayer, bacteria cell envelopes can have PGN, TA, and LPS, as well as membrane proteins. How AMPs initially traverse the non-lipid components of bacterial cell envelopes to reach the bilayer is still poorly understood. This is because most studies of AMP mechanisms have focussed on AMPs interacting with model lipid membranes, for example, using fluorescence-based permeabilization assays of vesicles or NMR of AMPs in liposomes [101–103]. One way to illustrate the potential importance of the non-lipid components is to compare the molar AMP-to-lipid (AMP: L) ratio needed to see the permeabilization of synthetic liposomes with the AMP:L ratio needed to see AMP activity in actual cells. In general, more AMP is needed to see activity in cells [54,104,105], suggesting that some AMP may not interact effectively with the membrane due to binding with components beyond the lipids.

One standard way to measure AMP activity against cells is by establishing the minimal inhibitory concentration (MIC), the minimum AMP concentration needed to prevent cells from growing. Several researchers have estimated or measured the AMP:L ratio at the MIC in whole cells and compared the values to those typical from *in vitro* experiments in model lipid vesicles. An early estimate proposed that, in liposomes, the bound AMP:L ratio needed to see activity is about 1:200 [106]. In stark contrast, in bacteria, the bound AMP:L ratio necessary to see effects is about 10–100:1. An alternate approach by Melo et al. [107] used the partition constant to understand the relationship between liposomes and bacterial experiments. Their *in vitro* and *in vivo* data for two AMPs, melittin and omiganan, indicated the cell-bound AMP:L ratio was from 2.3 to 9.2 times higher than the threshold to see effects in liposomes. In a more direct approach,

the Stella group [108] has developed an experimental approach using a special minimal medium where the bacteria are metabolically active but do not multiply. This has allowed them to investigate bactericidal activity against *E. coli* and AMP–cell association and show that, at the minimum bactericidal concentration (MBC), 10^7 fluorescently labelled AMP molecules are bound to each cell. This corresponds to an AMP:L ratio of ~1:3 to 5:1.

These studies suggest that AMPs may bind to molecules present in bacteria that are not present in liposomes. For Gram-negative bacteria, several studies indicate that AMPs interact with the LPS layer of the bacterial cell envelopes. Experiments on *E. coli* mutants where the LPS layer was absent increased the effectiveness of seven different AMPs, indicating that the LPS layer protects the bacteria from AMPs [109]. Such interactions between the AMPs and the LPS in the cell envelope of Gram-negative bacteria need to be accounted for to provide a complete view of AMPs' mechanism of action. Turning to Gram-positive bacteria with their thick PGN layers, it has been proposed that PGN does not prove to be a barrier for many AMPs, given PGN's lack of negative charge [110]. On the other hand, the AMP eosinophilic cationic protein has been shown to have strong interactions with both LPS and PGN using a fluorescent displacement assay [111]. Considering the importance of electrostatic interactions between positively charged AMPs and their targets, the negatively charged TA component of Gram-positive bacterial cell envelopes has been proposed to attract AMPs, sequestering them away from the lipid membrane and thus protecting the cells [112].

1.2.8 Cell selectivity of AMPs

AMPs have been known to exhibit cell selectivity, i.e., they selectively kill microorganisms at concentrations that are not toxic to host cells. This selectivity is thought to relate mainly to AMPs cationic character, which allows them to interact more strongly with bacterial membranes,

which have a more negative charge, than with host membranes, which are more zwitterionic in nature [39,113].

Hydrophobic interaction between the hydrophobic part of amphipathic AMPs and zwitterionic phospholipids on the cell surface of bacteria plays an important role in the interaction of AMPs with mammalian cell membranes. Matsuzaki et al. studied the correlation between hemolytic activity (which can be seen by monitoring the colour of hemoglobin) and lytic activity against phosphatidylcholine (PC) liposomes for several AMPs [114]. They found that hemolytic peptides exhibit strong interactions with PC liposomes (also a zwitterionic), whereas nonhemolytic AMPs do not [115].

Several studies focused on improving the cell selectivity of AMPs and suggest that strong antimicrobial activity and less cytotoxicity can be achieved by increasing the net positive charge of the peptide with minimal hydrophobicity above a threshold [116]. This is consistent with the hypothesis that the lipid composition of the cell surface is the main determinant of cell selectivity. A decrease in hydrophobicity can be achieved by introducing charged residues, D-amino acids [117], or by cyclization of the peptide [118].

Regardless of extensive research, study on the interaction of AMPs with mammalian cells has been limited. Most studies employ fluorescent assays as measures of cytotoxicity. However, erythrocytes are specialized cells without intracellular and extracellular cell organelles. Studies with mammalian cells have only examined cell viability [119,120][105]. A more detailed study on AMPs toxicities to mammalian cells and the mode of AMP-cell interaction is required.

1.2.9 Cell-penetrating peptides:

Cell-penetrating peptides (CPPs) are short-cationic or amphipathic peptides that can be conjugated with large macromolecules to facilitate their cell entry. Although the first study of a polycationic peptide capable of traversing the cellular plasma membrane was published in 1965, the Prochiantz group reported the cell-penetrating properties of penetratin in 1994 [121]. Later Lebleu et al. published that the short highly cationic peptide (Tat 48-60) from the Tat protein was sufficient for cell penetration[122]. From that date, an ever-increasing number of new CPPs have been discovered and characterized, however, the uptake mechanism still needs to be fully understood.

1.2.10 Mechanism of CPP membrane translocation:

Wimley et al. have explained the CPP mechanism of action by which CPP might translocate across the membrane and deliver a cargo molecule under a specific set of conditions, whether its internalization is mostly active by cell energy dependent or passive, i.e. without using cell energy [123]. One model proposed for the CPP mechanism (actively internalized) showed that polycationic CPPs interacted with the negatively charged phospholipids of the cell membrane, causing a local reorganization of the lipid bilayer, resulting in the formation of inverted micelles [75,123].

Many CPPs are reported to use the endocytic pathway (actively internalized) to gain access to the intercellular organelles. To understand the involvement of different endocytic pathways in the uptake of CPPs, most studies used pharmacological inhibitors or specific markers for a certain pathway. Some examples of endocytic uptake of CPPs are penetratin and Tat by micropinocytosis pathway. Transportan and TP-10 are known for caveolae-mediated pathways [123,124].

On the other hand, several studies have shown evidence that non-endocytic (passively internalized) mechanisms are involved in the uptake of some CPPs. For example, MPG peptide, both by itself and in complex with DNA, penetrates the membrane by a mechanism dependent on the GTPase Rac 1 [125,126]. Rac 1 activation stimulates actin network remodelling, increasing membrane fluidity and fusion [126]. Furthermore, one CPP might utilize different pathways depending on the cargo. Mutational analysis of the full-length HIV-tat protein showed that a short, highly basic and unstructured N-terminal sequence was necessary for cell entry and cargo delivery [123,127]. The cellular mechanism of Tat was initially thought to be energy-independent; however, a general agreement has emerged that endocytosis is the primary mechanism of entry [124,127].

1.2.11 Peptides used in this work

MSI-78 is one of a family of AMPs that are analogs of magainin, a family of amphipathic α-helical AMPs. Magainin was discovered in the skin of the African frog *Xenopus laevis*. MSI-78 is active against several bacterial strains, including strains resistant to conventional antibiotics [128]. MSI-78 has been screened for activity against *E. coli*, *P. aeruginosa*, *S. aureus*, and *C. albicans* [128]. It is a potent antibiotic with a MIC value of ≤ 64 μg/ml for *C. albicans* [128], a net cationic charge of +9, and a grand average hydropathicity index of −0.159 [129]. MSI-78, also known as pexiganan, was developed to treat infected diabetic foot ulcers [35,130]. MSI-78 is one of the best-studied AMPs [38,131].

MSI-78 was designed to be amphipathic and is one of a number of magainin analogues [132]. Hallock et al. studied MSI-78 in lipid bilayers using biophysical techniques like ^{31}P NMR and DSC to understand if MSI-78 operates by a similar mechanism to that of magainin. The ^{31}P-

NMR observations of samples containing 1-palmitoyl-2-oleoyl-phosphatidylcholine showed that MSI-78 induces significant changes in the bilayer structure, especially at high concentrations. However, at a low concentration, the peptide-induced membrane permeabilization is via toroidal pore formation [128]. Interestingly, MD simulations showed toroidal pores could be more dynamic or disordered, with only a few peptides being present at the center of the pore [133]. ^{15}N solid-state NMR data, on the other hand, showed that these peptides were aligned roughly parallel to the bilayer surface, indicating that they do not work via the barrel-stave membrane-disruption mechanism [134].

TP2 is a CPP [123] and contains the motif, LRLLR, called the spontaneous membrane translocation peptide (SMTP). TP2 is substantially more hydrophobic than MSI-78, with a grand average hydropathicity index of 0.423 and a +3 charge in a neutral solution [135]. CPPs can cross the bilayer spontaneously and enter cells by translocating directly across the membrane [77,135,136]. CPPs may result in cytotoxicity at a low peptide concentration. Thus membrane disruption is not a desired characteristic when designing CPPs [123]. A distinctive feature of CPPs is translocation without membrane disruption. A better understanding of the CPP-internalization mechanisms would allow for a better rational design of the selective and efficient CPPs [75].

1.3 Deuterium solid-state NMR

Deuterium solid-state nuclear magnetic resonance (^{2}H SS-NMR) has attracted attention as a tool for studying membrane perturbation and disruption due to a wide range of effects, including AMPs, because of its advantage over other analytical techniques. Compared to fluorescence analytical methods, which require large and potentially perturbing probe molecules, ^{2}H NMR is a non-invasive analytical technique that probes the lipid acyl chain orientational order parameter

profile and is sensitive to lipid chain dynamics in membranes, including deuterated bacterial membranes. ^{2}H NMR has been used with increasing frequency to understand better the antimicrobial interaction of AMPs and the mechanisms of their actions on the bacterial membrane [137–140].

1.3.1 Deuterium NMR for lipids

In order to use ^{2}H NMR for lipids, the hydrogens atoms on the lipid acyl chains are replaced with deuterons. If this replacement is done only at a single site, the sample is specifically deuterated. If deuterons are placed along the lipid acyl chain (**Fig. 1.4**), samples are designated as chain per-deuterated. In the next paragraph, I will describe how we extract information from the ^{2}H NMR lipid spectra.

In a model membrane vesicle sample, the bilayer normal is randomly oriented with respect to the external magnetic field. The resulting NMR spectrum for liquid crystalline bilayers has a characteristic line shape called a Pake doublet. For a chain perdeuterated sample, the NMR spectrum is a superposition of Pake doublets corresponding to all the deuterons on the lipid acyl chain, as shown in the upper panel of **Fig. 1.5**. The splittings of these doublets are determined by the averaged motion of the lipid acyl chains. Close to the lipid head groups, lipid acyl chain motion is more constrained, resulting in larger splittings, while, towards the end of the acyl chain, the large amplitudes of motion give rise to smaller splittings.

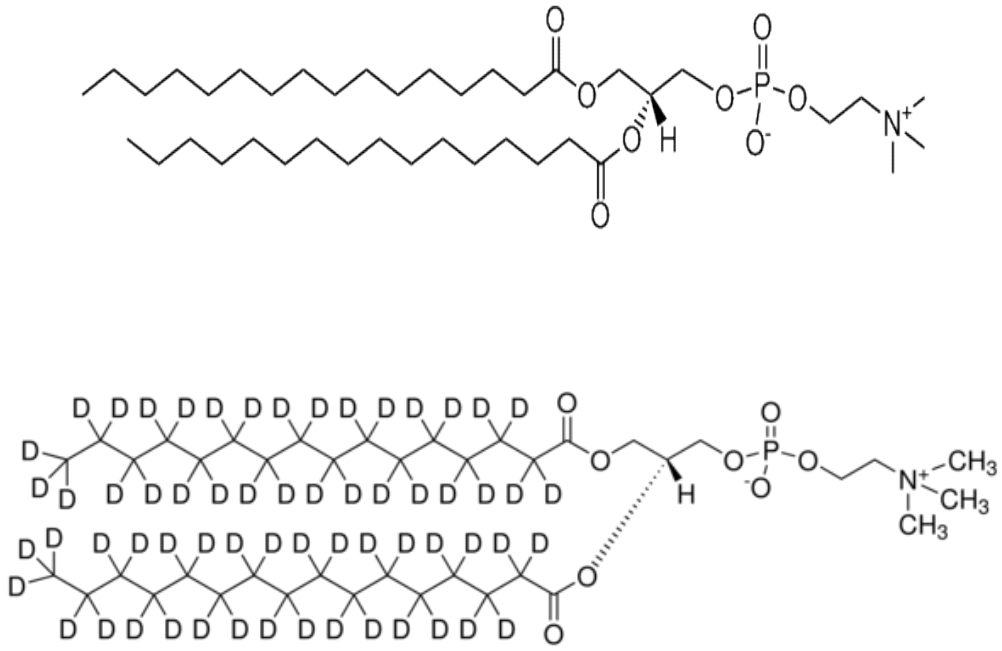

Fig. 1.4: Labelling strategy of DPPC-d_{62} for ^{2}H NMR.

Reorientation of the molecular frame of reference for a specific acyl chain segment with respect to the bilayer normal is characterized by the orientational order parameter. In order to calculate the orientational order parameter profile from the powder pattern of a chain perdeuterated sample with randomly oriented bilayers, it is helpful to extract the spectrum that would be obtained for a unique bilayer normal orientation by using a technique called "de-Paking" [141,142]. To get the orientational order parameter (S_{CD}) from the dePaked spectrum, quadrupole splittings ($\Delta\nu_Q$) for all the deuterons at different carbon postions can be calculated. The lower panel of **Fig. 1.5** shows the dePaked spectrum corresponding to the spectrum in the upper panel. The S_{CD} is 1 for rigid segments with CD bonds perpendicular to the bilayer normal and 0 for isotropically reorienting CD bonds. The plot shown in **Fig. 1.6** of the orientational order parameter vs. carbon position is called the orientational order parameter profile. The example shown here was obtained assuming a monotonic decrease of the orientational order along the acyl chain. For acyl chain segments close to the headgroup (the "plateau" region), orientational order may not change monotonically with position, but the profile shown here assigns common splittings to unresolved doublets. Therefore, this way of displaying the profile does not provide complete details of the orientational order parameter dependence on chain position for this part of the lipid acyl chain [143].

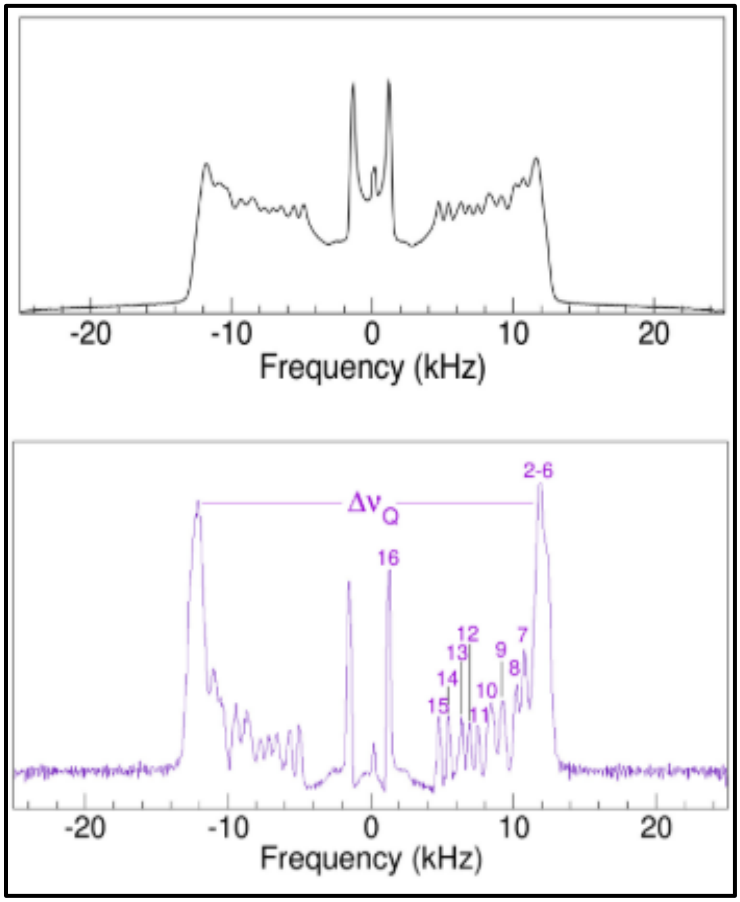

Fig. 1.5: Schematic representation of the powder pattern spectrum (black) and the de-Paked spectrum (purple) of a vesicle sample with multiple C-D bonds (DPPC-d_{62}). Larger splitting represents the C-D bonds closer to the lipid head groups. Numbers in the figure indicate the deuterated acyl chain segment giving rise to each peak in the spectrum. (Figure from [144] used with permission from Nury Paula Santisteban)

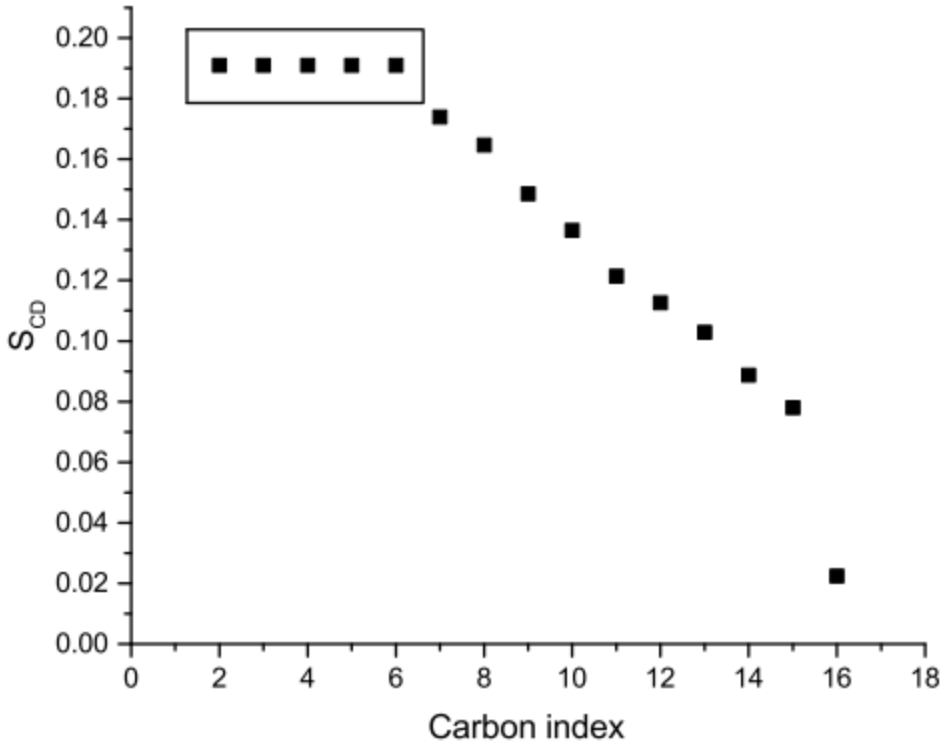

Fig. 1.6: Order parameter profile of DPPC-*d62* in liquid crystalline bilayers at 42°C. The box indicates the plateau region. (Figure from [144] used with permission from Nury Paula Santisteban)

1.3.2 Deuterium NMR of bacterial membrane

The Davis group obtained the first ^{2}H-NMR spectra of membrane-deuterated bacteria in the early 1980s [67]. ^{2}H-NMR has recently been used to study how AMPs interact with bacteria [137–140,145]. Although ^{2}H-NMR can be adapted to investigate the interaction of AMPs with model membranes, *in vivo* studies are of considerable value because of the complex structure of biological membranes. I successfully deuterated the membrane of wild-type strains of bacteria because their lipid metabolism and compositions are known.

Our group and others have employed two approaches to incorporating deuterium labels into the bacterial membrane [139,145]. The first approach uses a mutant strain of *E. coli* that is unable to metabolize fatty acids. The mutant bacteria were grown in the presence of deuterated palmitic acid (PA) and undeuterated oleic acids. The second approach used wild-type strain bacteria in which, during the bacterial growth phase, deuterated PA complexed with deodecylphosphocholine (DPC) micelles was added to facilitate uptake of the PA [103,140]. Apart from PA complexed with DPC, it is also important to provide oleic acids to PA to maintain a normal acyl chain composition in their membranes.

The deuterium NMR spectra for the bacterial membranes differ in some ways from the spectra of model membrane bilayers containing only lipid molecules. The bacterial membrane is more complex than systems comprising one or two lipid species. **Fig. 1.7** shows a lipid-only liquid-crystalline model membrane static spectrum and a membrane-deuterated *E. coli* ^{2}H NMR spectrum. The lipid-only spectrum shows prominent edges at ~± 12.5 kHz, mainly from the acyl chain deuterons near the lipid head groups where the motions of a few segments are constrained. This reflects the existence of an orientational order parameter plateau. The narrower parts of the

spectrum are derived from the opposite end of the acyl chain, near the bilayer center, where motions are less constrained. The intense peak near the center of the spectrum is from the highly mobile deuterated methyl groups at the ends of the acyl chains. The resolved doublets with intermediate splittings correspond to specific acyl chain segments in the model membrane. On the other hand, the bacterial spectrum does not show resolved doublets largely because of the complexity of the membrane and the likely deuteration of a range of lipid species in the bacterial membrane [131]. Nonetheless, the bacterial spectrum still displays evidence for spectral edges at ~± 12.5 kHz that correspond to the quadrupole splitting for deuterated acyl chain segments near the lipid headgroups for which motions are relatively more constrained than for segments closer to the bilayer centre [140,146],

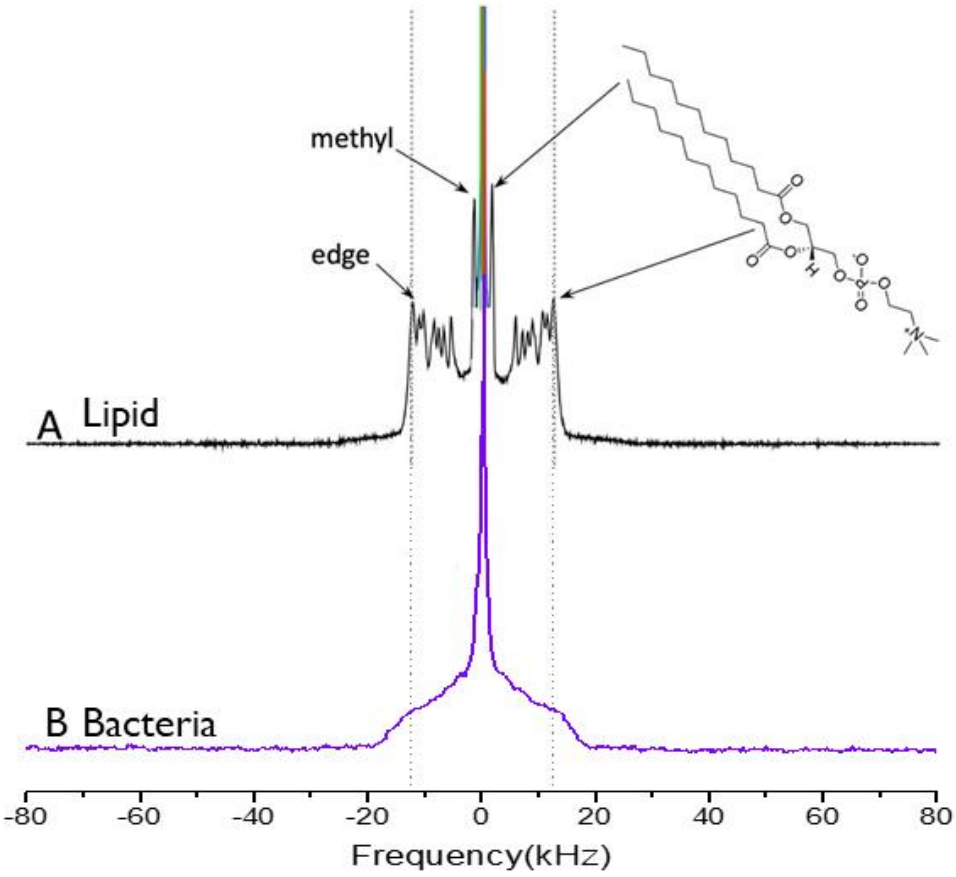

Fig. 1.7: Adapted from Booth et al. [147]. Static solid-state NMR spectra of (A) model lipids, i.e., dilauroyl phosphatidylcholine-$_{d46}$ (DLPC-$_{d46}$); (B) ^{2}H-membrane labelled *E. coli*.

1.3.3 Magic angle spinning experiments

While using static solid-state NMR takes more than 12 hours to record the NMR spectrum, a Magic Angle Spinning (MAS) (**Fig. 1.8**) experiment might only require 3 hours to record the NMR spectrum for membrane-deuterated bacteria. Rapidly spinning the sample about an axis oriented to 54.7° from the static magnetic field (the magic angle) collapses the quadrupole doublets into a sharp peak with sidebands from which, in principle, some of the information that would have been contained in the static spectrum can be recovered.

In the real MAS experiment, the spinning speed is much slower (2.5-10 kHz) than the speed needed to collapse the spectrum to a single peak. Spinning at slower speeds produces a set of sharp peaks called "spinning sidebands." The difference in frequency of adjacent spinning sidebands is the spinning rate. Compared to a static experiment, the MAS experiment greatly increases the resolution.

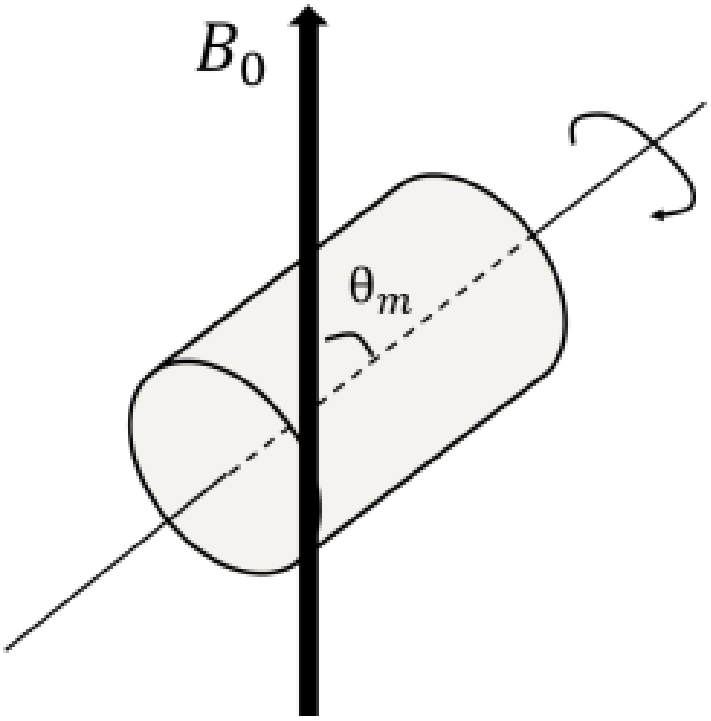

Fig. 1.8: Magic Angle Spinning Experiment: the sample is spun rapidly around an axis tilted by 54.7° relative to the external magnetic field.

Static ^{2}H solid-state NMR studies of deuterated bacterial membranes can be time-consuming (it takes 16-17 hours to obtain a good signal-to-noise ratio), which can be inimical for short-lived bacterial samples. The first ^{2}H MAS NMR experiment was introduced by Maricq et al. and Ackerman et al. in the late 1970s [148,149]. Clayden et al. in 1986 showed in their computer simulation study that MAS spectra can provide similar information to ^{2}H static solid-state NMR with better sensitivity [150]. Duer et al. and Cutajar et al. developed MAS techniques in the late 1990s [151,152] to extract dynamic information on model membranes and discovered an important application for membranes, which has been used to probe critical fluctuation in model membranes. Davis and Veatch et al. speculated that this critical fluctuation in domain-forming lipid mixtures on the model membrane would be measurable either on its sideband linewidths or the relaxation of ^{2}H MAS NMR [139,140]. These effects have been investigated and quantified on multilamellar dispersions of di-oleoyl-*sn*-glycero-3-phosphocholine/di-palmitoyl-*sn*-glycero-3-phosphocholine-d_{62}/cholesterol in water [153,154].

Recently, ^{2}H MAS NMR has been applied by the Marcotte group to study membranes in intact cells [155]. Therefore, along with the static NMR study described in Chapter 3 for membrane-deuterated *E. coli*, we also wanted to compare how bacterial membrane orientational order could be assessed using static and MAS ^{2}H NMR.

1.4 Hypothesis and Objectives

One important unanswered question is how AMPs traverse the non-lipid components of the cell envelope to reach the bilayer, either to permeabilize it or as the first step in reaching an intracellular target. This question has seen little attention. Most of the work on AMP-induced permeabilization has been performed with model lipid bilayers, which lack the peptidoglycan and lipopolysaccharide usually present in bacterial cell envelopes. We hypothesize that disrupting one of the non-lipid components of bacteria, particularly cell envelope components such as LPS, will affect AMPs interaction with the lipid membrane.

The membrane of a wild-type strain of bacteria can be successfully deuterated as their lipid metabolism is known. We have used *E. coli* bacteria in this study as we know they have a simple phospholipid profile including (75% PE, 20% PG and 5% CL) and the three main fatty acids are (C16, C17 and C18) [155].

The main objectives of this thesis are:

1) Establish ^{2}H NMR methods to independently prepare membrane-deuterated bacteria to get reproducible spectra and explore ^{2}H-MAS NMR of cells (Chapter 3).

2) The permeabilizing action of EDTA is usually considered to result from LPS release. We aimed to establish a protocol to prepare gently EDTA-treated cells for NMR and characterize the EDTA's effects on bacterial acyl chain orientational order using deuterium NMR (Chapter 4).

3) To evaluate the impact of the destabilization of the LPS layer on the interaction between the bacterial cell envelope and the AMP-MSI-78 (Chapter 5).

4) Compare the effect of AMP-MSI-78 and CPP-TP2 on deuterium NMR spectra of whole cells (Chapter 6).

5) Study AMP selectivity for bacteria over mammalian cells (Chapter 7).

Chapter 2. Materials and Methods

2.1 Materials:

Deuterated palmitic acid (PA-d_{31}) was acquired from CDN Isotopes (Pointe-Claire, QC, Canada). N-dodecyl phosphocholine (DPC) was purchased from Avanti Polar Lipids (Alabaster, AL, USA). Oleic acid (OA), ethylenediaminetetraacetic acid (EDTA), propidium iodide, yeast extract, tryptone and sodium chloride were purchased from Thermo Fisher Scientific BioReagents™ (Markham, ON, Canada). MSI-78 (GIGKFLKKAKKFGKAFVKILKK-NH_2) and TP2 (PLIYLRLLRGQWC-NH_2) peptides were C-terminally amidated and obtained from GenScript (Piscataway, NJ, USA) with ≥90% purity.

2.2 Peptide preparation:

MSI-78 and TP2 were desalted by buffer exchange using Spectrum™Spectra/Por™ dialysis membrane tubing (100–500 and 1000 Dalton MWCO). The dry peptide was dissolved with a small dialysate (5% acetic acid and 95% water) and added to the membrane tubing. Peptides were dialyzed against the dialysate for 24 hours at 4°C. Next, peptides were dialyzed against 100% purified water for another 24 hours. Dialysed peptides were lyophilized, weighed, and then stored at −20°C.

2.3 Preparation of membrane-deuterated *E. coli*

JM109 (ATCC-68862) strain *E. coli* bacteria were grown with a PA-d_{31}-DPC mixture incorporated in the growth medium described before [156] and outlined below.

Overnight cultures of JM109 were prepared by inoculating 20 mL of Luria Broth (LB) media (10 g/L tryptone, 5 g/L yeast extract and 5 g/L NaCl) with a 1 mL aliquot of frozen glycerol

cell stock and then incubating at 30°C with a shaking speed of 150 rpm. Large-scale cultures (200 mL) were grown at 37°C and 175 rpm starting with 2 mL of overnight culture in 200 mL of fresh LB media containing 0.25 mM deuterated palmitic acid (PA-d_{31}) complexed with 1 mM n-dodecyl phosphocholine (DPC) and 0.25 mM OA/DPC.

To prepare the fatty acid (PA-d_{31} or OA)/DPC complexes, a 5 ml solution containing 0.25 mM of PA-d_{31} or unlabelled OA and 1 mM DPC (final concentrations) was prepared with distilled water. Next, using a 0.2-micron syringe filter unit, each solution was filtered and transferred to a new 50 mL Falcon tube. Subsequently, the mixtures were heated in a boiling water bath for 3 minutes and then submerged in liquid nitrogen until each mixture froze solid. Next, both tubes were warmed in a water bath at room temperature until the ice melted. Finally, the mixture containing PA-d_{31} complexed with DPC micelles and OA was added immediately to the growth media as the large-scale (200 ml) culture was started.

Cells were harvested in the mid-log phase (after ~ 3.5 hours of growth) at an absorbance at 600 nm (A600) of 0.6 –0.8 and then pelleted by centrifugation at 5670 × *g* for 20 min at 4°C. The pellet was transferred into a 3.2 mm MAS NMR rotor, and NMR experiments were carried out as described in Section 2.5 below. Samples with EDTA or AMP treatment required additional pre-NMR steps described in Section 2.4.

2.4 AMP treatment of bacterial samples

The MIC defines AMP concentrations for a particular cell concentration. The MIC for MSI-78 to JM109 is 27μg/ml [139]. In our study, the cell concentration is many orders of magnitude higher than the cell concentrations used in MIC assays. Thus, the MIC does not help indicate if the amount of MSI-78 we use is likely to be inhibitory. We estimate peptide: lipid ratios, so we use AMP amounts as an AMP dry weight percentage relative to the dry weight of bacteria;

this facilitates comparing molar AMP:L ratios in this work with those from other studies [139,156]. Because the amount of cell pellets differ from one preparation to another, a relationship between A_{600}, just before centrifugation to harvest the cells, and the bacteria dry weight was required, and it was obtained as follows.

To derive this relationship, cells were grown under conditions explained in section 2.3. Cultures were harvested during different points of the log growth and pelleted by centrifugation at 5670 × *g* for 20 min. The final pellet was weighed and placed in a vacuum chamber for 48 hours. After 48 hours, each pellet was re-weighed. A linear fit of ln(dry weight) versus the absorption at 600 nm (A_{600}) gives the relationship equation that can be used to calculate the bacterial dry weight from observed absorption and, from this, the appropriate amount of AMP to add to each bacterial sample. For JM109 *E. coli,* the relationship obtained was ln (dry weight) = (1.28±0.28) A_{600} + (5.18±0.28), which yields the dry weight in mg per litre of cells grown. For example, at an A_{600} optical density of 0.62, this relationship was used to find that 23 mg of the peptide was required to obtain an AMP dry weight of 30% relative to the dry weight of bacteria for 0.2 litres of bacterial culture.

While cells were being harvested by centrifugation as described above, the appropriate amount of peptide was calculated, then weighed and suspended in 30 mL of LB medium. The media + AMP mixture was then used to resuspend the bacterial pellet, which was then incubated at room temperature for 20 minutes while undergoing mild shaking on a benchtop shaker. After 20 min, the sample was centrifuged at 5670 × *g* for 20 min at 4°C. Finally, the resulting pellet was transferred into the 3.2 mm NMR rotor, as detailed in Section 2.6. The cells need to be transferred to the NMR rotor immediately after the centrifugation to minimize the cell death.

2.5 EDTA treatment of bacterial samples

EDTA chelates the divalent cations that help stabilize the LPS layer of *E. coli* and thus destabilizes the LPS [56]. For this study, we needed to establish an EDTA treatment protocol that would destabilize the LPS gently without lysing the cells. To accomplish this, we treated *E. coli* samples for 45 minutes with a range of EDTA concentrations from 1.5 to 9.0 mM. Treatment times ranged from 5 to 45 minutes. At the end of each treatment time, I started the Gram staining protocol and looked at the bacteria under the compound microscope right after completing the staining. There was no change in Gram staining colour and shape until reaching EDTA concentration of 8.0 mM . The *E. coli* exhibited only minor changes up to 8.0 mM EDTA but showed changes in the shape and Gram-staining colour at 9.0 mM concentration. Thus, for the rest of the studies, 2.5 mM was chosen to represent the effects of a low concentration of EDTA and 9.0 mM to represent the effects of a high concentration of EDTA. For the samples treated with EDTA alone, discussed in **Chapter 4,** bacteria were grown and harvested at A_{600} values between 0.6 and 0.8 and then pelleted by centrifugation at 5670 × *g* for 20 min at 4°C. The resulting pellet was resuspended in 50 ml of LB media with 2.5 mM or 9.0 mM EDTA at room temperature for 45 minutes with gentle shaking on a benchtop shaker. For samples treated with both EDTA and AMP, cells were first treated with 2.5 mM or 9.0 mM EDTA and then pelleted by centrifugation at 5670 × *g* for 20 min at 4°C followed by AMP treatment as described above for 20 min. Finally, the samples were centrifuged at 5670 × *g* for 20 min. The samples treated with EDTA and AMP are discussed in **Chapters 5 and 6**.

2.6 Packing the rotor for NMR

The NMR rotor was cleaned, washed, and allowed to dry before each use. The actual weight of the bacterial paste that was ultimately packed into a rotor was determined by weighing the rotor before and after the bacterial paste (~ 40 mg) was added. Bacterial pellets were transferred to the 3.2 mm rotor with the help of 200 µl pipette tips. First, the pipette tip was trimmed slightly to enlarge the opening. Then the pipette tip was inserted into the rotor, and both were placed in a 1.5 ml Eppendorf tube. The bacterial paste was transferred into the pipette tip with a spatula, and the assembly was centrifuged for 30 sec at 3217 × *g* to transfer the bacteria into the rotor. The sample was packed similarly for static and MAS experiments. For both cases, the sample was packed in the MAS rotor and used in the MAS probe.

2.7 Performing static ^{2}H NMR measurements

^{2}H NMR experiments were performed at 37°C with a solid-state Bruker Avance II 600 MHz spectrometer (Milton, Ontario, Canada), operating at a frequency of 92.15 MHz for ^{2}H. All experiments were run with a triple resonance (HCD(N)) magic-angle spinning probe using 3.2 mm diameter rotors. All ^{2}H NMR samples were labelled SK-01, SK-02, etc. Please refer to Appendix C for the complete list of all 81 SK-XX NMR samples. SK numbers were labels to identify specific preparations, and this labelling scheme was used to distinguish replicants and facilitate the comparison of specific samples. The SK numbers correlate with the order in which samples were studied.

Static spectra were obtained using the solid-echo pulse sequence [145], with a 90° pulse width of 5 µs and a pulse separation of 60 µs. Spectra were derived from free-induction decays obtained by averaging 20,000 transients acquired with a dwell time of 5 µs (spectral width of 200

kHz) and a repetition delay of 500 ms. The total experiment time for each spectrum was 18 hours. Data were accumulated in 5-hour blocks so the spectra could be checked for any changes with time in the spectrometer.

To obtain spectra from free-induction decays (for processing), the data were left-shifted by up to 3 points to start the Fourier transform at the top of the echo [146]. Phasing, baseline correction, and 40 Hz line broadening were also applied. Most static spectra show two peaks near the centre, one from the lipids and the other presumably from HDO or some partially deuterated metabolic product. When two peaks were apparent, the larger peak closest to negative frequency was identified as 0 Hz. This ensured that the prominent edges of the spectra were symmetric at ±12.5 kHz.

To quantify the spectral shape and changes to it caused by the AMP, spectral moments (M_n) were calculated by using the equation

$$M_n = \frac{\int_0^\infty \omega^n f(\omega) d\omega}{\int_0^\infty f(\omega) d\omega} \qquad (1)$$

where ω is the angular frequency relative to the Larmor angular frequency, ω_0, and $f(\omega)$ is the spectral intensity. The first moment (with $n = 1$) is proportional to the average quadrupolar splitting and the average of the deuteron orientational order parameter. The second moment is proportional to the mean square quadrupolar splitting and the mean square order parameter.

The first and second moments, M_1 and M_2 were used to calculate Δ_2 [159], the relative mean square width of the distribution of order parameters. Δ_2 can be defined in terms of M_1 and M_2 as

$$\Delta_2 = \frac{M_2}{1.35 \times M_1^2} - 1 \qquad (2)$$

For static spectra, spectral moments $M_1$and M_2 from static spectra were calculated using an algorithm previously used in this group [139,140] but implemented through a new MATLAB script as follows. The average intensity value between 32.48 to 38.06 kHz and thus outside of the range containing spectral intensity from sample deuterons was subtracted from each point in the spectrum in order to correct for any offset of the spectral baseline from zero. To remove the effects of the water and metabolite peaks at the center of the spectrum (as described above), the intensity in the ± 0.61 kHz range was set uniformly to the average intensity in the 0.61 to 0.88 kHz range. The intensity of the spectrum between 0 and 24.8 kHz was then used to calculate the moments. The moment calculation was then repeated with the negative frequency half of the spectrum using the absolute value of the frequency. The moments obtained from the two halves, normally identical or nearly, were averaged to give the overall moment.

Since each sample preparation and NMR experiment was repeated several times, it became meaningful to conduct a statistical analysis. The moments and Δ_2 values for each composition were averaged and expressed as average ± standard deviation using Excel data analysis software. Different treatment groups were compared using a one-way ANOVA statistical test by OriginPro software.

2.8 Flow cytometry

Flow cytometry was performed to observe the AMP-induced cell permeability under the same sample preparation conditions used for the NMR work. Control samples were prepared by treating cells with 70% isopropanol to permeabilize them completely and by treating them with buffer alone to serve as healthy cell control. As was done for NMR, 200 ml of the cell suspension were harvested at OD 0.6 and pelleted by centrifugation at 5670 × g for 20 min at 4°C. The cell pellet was resuspended in 50 ml LB media containing EDTA at 2.5 mM or 9.0 mM concentration

for 45 minutes at room temperature and centrifuged at 5670 × *g* for 20 minutes. For the combined EDTA + AMP treatment, the EDTA treatment was performed first, followed by the AMP treatment described in Section 2.4. Regardless of treatment, all cell samples were harvested by centrifugation at 5670 x *g* for 20 minutes at 4°C. All samples were then diluted in phosphate buffer saline (PBS) (0.137 M NaCl, 0.05 M NaH_2PO_4, pH 7.4) to 2.5 × 10^5 CFU/ml (colony-forming unit)/ ml of bacterial suspension, followed by washing by adding PBS buffer and centrifuging at 5670 × *g*, after which the supernatant was discarded. Cells were resuspended in 100 µl PBS buffer with propidium iodide (PI).

To measure membrane permeability, 5-10 µl of propidium iodide (final concentration 10 µM) staining solution (PI Staining solution: 10 µg/ml PI in PBS) was added to the bacterial samples. Tubes were gently mixed and incubated at room temperature for 5-10 minutes in the dark. After the PI incubation, flow cytometry was started within 15 minutes. Data were acquired for 30 seconds (10,000 events) using a Beckman Coulter CytoFLEX flow cytometer using the ECD channel (610/20) with the 488 nm laser. Data were analyzed using CytExpert version 2.3 software (Beckman Coulter) by drawing a gate to include the significant cell events in the sample. Optical data (forward scatter and side scatter plots) are provided in Appendix **Fig. B1 and B2**. Each flow cytometry experiment was repeated at least 2 times, starting with new cells.

2.9 Gram Staining

Gram staining was used to obtain evidence for destabilizing the LPS layer of *E. coli* cells with EDTA treatment. A 1 ml aliquot of the bacterial sample was set aside in a 1.5 ml microcentrifuge tube before the final centrifugation harvest in Section 2.3. These bacterial cells were spread onto a microscope slide using a sterile cooled loop. Next, the cells were heat-fixed onto the microscope

slide by passing them through the Bunsen burner flame three times. The slide was allowed to air dry. Next, 90% crystal violet was gently added to the slide, assuring full coverage of the smear, and left to stand for 1 minute. The 90% crystal violet was gently rinsed off with distilled water. Next, the iodine at a concentration of 1% was gently added to the slide and let stand for 1 minute. The iodine solution was gently rinsed off with distilled water. The fixed smear was decolorized using 95% ethyl ethanol for about 5 to 10 seconds or until the ethanol ran almost clear. The ethanol was gently rinsed off with distilled water. Safranin at a concentration of 0.1% was gently added to the slide, assuring full coverage of the smear, and let stand for 45 seconds. Finally, the safranin was gently rinsed off with distilled water. The slide was placed on a paper towel and allowed to air dry. Once the slide was completely dry, bacterial samples were observed under a conventional light microscope using a 100× immersion oil lens equipped with a built-in camera.

2.10 Performing MAS ^{2}H NMR measurements

Because of the potential for MAS to improve NMR signal acquisition from deuterated bacterial samples, a limited number of samples were also studied using deuterium MAS NMR. To extract quantitative measurements from the MAS spectra we calculated moments from the MAS spectra using the following procedure:

MAS (**Fig. 3.4**) solid-state spectra were obtained from a 600 MHz magnet, and the spinning speed was 5 and 10 kHz. MAS data was processed with Topspin NMR software with 100 Hz line-broadening. The largest centre peak was taken as the reference at 0 Hz. Frequency referencing was checked with the spinning sidebands to ensure they were exactly at ± 10 kHz and ± 20 kHz. MAS data show two peaks in the centre – one from the lipids and the other presumably from water or some other metabolic product. For this reason, decomposition was needed to measure the areas.

The areas of the MAS peaks were measured by fitting the sidebands and decomposing the centre peaks. I used OriginPro for fitting each sideband.

The peak areas from the fits were used to calculate the M_1, M_2, and Δ_2 parameters with the equations as in:

$$M_n = \omega_r^n \frac{\Sigma_{N=0}^{\infty} N^n A_N}{\Sigma_{N=0}^{\infty} A_N} \quad (3)$$

$$\Delta_2 = \frac{M_2}{1.35 M_1^2} - 1 \quad (4)$$

Where ω_r is the spinning rate ($\omega_r = 2\pi\upsilon_r$, where υ_r is expressed in Hz), and A_N is the area of the Nth sideband.

2.11 Preparing Ramos cells

In order to understand the competitive binding of AMP to the bacterial and mammalian cells, Ramos cells are used in a mixture with *E. coli* cells. Dr. Sherri Christian, Biochemistry Department, MUN, generously provided the Ramos cells (CRL-1596). Ramos cells were grown in RPMI medium (Sigma Aldrich) supplemented with 10% fetal bovine serum (Gibco) and 1% penicillin/streptomycin. The cells were grown in 50 ml RPMI medium in a tissue culture dish for 24 h at 37°C in a CO_2 chamber. The next day, cells were counted by cell counter under the compound microscope and centrifuged at 3000 rpm for 5 minutes. The pellet was then mixed with another 50 ml of RPMI medium and kept growing for another 2 days. After 2 days, cells were counted, centrifuged, and pellets were weighed. We judged that the pellet was not enough to fill the NMR rotor, so the cells were re-cultured for another 2 weeks by changing with new RPMI medium at 2-day intervals. After a total of 2 weeks and 3 days, the cells were centrifuged at 3000

rpm for 5 minutes. After centrifugation, the total number of cells was 2.9×10^9 cells, and these cells were suspended in 50 ml of media.

For the preliminary experiment, in which the objective was to determine whether competitions between the bacteria and Ramos cells for bound AMP would effectively increase, decrease or not affect the effective amount of AMP available to perturb the bacterial membrane. For this purpose, it was sufficient to obtain a rough estimate of the amount of Ramos cell membrane lipids. To obtain that estimate, we took advantage of knowing the diameter of the Ramos cells as measured by microscopy to obtain the cell surface area. To obtain a more precise determination of Ramos cell lipid content, we would need to measure the dry weight of extracted lipid. Because we were initially interested primarily in showing whether Ramos cells bound lipid in amounts that were much more than much less than or similar to the bound quantities by bacteria having comparable amounts of membrane lipid, the rough estimate of Ramos cell membrane lipid provided by this geometric approach was deemed to be sufficient.

Next, the objective for growing Ramos cells was to experiment to assess the extent to which AMP binds to Ramos cells relative to bacteria. We decided to examine how the presence of Ramos cells affects the response of bacteria to MSI-78. To facilitate comparison, we wanted to use a similar peptide-to-lipid ratio in the mixed cell samples as in our study of MSI-78 interacting with bacteria. In order to do this, firstly, we need to know the amount of lipids present in the bacterial sample and Ramos cells.

Starting with the bacterial cells, the molar amount of lipids was calculated from the bacterial dry weight, knowing that lipids comprise 5.2% of the bacterial dry weight [160]. For example, the bacterial sample had an absorbance at 600 nm of 0.658. The absorbance vs bacterial dry weight relationship explained in section 2.4 gave a bacterial dry weight of 82.19 mg. Then, the

approximated lipid mass was 4.27 mg. The LPS mass was not included in this total mass of lipid. The average molecular weight of the lipids is 705 g/mol, which estimated that this sample had 6.0 $\times 10^{-6}$ moles of lipids. To get the number of lipids, we can multiply this number by Avogadro's number, giving us 3.61×10^{18} lipids.

Once we knew the number of lipids in our bacterial sample, we estimated the number of lipids present in the Ramos cells. To do this, we made use of the cell diameter. The Ramos cell diameter was 0.02 mm as measured from a microscope image obtained from Dr. Christian's Lab. From the diameter, we can calculate the surface area of each cell. Then we can look up the surface area per lipid (0.5 nm^2, i.e. 5×10^{-13} in mm^2) [161] to estimate how many lipids are in the cytoplasm of cells. The number of cell membrane lipids can then be obtained from the cell surface area using the typical surface area per lipid in a cell membrane. We are not aware of a specific estimate of surface area per lipid for Ramos cells but the purposes of this preliminary experiment, an estimate based on the reported area of 0.5 nm^2 for the surface area per lipid in eukaryotes was deemed to be sufficient [161]. Based on the measured diameter, the surface area for each cell is 1.25×10^{-3} mm^2. Multiplying the number of cells by the surface area of each cell gives us 2.9×10^9 x $1.25 \times 10^{-3} = 3.62 \times 10^6$ mm^2 total cytoplasmic membrane surface area. To get the number of lipids present, we can divide the total cell surface area by the surface area per lipid and times by two since the membrane is a bilayer, giving us a number of lipids in the cytoplasmic membrane (7.24×10^6 mm^2 / 5×10^{-13} mm^2 = 1.45×10^{19}).

Next, I calculated the amount of peptide needed for the peptide-to-bacterial lipid ratio. The membrane-deuterated *E. coli* treated with 30% MSI-78 is mentioned in Section 2.4. A equivalent amount of 30% MSI-78 was calculated, then weighed and suspended in 30 mL of LB medium. The media + AMP mixture was then used to resuspend the bacterial pellet and Ramos cell pellet,

which was then incubated at room temperature for 20 minutes while undergoing mild shaking on a benchtop shaker. After 20 min, the sample was centrifuged at 5670 × *g* for 20 min at 4°C.

The pellet was weighed, and it was 110 mg. The NMR rotor can only fill up to 40 mg of pellets, so some pellets are left over in the falcon tube. Next, 40 mg of the mixed pellet was transferred into the 3.2 mm NMR rotor, as detailed in Section 2.6.

Preparing deuterated Ramos cells

To deuterate the Ramos cells, I have adapted the protocol from Davis et al. [162], where they studied deuterated erythrocyte membranes. First, Ramos cells were grown for two weeks and 3 days and centrifuged at 3000 rpm. The pellet was incubated with 0.72 ml of 50 mM deuterated palmitic acid in methanol for 15 minutes at room temperature. The mixture was centrifuged at 30000 rpm for 30 minutes [162]. Immediately, the NMR rotor was packed with the pellet.

Chapter 3. Obtaining ^{2}H NMR spectra from *E. coli* by using static and MAS techniques

In this chapter, I present the most reproducible static ^{2}H NMR spectra of membrane-deuterated bacteria to date and explore the MAS NMR of these membrane-deuterated bacteria.

3.1 ^{2}H NMR static spectra of deuterated *E. coli*

The Davis group obtained the first ^{2}H-NMR spectra of membrane-deuterated bacteria in the early 1980s [146]. The first application of whole bacteria ^{2}H NMR to systems affected by the presence of AMPs came in 2012 by Pius et al. [139], where the AMP MSI-78 was shown to impact intact cells' lipid acyl chain order drastically. This work employed a modified strain of *E. coli* which could not metabolize or synthesize the fatty acids and thus incorporated into cell membranes high levels of deuterated acyl chains from deuterated palmitic acid (PA) provided in the growth media [139,156]. These studies employ bacteria that have deuterons in place of hydrogens in the acyl chains of a number of different phospholipid species in their membranes [156,163], in both the inner and outer membranes. Shortly after, the Marcotte group developed a method for membrane-deuterating bacteria without mutants by adding deuterated PA in a complex with dodecyl phosphocholine (DPC) to the growth media [145].

Several factors have been identified in this and subsequent work supporting the acquisition of reproducible ^{2}H NMR spectra from the bacteria. These include adjusting the relative amounts of palmitic and oleic acids for the type of bacteria being grown, being very consistent with the growth and harvesting protocols used, transferring the cells into the NMR spectrometer quickly after growth to understand the viability of the cells, acquiring spectra in sequential blocks to

monitor for changes in spectra over time, and using cell viability assays to assess how many bacteria are alive and metabolizing after their time in the NMR spectrometer [139,156]. With the initial studies of AMPs in whole deuterated bacteria [139,145], it was exciting to see how the ^{2}H experiments traditionally done with AMPs in model lipids could be recapitulated in the context of whole bacteria. Before examining how whole-cell ^{2}H NMR speaks to the membrane perturbing mechanisms of AMPs, this chapter first discusses the information contained in the general ^{2}H NMR spectra of whole-cell membranes.

In order to understand the ^{2}H NMR spectra of *E. coli*, we need to know how we can compare the model lipid ^{2}H NMR spectra to *E. coli* membrane-deuterated samples. ^{2}H NMR spectra of lipids in model membranes or membranes-deuterated bacteria encode information about the lipid acyl chain dynamics at various positions along the chain. The more constrained the motion at a particular carbon–deuteron bond on the acyl chain, the wider the ^{2}H NMR doublet splitting will be for that chain position. Thus, the prominent edges at ±12.5 kHz (**Fig. 1.7**) are dominated by the acyl chain deuterons, closest to the lipid head groups, with the most constrained motions.

On the other hand, deuterons near the methyl end of the lipids, and thus near the center of the bilayer, have much freer motion and thus contribute intensity near the center of the NMR spectra [158]. When a lipid-membrane-perturbing AMP is added to the sample, this is commonly seen as a change in the shape of the NMR spectrum with intensity transferred from the outer edges (that correspond to more constrained motion) to nearer the center of the spectra (that indicate less constrained motion). This likely reflects a peptide-induced increase in dynamic local curvature of bilayer surfaces.

For ^{2}H NMR of *E. coli* deuterated membrane, spectra are thus sensitive to the dynamics of the deuterated lipid acyl chains in the sample, particularly the degree of disorder of each segment

along the chain. Obtaining consistent spectra from intact membrane-deuterated bacteria can be challenging. It is, therefore, important to demonstrate the reproducibility of independently prepared samples before probing how different treatments affect the bacterial spectra. **Fig. 3.1** shows the ^{2}H NMR spectra of three different preparations of untreated membrane-deuterated *E. coli* from independent cell preparations.

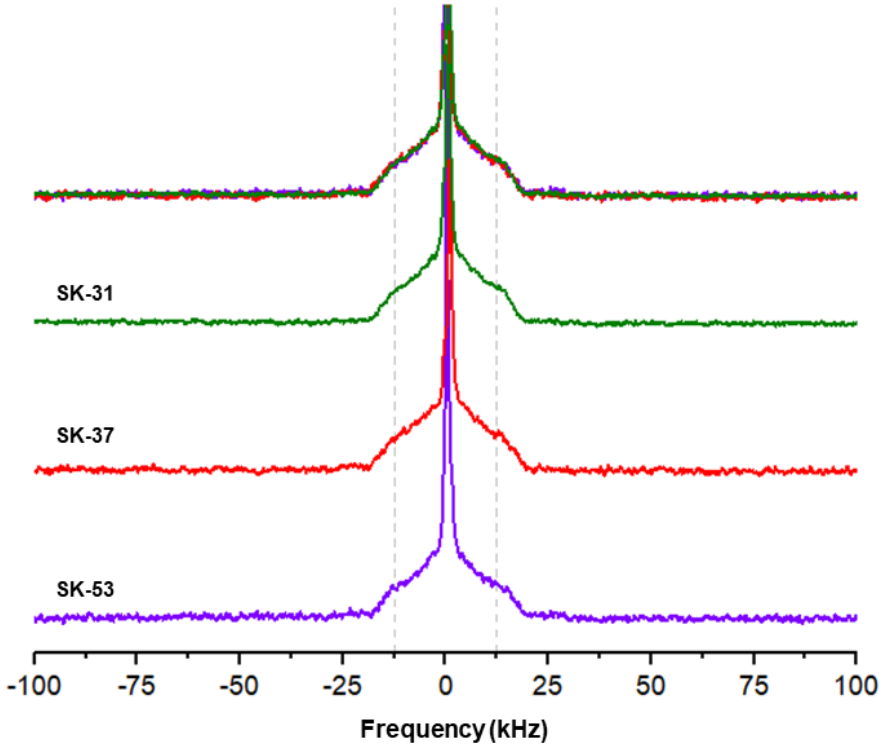

Fig. 3.1: ^{2}H NMR spectra of membrane-deuterated *E. coli* are reproducible. Shown are spectra from 3 independent preparations of bacteria (purple, SK-53; red, SK-37; green, SK-31). Dashed lines at ±12.5 kHz are included to facilitate the comparison of the spectra. Each spectrum is obtained from 110,000 scans recorded over 12 h at 37°C in a 600 MHz NMR spectrometer and normalized by area. The high degree of overlap in the stacked spectra on top shows that the spectra are reproducible.

As seen in the overlay at the top of **Fig. 3.1**, the spectra from the different samples are highly reproducible. All spectra in **Fig. 3.1** display spectral edges at ~ ± 12.5 kHz; these edges correspond to the quadrupole splitting for acyl chain carbon-deuterium bonds near the headgroup [140,146], which have relatively constrained motions compared to the segments closer to the center of the bilayer.

The spectral shapes were quantified by calculating their moments, M_1 and M_2, along with their Δ_2 values (**Fig. 3.1, Table 3.1**). These are shown with averages and standard deviations to indicate the variability between different preparations using the same bacterial strain and protocol with biological replicates. ^{2}H NMR parameters for different bacterial preparations are quite reproducible. As detailed in the Methods section 2.7, M_1 and M_2 relate to the order of the lipid acyl chains, while Δ_2 describes the shape of the spectrum.

Table 3.1: M_1, M_2, and Δ_2 values for all the spectra with averages and standard deviations of *E. coli* are shown in **Fig.3.1**

Experiment	$M_1 \times 10^4 (s^{-1})$	$M_2 \times 10^9 (s^{-2})$	Δ_2
No treatment SK-31	3.66	2.04	0.12
No treatment SK-37	4.40	3.02	0.15
No treatment SK-53	4.23	2.77	0.15
Average ± Standard deviation	4.09 ± 0.38	2.61 ± 0.50	0.14 ± 0.02

3.2 ^{2}H NMR MAS spectra of deuterated *E. coli*

As discussed in Section 1.3.3, ^{2}H solid-state NMR can be time-consuming (it takes 16-17 hours to obtain a good signal-to-noise ratio for this sample), which can be a problem for short-lived bacterial samples. The cell viability experiment presented by Pius et al. showed that the spectral shape obtained from *E. coli* LA8 samples remained unchanged after 12 to 18 hours of

measurements despite a cell viability reduction of approximately 50% [133]. One approach to speed up sample characterization relative to conventional ^{2}H static solid-state NMR experiments is to use magic-angle spinning (MAS).

To understand the information available from MAS spinning ^{2}H NMR experiments, I first tried to extract the information from ^{2}H MAS NMR spectra of model lipid bilayers of DPPC-d_{62} and compare the results with those from the ^{2}H static NMR on DPPC-d_{62} bilayers (**Fig. 3.2**). As discussed in section 2.7, the best way to quantify the ^{2}H NMR spectra is by moment calculation, which can be performed for both static and MAS spectra. In order to establish the reliability of the ^{2}H NMR MAS moments, the information extracted from MAS is compared to the moments from the ^{2}H NMR static samples.

To do this, we calculated the moments from static ^{2}H NMR spectra (**Fig. 3.2A**) and 5 kHz (**Fig. 3.2B**) and 10 kHz MAS (**Fig. 3.2C**) sidebands for DPPC-d_{62} bilayers as described in section 2.10. We found that our static ^{2}H NMR moments for DPPC-d_{62} were identical to the values reported in the literature [159]. M_1 and M_2 for 10 kHz MAS spectra of DPPC-d$_{62}$ compared well to the static moments, with percent differences of 2.7% and 4.6%, respectively. The Δ_2 values for the liquid-crystalline phase should be close to zero, which is consistent with the small value of Δ_2 observed in **Table 3.2**.

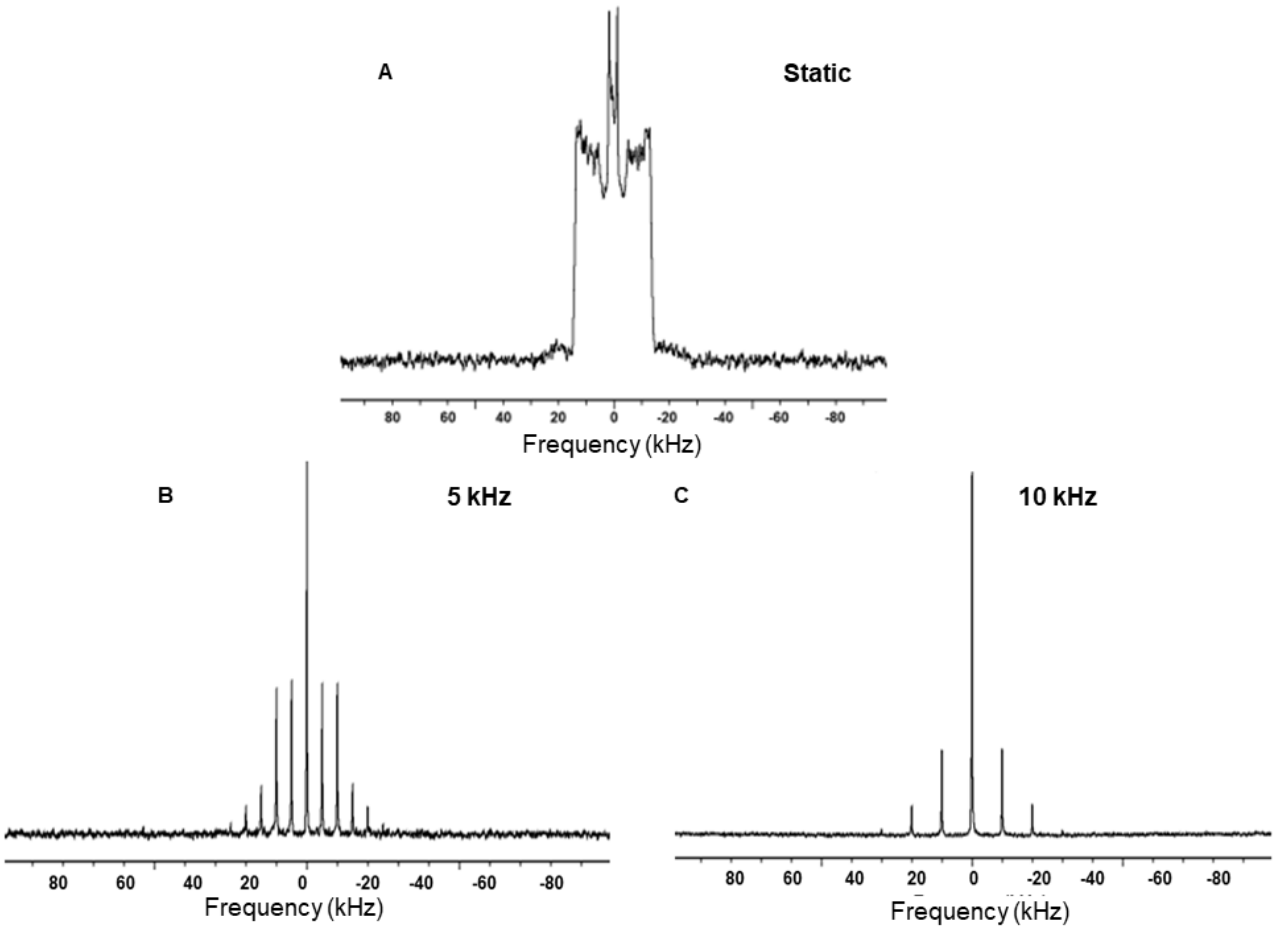

Fig. 3.2: Static ^{2}H NMR and MAS spectra of (5 and 10 kHz) of DPPC-d_{62} at 37°C. **A**: ^{2}H static NMR spectra of DPPC-d_{62}. **B**: ^{2}H MAS spectra of DPPC-d_{62} at a spinning rate of 5 kHz. **C**: ^{2}H MAS spectra of DPPC-d_{62} at a spinning rate of 10 kHz. The static spectra were obtained with 10,000 scans, and MAS spectra were obtained with 1000 scans.

Table 3.2: M_1, M_2, and Δ_2 values for all the spectra with % difference of static and MAS DPPC-d_{62} are shown in **Fig. 3.2**

Experiment	$\boldsymbol{M_1 \times 10^4 (s^{-1})}$	$\boldsymbol{M_2 \times 10^9 (s^{-2})}$	$\boldsymbol{\Delta_2}$
DPPC- d_{62} Static (Davis.et.al [159])	5.32	3.88	0.01
DPPC- d_{62} Static (SK-20)	5.10	3.73	0.06
DPPC- d_{62} MAS 10 kHz (SK-21)	5.24	3.90	0.05
% Difference	2.74%	4.55%	16%

Once the MAS experiment was validated with the model DPPC-d_{62} sample, we moved to apply this approach to ^{2}H MAS NMR spectra of membrane-deuterated *E. coli*. Firstly, we tried to optimize the experiment time. We had been attempting to record the MAS spectra of membrane-deuterated *E. coli* samples in 20 minutes. However, we could not get a good signal-to-noise ratio at this time. Thus, we decided to increase the number of scans and record the spectra for 3 hours, which provided a good signal-to-noise ratio with a good baseline.

Next, we recorded many 5 kHz membrane-deuterated *E. coli* MAS spectra and compared the MAS moments with the static ^{2}H NMR values. A closer look at one of the membrane-deuterated *E. coli* MAS spectra (**Fig. 3.4A**) shows two distinct peaks in the center, one from lipid and another probably from water. One possible way to confirm the assignment of the central peaks might be to use deuterium-depleted water which may reduce the amplitude of any HDO peak. The extra central peak was not seen for the model DPPC-d_{62} MAS (**Fig. 3.2B**) sample, and we suspect it represents the outcome of a metabolic process. In any case, we needed to decompose the membrane-deuterated *E. coli* sample's center peak to get the area under the curve for the lipid. Doing this allowed us to calculate the moments using Equations 3 and 4 in Section 2.10.

We explored suitable spectral analysis software packages to decompose the center peak and fit the sidebands. Several spectral analysis programs (Dmfit, Topspin, Origin Pro) were tried. Dmfit was the first spectral analysis program that I used. Dmfit could fit the MAS sidebands but could not decompose the center peak. So, I moved to another NMR spectral analysis program, Topspin. However, Topspin also could not decompose the two central peaks and didn't give us the area under the curve for each separate peak in the center. Origin pro (2020b) provided the most useful fits to the sidebands and two center peaks (**Fig. 3.3 A and B**).

Once we decided on the suitable spectral analysis software, we started analyzing with 5 kHz MAS spectra of membrane-deuterated *E. coli* (**Fig. 3.4A**). Initially, we recorded many 5 kHz MAS spectra and calculated the resulting spectral moments and compared them with static moments from the same samples. For example, **Table 3.3** shows one of the analyzed 5 kHz MAS moment analysis sets. We found that the moments obtained from MAS with a 5 kHz spinning rate did not match those obtained from the static experiments. Warnet et al. [155] noted line broadening at both 5 kHz and 10 kHz, and they noted it was worse at 5 kHz than at 10 kHz. We likewise found a better agreement between MAS and static moments at 10 kHz than at 5 kHz (**Table 3.3**). Also, we noticed that 5 kHz MAS spectra have 3 sidebands, with the 3rd sideband at 15 kHz having very low intensity, likely increasing the error in moments (**Table 3.3**).

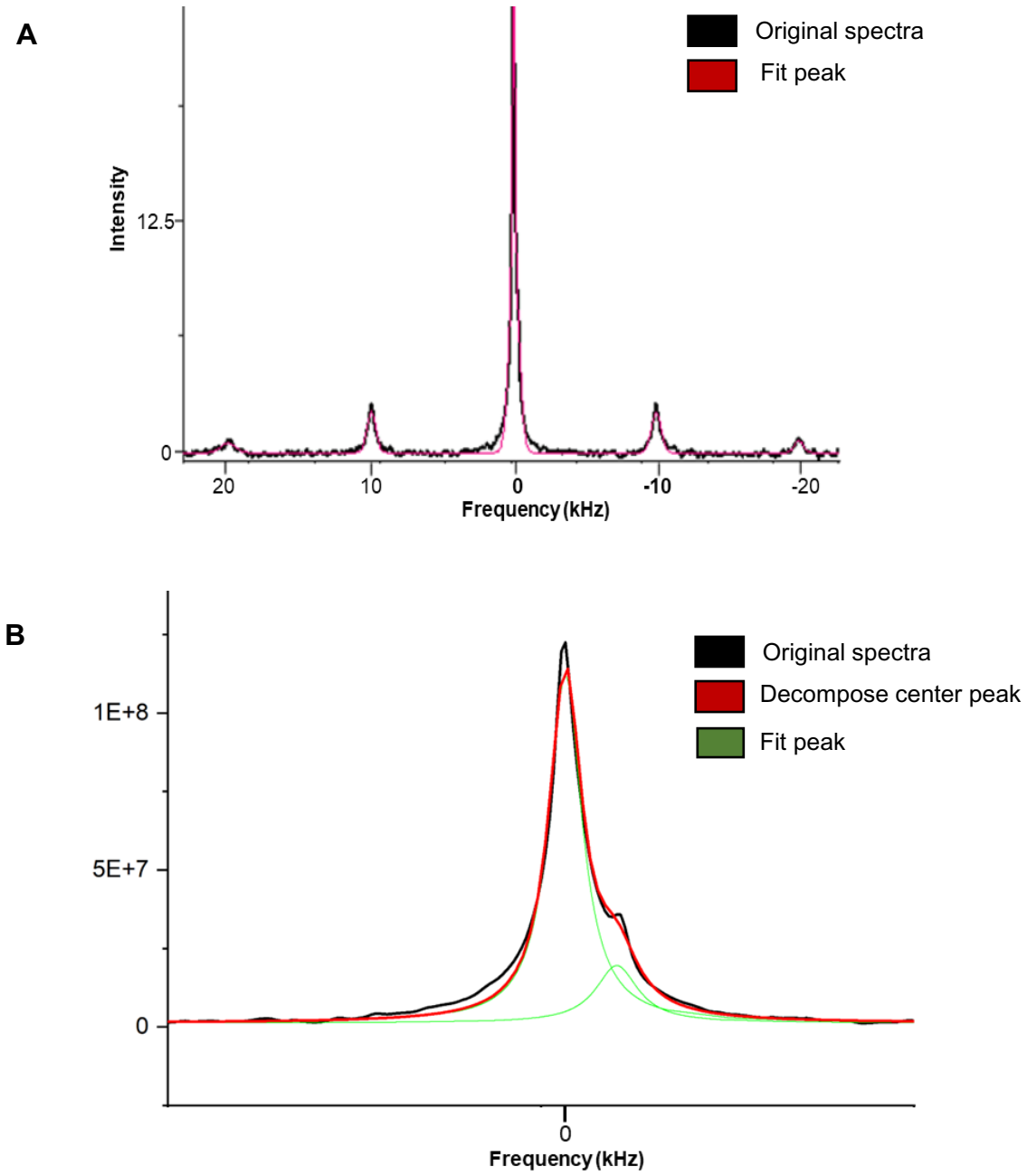

Fig. 3.3: A: Snapshot of sidebands fitting SK-73 MAS spectra **B**: Snapshots decompose the center peak for SK-73 MAS spectra with Origin Pro.

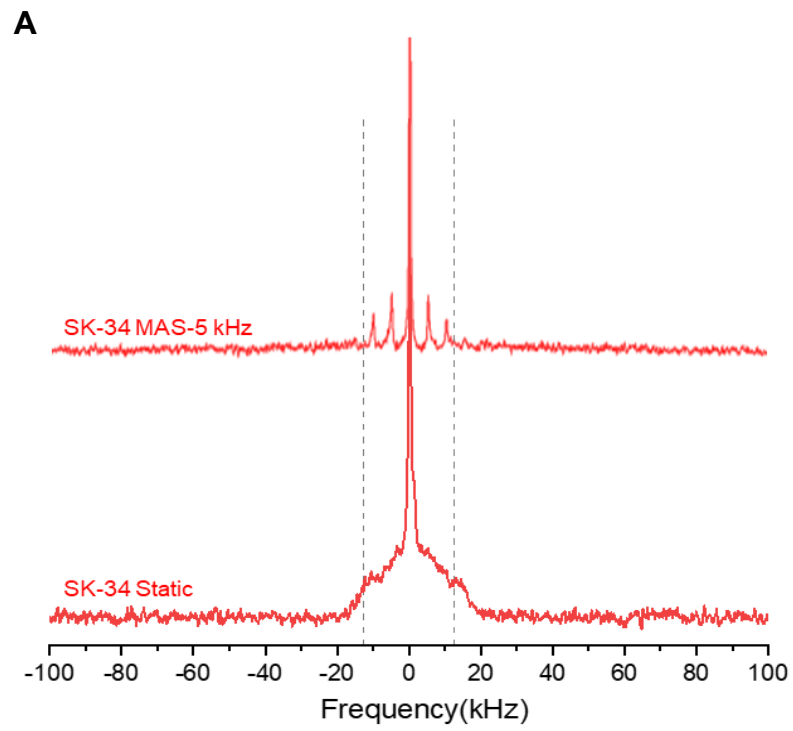
A
SK-34 MAS-5 kHz
SK-34 Static
-100 -80 -60 -40 -20 0 20 40 60 80 100
Frequency(kHz)

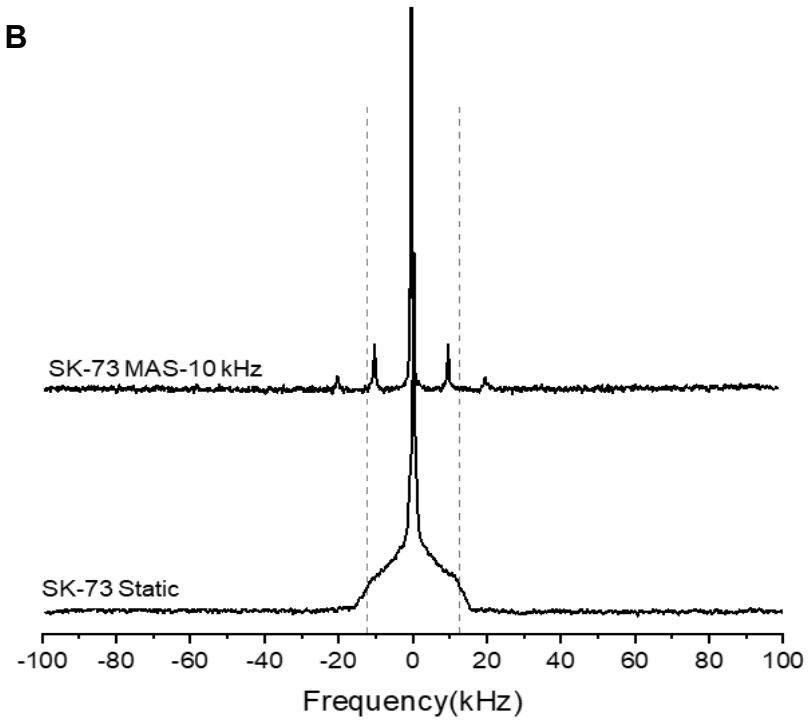
B
SK-73 MAS-10 kHz
SK-73 Static
-100 -80 -60 -40 -20 0 20 40 60 80 100
Frequency(kHz)

Fig. 3.4: A: ^{2}H NMR spectra of membrane-deuterated *E. coli* obtained by MAS ^{2}H NMR (upper) and static ^{2}H NMR (lower). The MAS sample spinning rate is 5 kHz. Dashed lines at ±12.5 kHz are included to facilitate the comparison of the spectra. Each MAS spectrum is obtained from 20,000 scans recorded over 3 h at 37°C in a 600 MHz NMR spectrometer. The static spectrum is obtained from 110,000 scans recorded over 12 h at 37°C in a 600 MHz NMR spectrometer and normalized by area. **B**: ^{2}H NMR spectra of membrane-deuterated *E. coli* obtained by MAS ^{2}H NMR (upper) and static ^{2}H NMR (lower). The MAS sample spinning rate is 10 kHz. Dashed lines at ±12.5 kHz are included to facilitate the comparison of the spectra.

Table 3.3: M_1, M_2 and Δ_2 values for no treatment *E. coli* SK-34 (Static) and SK-34 (5 kHz MAS) spectra. M_1, M_2 and Δ_2 values for no treatment *E. coli* SK-73 (Static) and SK-73 (10 kHz MAS).

Experiment	$M_1 \times 10^4 (s^{-1})$	$M_2 \times 10^9 (s^{-2})$	Δ_2
No treatment SK-34 (Static)	4.17	2.17	0.14
No treatment SK-34 (MAS-5 kHz)	2.04	1.01	0.80
% Difference	51 %	53%	471%
No treatment SK-73 (Static)	4.64	3.34	0.15
No treatment SK-73 (MAS-10 kHz)	4.76	3.97	0.29
% Difference	2.5%	18%	93%

As Warnet et al. [155] noticed, increasing the spinning rate increases the sensitivity, reduces the number of sidebands needed to calculate the spectral moments, and increases the heating by friction. An infinitely fast rotation would result in no spinning sidebands and no possible moment measurement. A compromise must be found, and Warnet's results [155], along with our experiments, showed us that, provided the signal-to-noise was good enough, 10 kHz spinning sidebands could be sufficient to provide MAS spectral moment values that are comparable to those from static experiments for membrane deuterated *E. coli* samples. Private communication with members of the Marcotte group confirmed the suggestion that MAS at a higher spinning rate (10 kHz) was better suited to the determination of spectral moments.

As discussed above, a good signal-to-noise ratio is required to calculate the MAS spectra. Next, I thought that recording the spectra for a longer time and increasing the number of scans would give us better signal-to-noise MAS spectra, as I opened the NMR rotor cap and observed that the sample was not hydrated enough at the end of the experiment to conclude if increasing the acquisition time will provide us with the better signal-to-noise ratio.

Discussion

This chapter first describes the reproducibility of ^{2}H static NMR spectra obtained from membrane-deuterated *E. coli*. All the spectra exhibit characteristics that indicate the presence of a lipid liquid-crystalline phase [146], despite the complexity of the lipid compositions and bacterial cell envelope compositions. All the membrane-deuterated *E. coli* samples produced similar static spectra (**Fig. 3.1**). The M_1, M_2 and Δ_2 values for untreated cells found in this study are within the range observed for untreated *E. coli* in previous studies [139,140]. The average M_1 , M_2, and Δ_2 values were more replicable compare to M_1 , M_2, and Δ_2 values reported in previous work

[139,140]. For Santisteban et al., the average M_1 , M_2, and Δ_2 values with standard deviation for two untreated sample was noted as $M_1 = 9 \pm 1 \times 10^4$ (s^{-1}), M_2, = 17± 3 ×10^9(s^{-2}) and $\Delta_2 = 0.47 \pm 0.07$. For my three untreated was M_1= 4.08 ± 0.38 × 10^4 (s^{-1}), M_2 = 2.61± 0.50 ×10^9(s^{-2}) and Δ_2 = 0.14±0.02.

Another approach discussed in this chapter is using ^{2}H MAS NMR to characterize membrane-deuterated bacteria in whole cells in 3-4 hours. The shorter spectral acquisition time may help reduce the possibility of sample degradation and be better suited to *in vivo* study of biological samples. We have tried to reproduce and validate the MAS approach that has already been published by Warnet et al. [155]. However, we still need to analyze more samples to fully assess the reproducibility of spectral analysis and moment calculation using MAS data. In our 10 kHz MAS spectra analysis, we found that to get the accurate area under the curve from the sidebands, we need to fit each sideband of the MAS samples, and the center peak needs to be decomposed. The signal-to-noise ratio must be very good to get moment calculations that compare the static moments. It is unclear at this point if the information gained from the faster MAS experiments is as complete and useful as that obtained from static experiments. However, we still need to analyze more samples to fully assess the reproducibility of spectral analysis and moment calculation using MAS data.

Chapter 4. Effect on *E. coli* bacteria of gentle destabilization of LPS layer

The main goal of this thesis is to determine if the lipopolysaccharide layer in the Gram-negative cell envelope impacts the interaction between the lipid cell membrane and AMPs and CPPs. In order to do this, we need to first develop a method that can gently destabilize the LPS layer of *E. coli.* We have used EDTA to gently destabilize the LPS layer in the next section of this chapter. I will talk next about how EDTA works on the outer membrane.

EDTA is one of the classical examples of a permeabilizer, sequesters divalent cations contributing to the stability of the outer membrane by providing electrostatic interactions with LPS and proteins [164,165]. In Gram-negative bacteria, EDTA and other metal chelators (e.g., nitrilotriacetic acid, CDTA, and HDTA) induce OM permeabilization [164,166]. **Fig. 4.1** shows a schematic view of EDTA activity on *E. coli* OM.

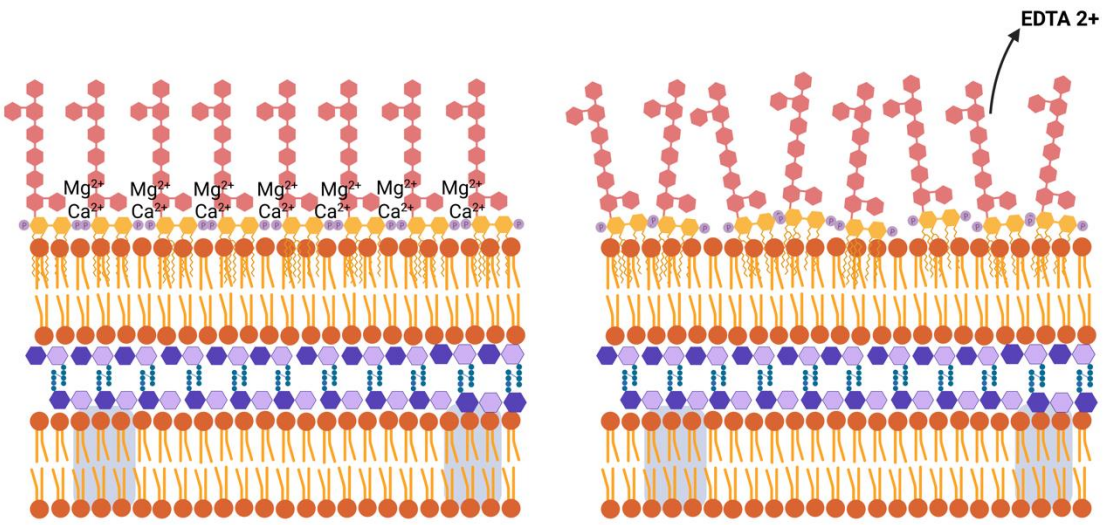

Fig. 4.1: Permeability barrier and destabilization of the LPS layer. The intact outer membrane of Gram-negative bacteria (left-hand side of the figure) functions as a permeability barrier against hydrophobic molecules. Removal of stabilizing divalent cations (Mg^{2+} and Ca^{2+}) from the LPS layer by chelating agents such as EDTA destabilizes the LPS (right-hand side of the figure).

Given the permeabilizing effect of EDTA and the objectives of this work, it was necessary to optimize the EDTA concentration and treatment time that gently destabilized the LPS layer. Vaara et al. reported that bacteria treated for 10 minutes with up to 10 mM EDTA only released 9-11 % of the LPS, and the lowest EDTA concentration where they saw an effect was 2.5 mM [164,165]. Thus, my first experiment was to optimize the EDTA concentration and treatment time to gently destabilize the LPS layer. The goal was to ensure the LPS was modified without killing the cells.

Gram-staining is one of the most widely used staining procedures in bacteriology to observe the change in bacterial cells and shape [167]. I observed the bacteria under the microscope when treated with EDTA at concentrations of 2.5, 3.0, 4.0, 5.0, 6.0, 7.0, 8.0, 9.0 up to 10 mM. Treatment times ranged from 5 to 45 minutes. At the end of each treatment time, I started the Gram staining protocol (section 2.9) and looked at the bacteria under the compound microscope right after completing the staining. There was no change in Gram staining colour and shape until 8.0 mM of EDTA. Interestingly, at 45 minutes of treatment time for 9.0 mM EDTA, I saw a change in Gram staining colour from pink to purple and a change in cell shape from rod-like to spherical. The same difference was observed for 10 mM EDTA concentration.

Because 45 minutes and 9.0 mM EDTA was the shortest time and EDTA concentration combination for which I saw a definite change in Gram-staining. I chose this as my strongest EDTA treatment. I also included 2.5 mM EDTA as Vaara et al., and Leive et al. [164,165] had seen some LPS release at this concentration.

I then went on to do deuterium NMR and flow cytometry for cells treated with these two (2.5 and 9.0 mM) EDTA treatments. Representative spectra shown in **Fig. 4.2A** are of *E. coli* in the absence of EDTA treatment (black), after treatment with 2.5 mM EDTA (blue), and after

treatment with 9.0 mM EDTA (red). Appendix A contains additional spectra from independent samples treated with 2.5 mM EDTA and 9.0 mM EDTA samples **(Fig. A1** and **A2**).

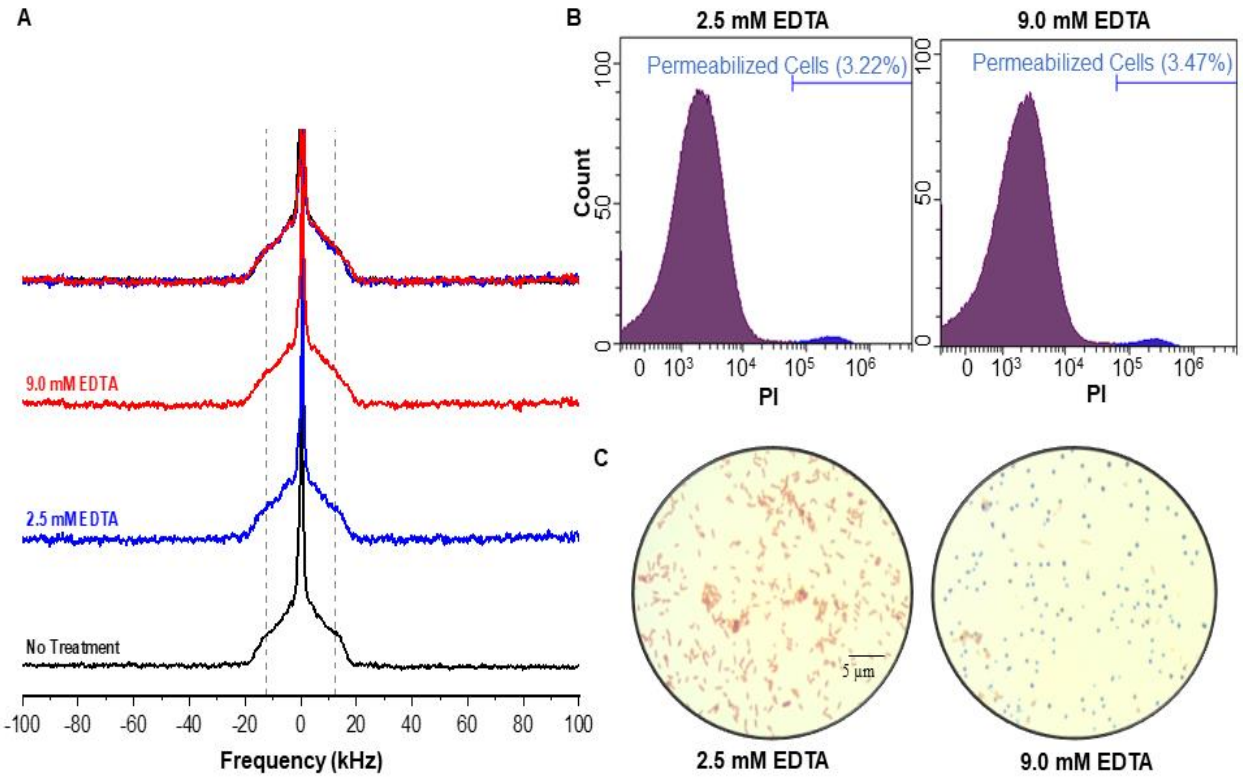

Fig. 4.2: EDTA effects on lipid chain order, cell permeability and cell wall staining. **A**: ^{2}H NMR spectra of deuterium-enriched *E. coli* that are untreated (black, SK-53); treated with 2.5 mM EDTA (blue, SK-38) and treated with 9.0 mM EDTA (red, SK-39). Dashed lines at ±12.5 kHz are included to facilitate the comparison of the spectra. Each spectrum is obtained from 110,000 scans recorded over 12 h at 37°C in a 600 MHz NMR spectrometer and normalized by area. The top panel shows the overlaid spectra. Additional spectra obtained from samples with EDTA added are shown in Fig. A1 and A2. **B**: Cell count versus PI fluorescence intensity for *E. coli* cells treated with 2.5 mM and 9.0 mM EDTA as probed by flow cytometry with PI. The small count numbers for high PI fluorescence intensity show that PI cannot penetrate 2.5 mM and 9.0 mM EDTA-treated cells. **C**: Microscope images of cells treated with 9.0 mM EDTA and 2.5 mM EDTA after

Gram staining. These show that 9.0 mM EDTA (but not 2.5 mM EDTA) treatment drastically changes bacterial shape and susceptibility to Gram staining.

The NMR spectra of the EDTA-treated cells are very similar to those of untreated cells. NMR observations were complemented by flow cytometry (**Fig. 4.2B**) and light microscopy of Gram-stained cells (**Fig. 4.2C**) in order to assess the effects of LPS destabilization on membrane permeability. Flow cytometry showed that for bacteria treated with either 2.5 mM or 9.0 mM EDTA, only ~3% of the cells became PI-permeable.

In contrast to the flow cytometry observations, Gram-staining did show a clear difference between the effects of the two EDTA treatments (**Fig. 4.2C**). Once the cells are treated with different concentrations of EDTA for 45 minutes, the cells are washed and fixed on glass slides to observe under a compound microscope by Gram-stain. Treatment with 9.0 mM EDTA led to the destabilization of the LPS layer, as seen by the change in Gram staining colour from pink to purple and a change in cell shape from rod-like to spherical. Taking the results of flow cytometry and microscopy together, it appears that treatment with 9.0 mM EDTA disrupts LPS without killing the cells.

Statistics carried out with the Δ_2 values from the three control spectra, and three 9.0 mM EDTA spectra indicate a p-value of 0.09 for the comparison, suggesting there may be a small change in the distribution of lipid acyl chain order along the acyl chain following EDTA treatment. Nevertheless, it is striking that while EDTA treatment leads to drastic changes in overall cell shape (**Fig. 4.1C**), there is effectively little to no observable change in the ^{2}H NMR spectra that characterize the orientational order of bacterial lipid-acyl chains.

In summary, LPS layer destabilization by the removal of divalent cations affected the ability of the bacterial cell to maintain their rod-like shapes. Destabilizing the LPS layer seems to

affect the cell wall over length scales that affect cell shape, but that membrane organization, on a much smaller length scale, is not significantly affected.

Table 4.1: M_1, M_2, and Δ_2 values for all the spectra with averages and standard deviations. P-values for ANOVA comparison of selected treatment groups are also included. *E. coli* was treated with different concentrations of EDTA, as shown in **Fig. 4.2**.

Experiment	$\boldsymbol{M_1}$**× 10^4(s^{-1})**	$\boldsymbol{M_2}$**× 10^9(s^{-2})**	$\boldsymbol{\Delta_2}$
No treatment SK-31	3.66	2.04	0.12
No treatment SK-37	4.40	3.02	0.15
No treatment SK-53	4.23	2.77	0.15
Average ± Standard deviation	4.09 ± 0.38	2.61 ± 0.50	0.14 ± 0.02
2.5 mM EDTA SK-38	4.47	3.02	0.11
2.5 mM EDTA SK-40	4.32	2.84	0.12
Average ± Standard deviation	4.39 ± 0.11	2.61 ± 0.13	0.11 ± 0.01
9.0 mM EDTA SK-39	4.04	2.64	0.19
9.0 mM EDTA SK-41	4.61	3.33	0.15
9.0 mM EDTA SK-66	4.4	3.22	0.19
Average ± Standard deviation	4.35 ± 0.29	2.73 ± 0.36	0.18 ± 0.02
p-value (no treatment vs. 9.0 mM EDTA)	*0.40*	*0.28*	*0.09*

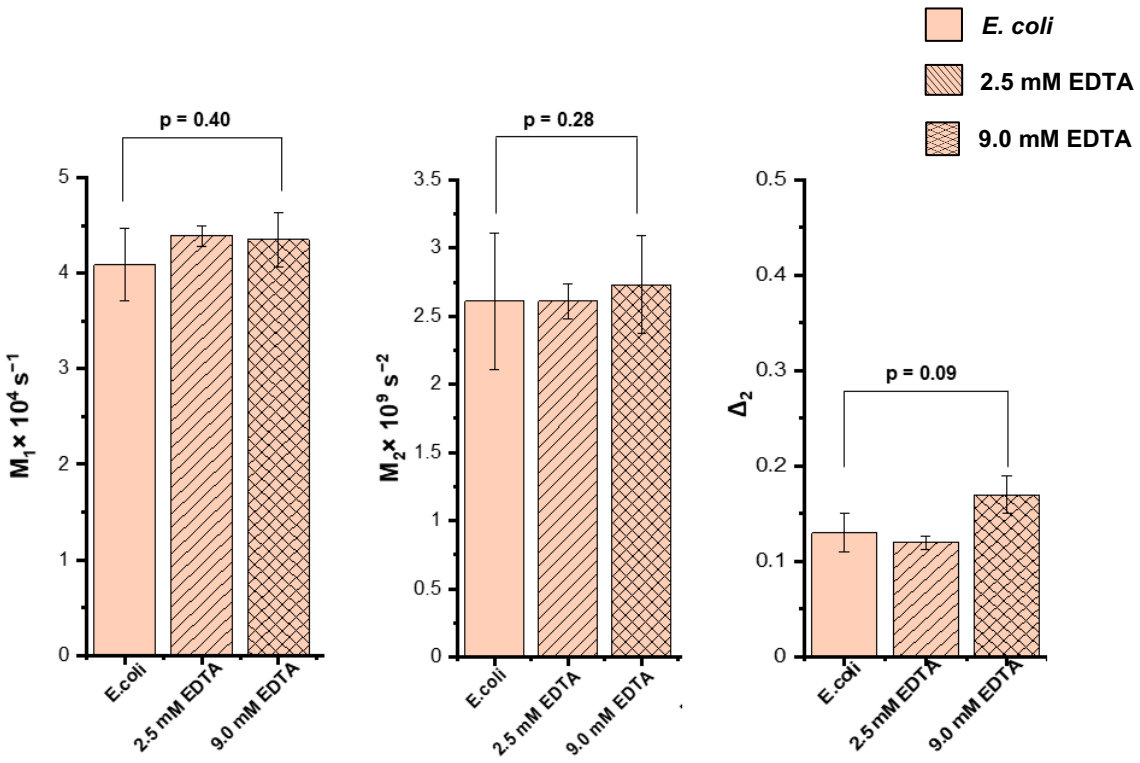

Fig. 4.3: M_1, M_2, and Δ_2 values for all the spectra with averages and standard deviations. p-values for ANOVA single-factor comparison of treatment groups are indicated for all comparisons.

Discussion

In this chapter, I show that destabilizing the LPS layer has no substantial impact on the ^{2}H NMR spectra or membrane integrity. Spectra for bacteria treated with EDTA at both concentrations (2.5 mM and 9.0 mM) have similar characteristics to untreated bacteria, including edges at ±12.5 kHz, indicating that the lipid organization in the membrane remains similar to that in untreated bacteria. The lack of observable difference between the spectra from the EDTA-treated and untreated samples indicates that the membrane organization is not affected by any indirect effects from the disruption of the carbohydrate part of the LPS, which includes other part of OM and does not seem to disrupt chain order. Comparing membrane permeabilization effects of the 2.5 and 9.0 mM EDTA concentrations, a similar observation was noticed for the membrane permeabilization effects.

Given that the Gram-staining shows the cells are strongly affected by 9.0 mM EDTA (**Fig. 4.2C)**, it is helpful to analyze further the NMR spectra (**Fig. 4.1A)** that, from inspection, appear to show little difference between untreated and EDTA-treated cells.

Notably, Δ_2 is a measure of the overall shape in the spectrum, i.e., the distribution of splittings. As reported in earlier studies, and also, observed below in this study, the most significant changes in Δ_2 occur when bacteria are treated with AMP [139,140,145]. Looking at **Fig. 4.1A** and **Table 4.1**, interestingly, it is seen that the Δ_2 parameters calculated from the spectra (**Table 4.1 and Fig. 4.3**) increase slightly with 9.0 mM EDTA treatment. `

Chapter 5. Effect of LPS destabilization on bacterial membrane susceptibility to AMP-induced disruption

After assessing the gentle destabilization effect of the LPS layer by EDTA treatment, the next stage of this project was to evaluate the impact of LPS layer destabilization on the sensitivity of the bacterial cell envelope to treatment with AMP MSI-78.

Since AMPs must traverse the carbohydrates of the LPS layer before reaching the lipid acyl chains, it was important to find out if LPS disruption would sensitize the cells to AMP-induced acyl chain disruption. To address this question, we used ^{2}H NMR spectroscopy and flow cytometry to examine the effects of treating *E. coli* with EDTA to destabilize the LPS layer prior to treatment using 30% MSI-78 and then compared the results with the effects of AMP treatment alone. **Fig. 5.1** and **5.2** compare the effects of 30% MSI-78 on ^{2}H NMR spectra and flow cytometry of *E. coli* with and without prior treatment using 2.5 mM EDTA and 9.0 mM EDTA.

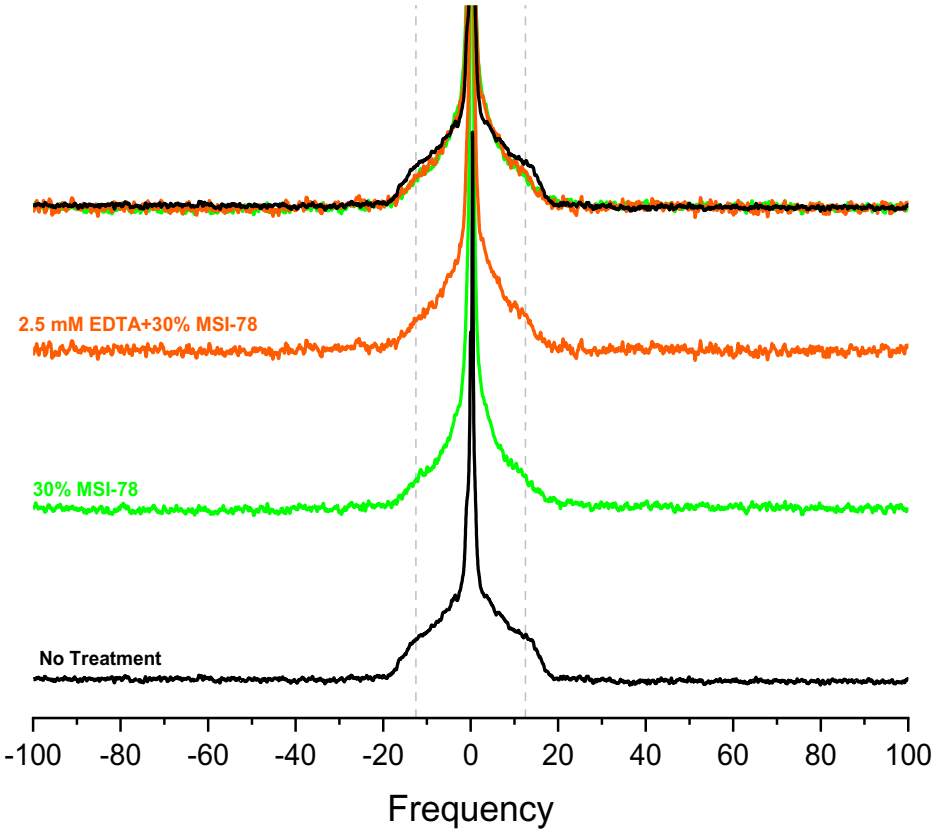

Fig. 5.1: ^{2}H NMR spectra of deuterium-enriched *E. coli* treated with 2.5 mM EDTA+30% MSI-78 that are untreated (black, SK-53); after treatment with 30% MSI-78 (green, SK-47) (% by dry weight of bacteria), and after treatment with 2.5 mM EDTA followed by 30% MSI-78 (orange, SK-49). The top panel shows the overlaid spectra. Dashed lines at ~ ±12.5 kHz are shown to facilitate the comparison of the spectra. Each spectrum is obtained from 110,000 scans recorded over 12 h at 37°C in a 600 MHz NMR spectrometer and normalized by area. Only selected spectra are shown. Additional spectra are shown in Figs. **A4** and **A5**.

Fig. 5.1 showed no observable difference between the ^{2}H NMR spectra obtained from the sample treated with 30% MSI-78 and the sample treated with 2.5 mM EDTA followed by 30% MSI-78 treatment. Representative ^{2}H NMR spectra shown in **Fig. 5.1** include the spectra for *E. coli* with no treatment, *E. coli* treated with MSI-78 only, and cells treated with 2.5 mM EDTA followed by MSI-78. Appendix A contains additional spectra from independent samples treated with 30% MSI-78 (**Fig. A3**) and samples with 2.5 mM EDTA and 30% MSI-78 (**Fig. A4**).

Fig. 5.2 compares the effects of 30% MSI-78 on ^{2}H NMR spectra and flow cytometry of *E. coli* with and without prior treatment using 9.0 mM EDTA. Flow cytometry (**Fig. 5.2B**) showed that treatment with 30% MSI-78 alone permeabilized ~68% of cells while treatment with 9.0 mM EDTA followed by 30% MSI-78 permeabilized 92% of cells, i.e., more permeabilization than for cells treated with MSI-78 alone. The flow cytometry experiments were repeated with two independently prepared samples and gave similar results (data not shown). Thus, as judged by cell permeabilization, disruption of LPS does sensitize the cells to MSI-78. Additionally, 9.0 mM EDTA+MSI-78 shows an increase in the side scatter spread of the cells (Appendix Fig. **B2**), suggesting an increase in intracellular granularity.

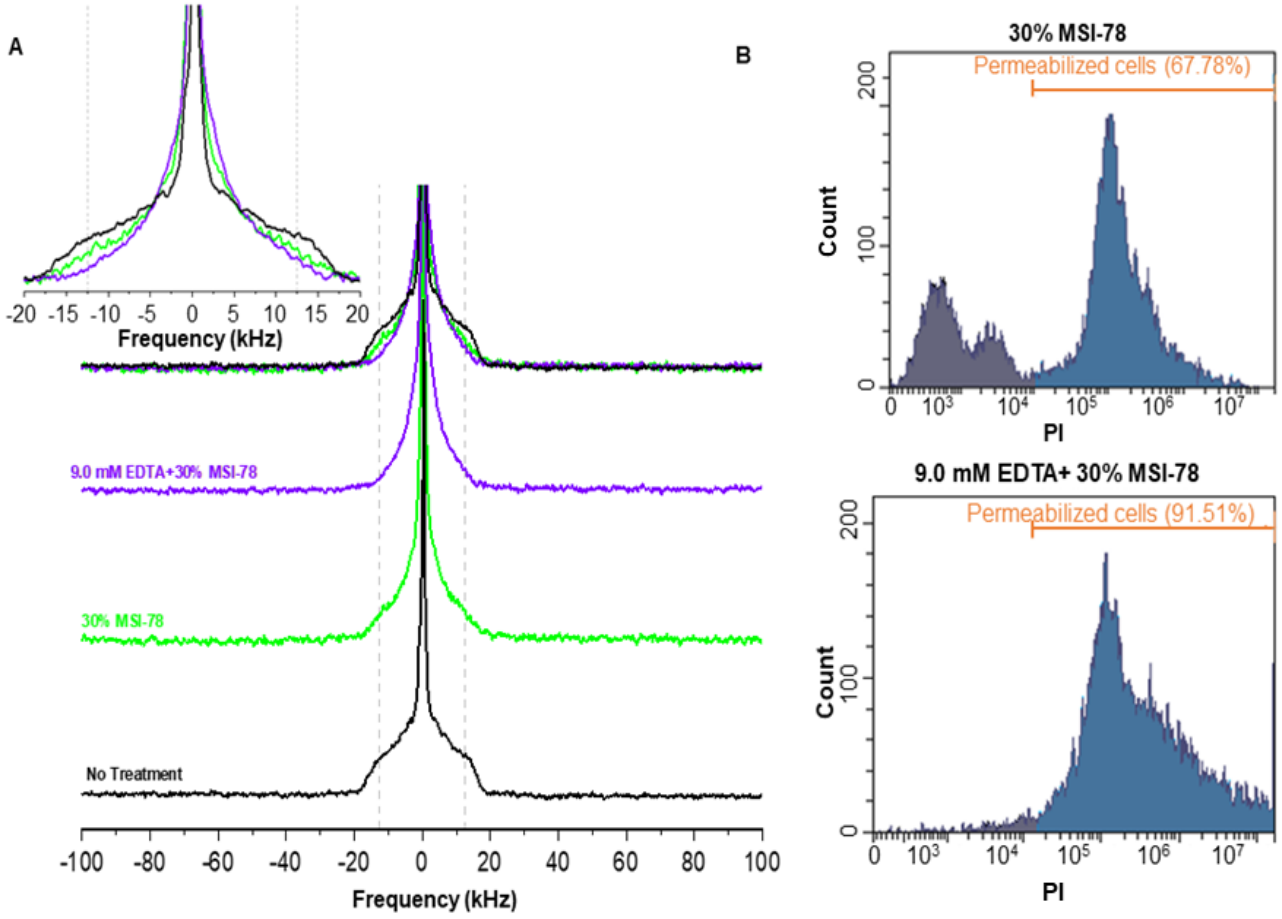

Fig. 5.2: LPS pre-treatment increases the susceptibility of bacteria to AMP as judged by ^{2}H NMR and flow cytometry. **A**: ^{2}H NMR spectra of deuterium-enriched *E. coli* that are untreated (black, SK-53); after treatment with 30% MSI-78 (green, SK-47) (% by dry weight of bacteria), and after treatment with 9.0 mM EDTA followed by 30% MSI-78 (purple, SK-49). The top panel shows the overlaid spectra. Dashed lines at ~ ±12.5 kHz are shown to facilitate the comparison of the spectra. Each spectrum is obtained from 110,000 scans recorded over 12 h at 37°C in a 600 MHz NMR spectrometer and normalized by area. Only selected spectra are shown. Additional spectra are shown in Figs A4 and A5. **B:** Cell count vs. PI fluorescence intensity for treated *E. coli* cells treated with 30% MSI-78 alone and 9.0 mM EDTA+MSI-78, as probed by flow cytometry with PI.

Unlike the flow cytometry results, which indirectly report on the state of the membrane by indicating if the dye can reach DNA inside the cells or not, ^{2}H NMR spectra report directly on the lipid acyl chains. Representative ^{2}H NMR spectra shown in **Fig. 5.2A** include the spectra for *E. coli* with no treatment, *E. coli* treated with MSI-78 only, and cells treated with 9.0 mM EDTA followed by MSI-78. Appendix A contains additional spectra of independent samples prepared with 30% MSI-78 and 9.0 mM EDTA and 30% MSI-78 (Figs. **A3, A4** and **A5)**.

Firstly, we confirm that the effect on the bacterial membrane of 30% MSI-78 alone is similar to that of previous studies [139,140]. Specifically, the ^{2}H NMR observations shown in **Fig. 5.2A** demonstrate that MSI-78 induced substantial changes in the *E. coli* spectra, including decreased intensity at the ~ ± 12.5 edges and increased intensity at smaller splittings (~<5 kHz). These ^{2}H NMR observations are consistent with an MSI-78-induced decrease in bacterial membrane lipid acyl chain orientational order, i.e., an increased angular amplitude of lipid chain motions.

To address how pre-treatment with EDTA to destabilize the LPS affects the bacteria's sensitivity to AMP-induced lipid-acyl chain disruption, we next compare the spectra for cells treated with MSI-78 alone to the spectra of cells pretreated with 9.0 mM EDTA before AMP treatment. Compared to treatment with MSI-78 alone, spectra of cells treated with EDTA before MSI-78 displayed less intensity at ~ ± 12.5 kHz and substantially more intensity in the ~ ± 2.5 kHz range of the spectrum **(Fig. 5.2A inset)**. This observation is consistent with there being more AMP-induced lipid acyl chain disruption in LPS-destabilized cells. Hence, LPS does appear to provide some protection to the cells from membrane disruption by MSI-78.

To compare, more quantitatively, the effects of the AMP alone with those of EDTA-pre treatment + MSI-78, we performed a statistical analysis of M_1, M_2, and Δ_2 values. These

comparisons are shown in **Table 5.1** and **Fig. 5.3**. It is first noted that treating with 9.0 mM EDTA alone has no statistically significant effect on the average M_1, although M_1 did tend to increase from 4.09×10^4 s^{-1} for untreated cells to 4.35×10^4 s^{-1} for cells treated with 9.0 mM EDTA (p-value 0.40). Interestingly, treatment with EDTA has the opposite effect on M_1 to that of treatment with AMP alone; $M_1$was significantly (p-value 0.05) smaller for the spectra of cells treated with AMP (3.44×10^4 s^{-1}) than for the spectra of untreated cells. This observation is in keeping with previous studies (e.g., [139,140]) that noted that treatment with AMP leads to a decrease in average chain orientational order in model lipids. As expected from visual inspection of the spectra in **Fig. 5.2A**, treatment with 9.0 mM EDTA and 30% AMP together results in M_1 reduced even more than for cells treated with AMP alone, 3.44×10^4 s^{-1} and 3.12×10^4 $s^{-1,}$ respectively, with a (p-value of 0.07).

Table 5.1: M_1, M_2, and Δ_2 values for all the spectra shown in **Fig. 5.1 and 5.2A** with averages and standard deviations. p-values for ANOVA comparison of selected treatment groups are also included. SK-XX are the sample numbers, and referenced spectra not shown in the main text are shown in Appendix A.

Experiment	$M_1 \times 10^4 (s^{-1})$	$M_2 \times 10^9 (s^{-2})$	Δ_2
30% MSI-78 SK-47	3.60	2.26	0.30
30% MSI-78 SK-57	3.29	2.05	0.36
30% MSI-78 SK-64	3.44	2.11	0.32
Average ± Standard deviation	3.44 ± 0.16	2.14 ± 0.11	0.33 ± 0.03
p-value (no treatment vs. MSI-78)	*0.05*	*0.19*	*0.0008*
2.5 mM EDTA+30% MSI-78 SK-49	3.23	2.43	0.32
2.5 mM EDTA+30% MSI-78 SK-54	3.73	2.52	0.34
Average ± Standard deviation	3.48 ± 0.35	2.45 ± 0.06	0.33 ± 0.01
9.0 mM EDTA+30% MSI-78 SK-55	3.16	1.86	0.38
9.0 mM EDTA+30% MSI-78 SK-67	3.09	1.82	0.41
Average ± Standard deviation	3.12 ± 0.05	1.84 ± 0.03	0.39 ± 0.02
p-value (9.0 mM EDTA alone vs 9.0 mM EDTA+30% MSI-78)	*0.01*	*0.03*	*0.002*
p-value (30% MSI-78 vs. 9.0 mM EDTA+ 30% MSI-78)	*0.07*	*0.02*	*0.07*

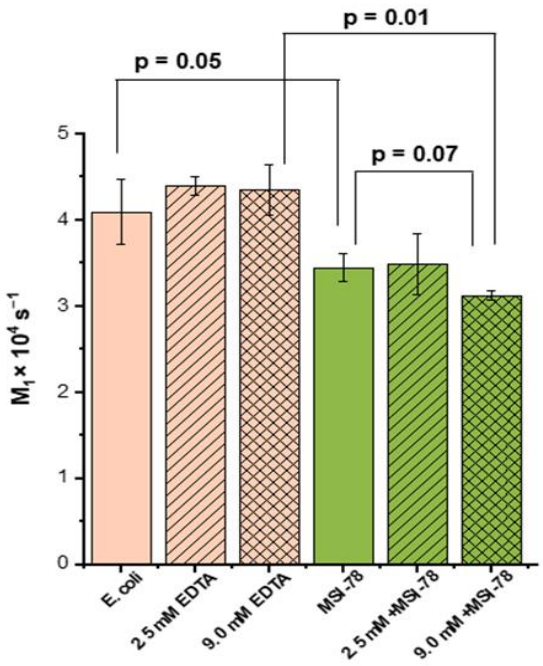
p = 0.01
p = 0.05
p = 0.07
$M_1 \times 10^4\ s^{-1}$
0
1
2
3
4
5
E. coli
2.5 mM EDTA
9.0 mM EDTA
MSI-78
2.5 mM +MSI-78
9.0 mM +MSI-78

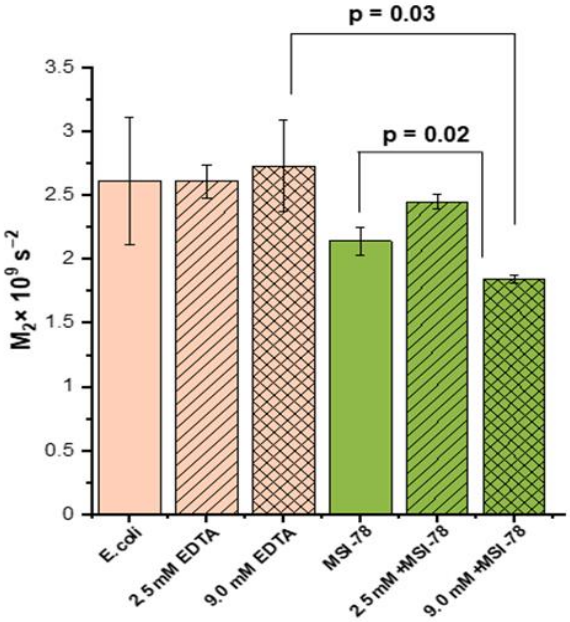
p = 0.03
p = 0.02
$M_2 \times 10^9\ s^{-2}$
0
0.5
1
1.5
2
2.5
3
3.5
E. coli
2.5 mM EDTA
9.0 mM EDTA
MSI-78
2.5 mM +MSI-78
9.0 mM +MSI-78

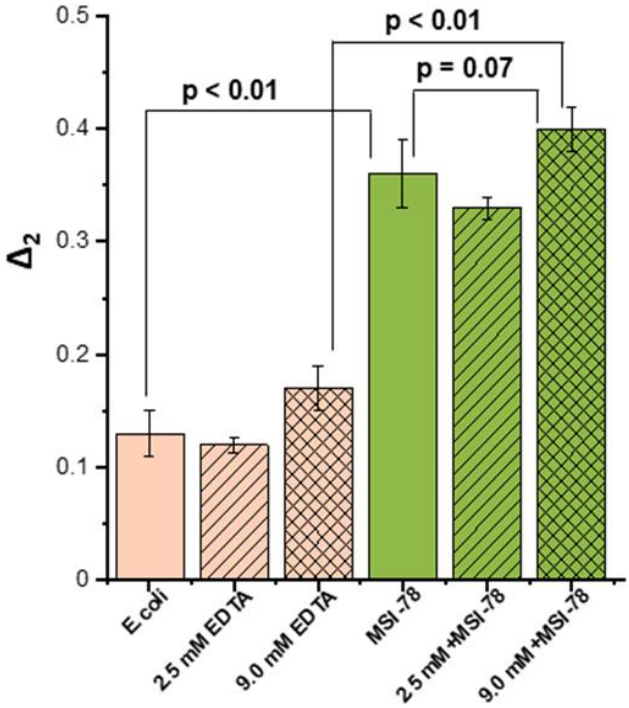
p < 0.01
p < 0.01
p = 0.07
Δ_2
0
0.1
0.2
0.3
0.4
0.5
E. coli
2.5 mM EDTA
9.0 mM EDTA
MSI-78
2.5 mM +MSI-78
9.0 mM +MSI-78

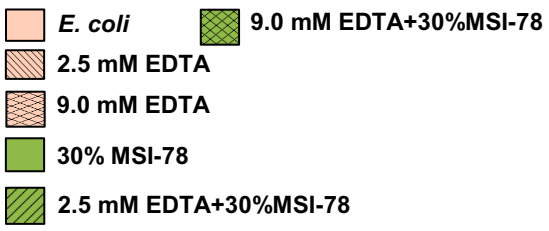
E. coli
2.5 mM EDTA
9.0 mM EDTA
30% MSI-78
2.5 mM EDTA+30%MSI-78
9.0 mM EDTA+30%MSI-78

Fig. 5.3: M_1, M_2, and Δ_2 values for all the spectra with averages and standard deviations. p-values for ANOVA single-factor comparison of treatment groups are indicated for all comparisons.

Table 5.1 shows the calculated values of the first and second moments, M_1 and M_2, along with the Δ_2 values for all the spectra shown in **Fig.** 4.3. The moment values M_1 and M_2 and Δ_2 of EDTA treated and EDTA treated with 30% MSI-78 samples were averaged and the standard deviation was reported to indicate the variability between different samples. As noted, the standard error for Δ_2 value is small since. Taking that in account Δ_2 is a function with M_2 over M_1 squared so M_2 and M_1 values are correlated so that the ratio does not vary as much as the individual values.

Similar to the observations for M_1, treatment with 9.0 mM EDTA alone does not make a significant change in the observed value of M_2. The average M_2 increases slightly from 2.61 x10^9 s^{-2} for the spectra of untreated cells to 2.73 x10^9 s^{-2} for the spectra of cells treated with 9.0 mM EDTA (p-value 0.28). Treatment with AMP moves M_2 in the opposite direction to that seen for treatment with EDTA, i.e., to a lower value (2.14 x10^9 s^{-2}), although the difference between no treatment and AMP treatment is not statistically significant (p-value 0.19). With 9.0 mM EDTA followed by MSI-78 treatment, the average value of M_2 decreased even more to 1.84 x10^9 s^{-2}. This value of M_2 was significantly different from both the M_2 values for cells treated with MSI-78 alone (p-value 0.03) and cells treated with EDTA alone (p-value 0.02).

It is important to note that while treatment with EDTA tends to increase the spectral moments slightly, AMP does the opposite. With the joint EDTA + AMP treatment, the spectral moments decrease even more than for AMP alone, implying a synergistic effect exists between the two treatments. That is to say, the EDTA followed by AMP treatment decreases acyl chain orientational order more than the sum of the effects of EDTA or AMP applied separately. For M_1,

the comparison between AMP alone and EDTA followed by AMP is on the edge of statistical significance with a p-value of 0.07, while the M_2 comparison is more significant, with a p-value of 0.02. Importantly, since EDTA and AMP alone have opposite effects on M_1 and M_2, the effects of AMP and EDTA are not additive rather, the effect of EDTA treatment on AMP-induced reduction in M_1 and M_2 is synergistic.

Moving to the Δ_2 values, which reflect the spectral shape, the average Δ_2 value increases significantly from 0.14 for untreated cells to 0.33 for AMP-treated cells (p-value 0.0008). With the 9.0 mM EDTA followed by MSI-78 treatment, Δ_2 values increased slightly more to 0.39 (p-value for AMP alone vs EDTA+MSI-78 is 0.07). While the effects of EDTA and MSI-78 on average chain order, as indicated by M_1, and M_2, were synergistic, the effects on Δ_2 were more additive in nature, i.e., both EDTA and MSI-78 tended to increase the relative mean squared deviation of the quadrupolar splittings, consistent with both treatments altering the distribution of orientational order parameters along the acyl chains.

At this point, it is helpful to examine more closely what parameter Δ_2 means. AMPs tend to decrease spectral intensity at splittings corresponding to the plateau region of the order parameter profile, i.e. close to the lipid headgroups of model membranes [157]. Δ_2 reflects the shape of the distribution in ^{2}H splittings [146]. Since in unperturbed membranes, a large fraction of the observed splittings come from the plateau region and have similar values, the distribution of splittings peaked near the upper range of the observed splittings, and Δ_2 is relatively small. In the presence of AMP, the distribution of splittings becomes flattened (the order parameter profile becomes more linear) and Δ_2 increases. In a typical liquid crystalline bilayer, packing constraints near the headgroup end of the acyl chains lead to the persistence of higher orientational order through the plateau region segments [159]. Interaction with AMPs appears to relax these

constraints in a way that removes the prominent spectral edges characteristic of the plateau in the orientational order parameter. The resulting spectrum appears to reflect a more uniform change in orientational order parameters with position along the acyl chains. This probably reflects an AMP-induced increase in the amplitude of fluctuations in bacterial membrane bilayer shape and thickness, likely due to effects on lipid headgroup packing. As suggested above, this, in turn, may reflect a peptide-induced increase in local bending of bilayer surfaces.

Discussion

The findings in this chapter directly relate to a well-known open discussion in the AMP area of research about whether LPS promotes the accumulation of the AMPs on the cell membrane or instead entraps the AMPs, thus preventing them from reaching the lipid bilayer. A comparison of previous *in vitro* and *in vivo* studies for two AMPs, melittin and omiganan, indicated that the cell-bound AMP:L ratio was 2.3 to 9.2 times higher than the threshold to see effects in liposomes [107]. In a more direct approach, the Stella group [108] showed that, at the minimum bactericidal concentration (MBC), 10^7 fluorescently labelled AMP molecules are bound to each cell. This corresponds to an AMP:L ratio of ~1:3 to 5:1. This study by the Stella group suggests that AMPs may bind to molecules present in bacteria but not in liposomes. For Gram-negative bacteria, several studies indicate that AMPs interact with the LPS layer of the bacterial cell envelopes. Experiments on *E. coli* mutants where the LPS layer was absent increased the effectiveness of seven different AMPs, indicating that the LPS layer contributes some protection to the bacteria from AMP [109].

I have shown that gently destabilizing the LPS layer of *E. coli* bacteria has given a little more access for MSI-78 to reach the lipid bilayer. The presence of an effect of LPS destabilization

on MSI-78-induced changes observable directly in the ^{2}H NMR spectra is also supported by Δ_2 values calculated from the spectra (**Table 5.1**).

In summary, M_1, M_2, and Δ_2 values for samples treated with MSI-78 alone vs. samples pre-treated with EDTA followed by MSI-78 demonstrating that LPS helps protect bacteria from lipid acyl chain disruption by MSI-78.

Chapter 6. Comparison of cell-penetrating peptide's effect with antimicrobial peptides

In this chapter, we compare the lipid acyl chain disorder induced by MSI-78, which permeabilizes cells to a fluorescent dye, with the effect of a cell-penetrating peptide (CPP) (TP2). This peptide has been shown to cross the membrane without making it permeable to dye [135].

Our flow cytometry observations confirmed Wimley et al.'s findings [135] that bacteria were not dye-permeable after treatment with TP2. So, we were quite surprised to find that TP2's effects on membrane lipid orientational order, as indicated by ^{2}H-NMR observations, were similar to those of MSI-78, which does make cells permeable to the dye.

Representative ^{2}H NMR spectra shown in **Fig. 6.1A** are for membrane-deuterated *E. coli* with no treatment and *E. coli* treated with 30 % TP2 alone. **Fig. 6.1B** compares spectra for bacteria treated with TP2 alone and for bacteria treated with 9.0 mM EDTA followed by 30% TP2. Appendix Fig. **A6** contains additional spectra from independent samples treated with 30% TP2 and treated with 9.0 mM EDTA followed by 30% TP2. While the NMR spectra show not much difference between the effects of TP2 and MSI-78 on lipid chain order, flow cytometry confirms that, unlike MSI-78, TP2 does not permeabilize the cells to PI (**Fig. 6.1C**).

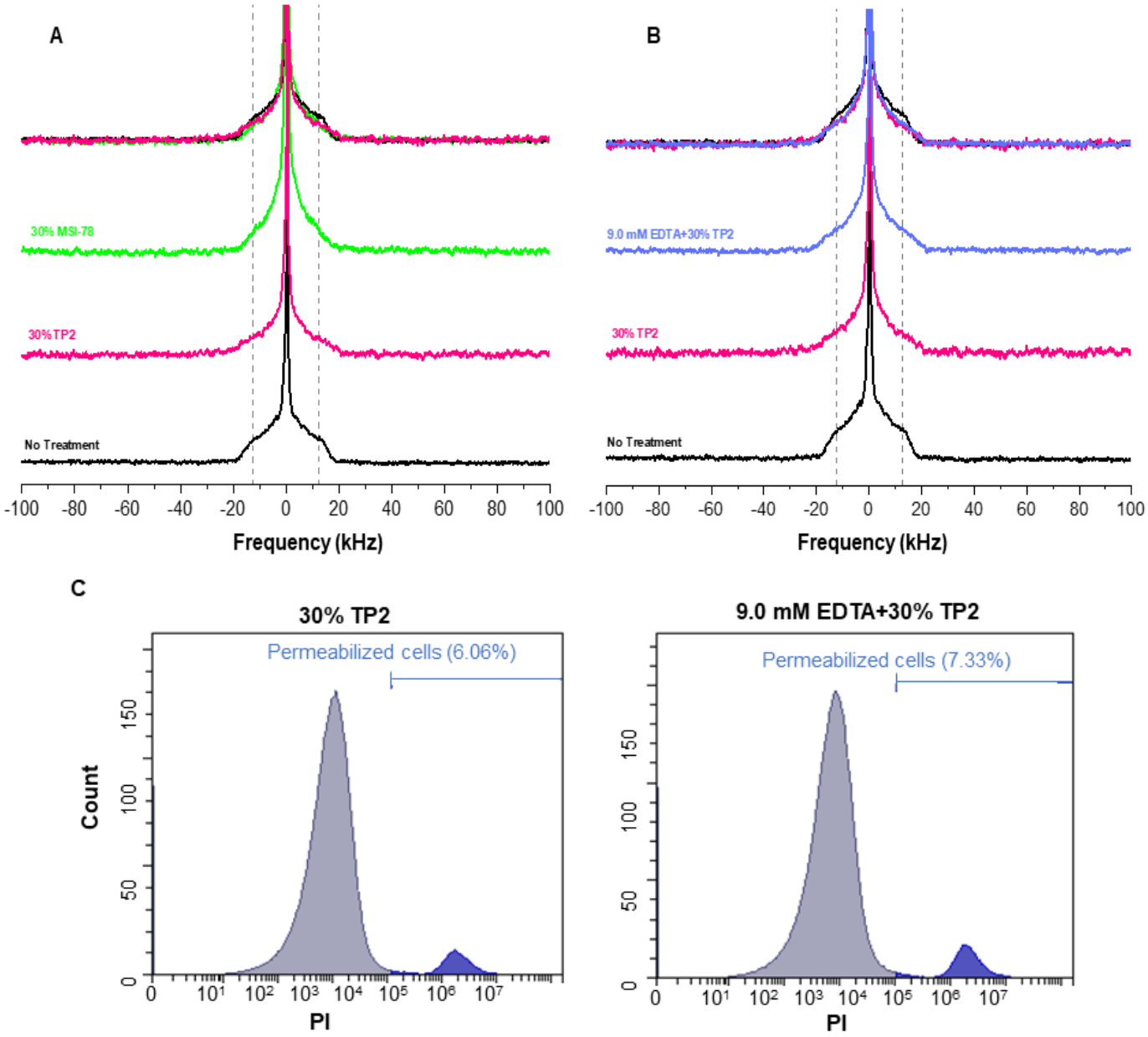

Fig. 6.1: The CPP peptide TP2 increases the amplitude of lipid chain motions but does not induce membrane permeabilization. **A**: ^{2}H NMR spectra of deuterium-enriched *E. coli* that are untreated (black, SK-53); after treatment with 30% TP2 (pink, SK-71); and after treatment with 30% MSI-78 (green, SK-47) **B:** ^{2}H NMR spectra of deuterium-enriched *E. coli* that are untreated (black, SK-53); after treatment with 30% TP2 (pink, SK-71) and after treatment with 9.0 mM EDTA followed by 30% TP2 (blue, SK-72). Dashed lines at

±12.5 kHz are shown to facilitate the comparison of the spectra. Each spectrum is obtained from 110,000 scans recorded over 12 h at 37°C in a 600 MHz NMR spectrometer and normalized by area. Only selected spectra are shown; additional spectra are shown in Fig. A6. **C:** Flow cytometry cell count vs. PI fluorescence intensity for *E. coli* cells treated with 30% TP2 and 9.0 mM EDTA+TP2.

Having shown that pre-treatment to destabilize the LPS affects the bacteria's sensitivity to lipid acyl chain disruption by MSI-78, we asked if destabilization of the LPS layer also affects acyl chain disruption induced by TP2 (**Fig. 6.1B**). From inspection of spectra, any differences were hard to discern, so we examined the Δ_2 values calculated from these spectra.

As for MSI-78, there was a significant increase in Δ_2 with TP2 treatment (**Table 6.1, Fig. 6.2**). Interestingly, unlike the case for MSI-78, the Δ_2 for the spectrum resulting from pre-treatment with 9.0 mM EDTA followed by TP2 decreased to 0.25. This was smaller than the Δ_2 value of 0.29, resulting from treatment with TP2 alone (p-value 0.03). This comparison of Δ_2 values indicates that membrane perturbation due to TP2 is larger than that due to treatment with EDTA followed by TP2.

In other words, while the presence of intact LPS protects cells from MSI-78, it appears to sensitize them to TP2. Overall, MSI-78 has a stronger effect on LPS-disrupted cells than TP2, with Δ_2 values of 0.39 and 0.25, respectively, and this was a statistically significant difference (p-value 0.01).

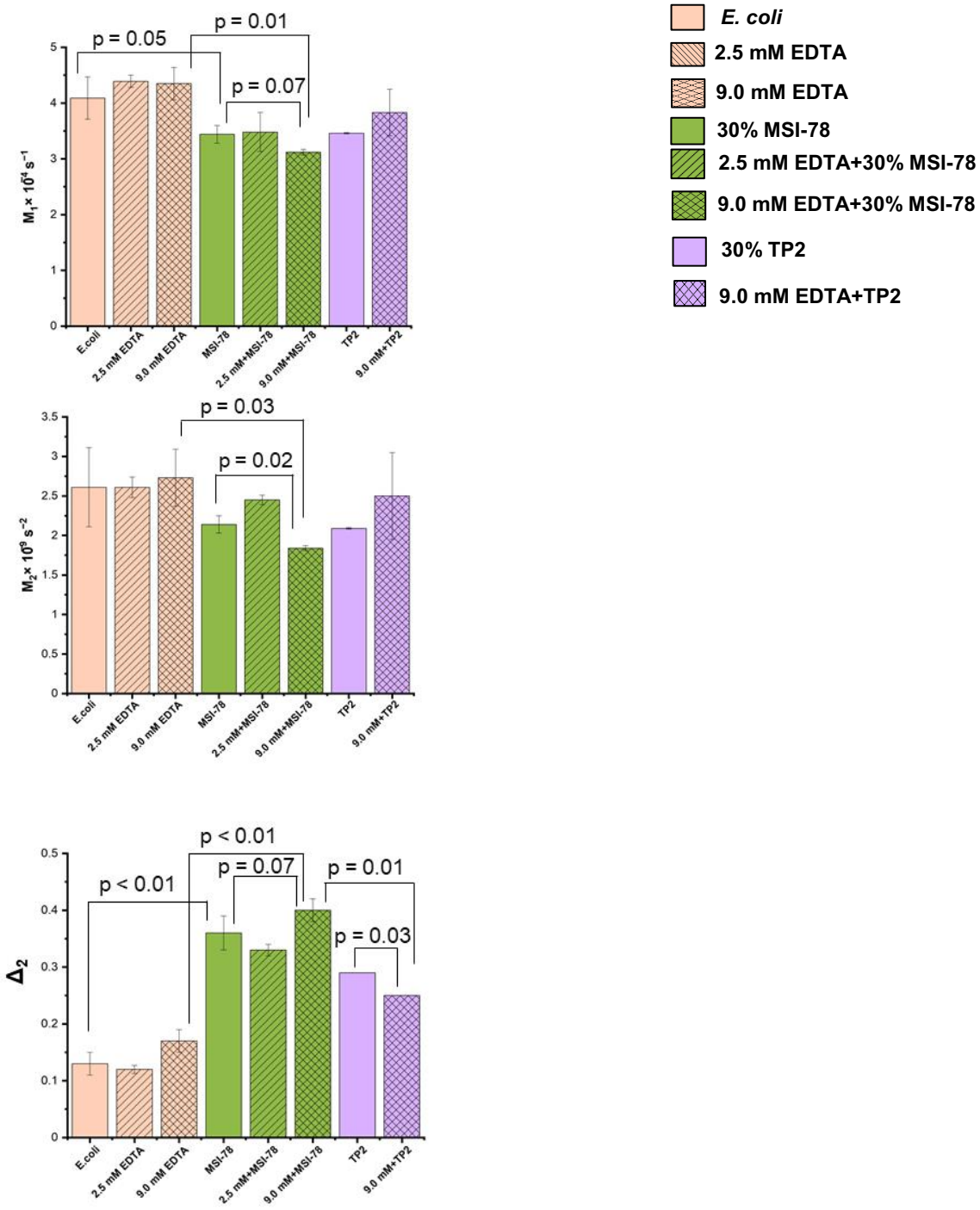

Fig. 6.2: M_1, M_2, and Δ_2 values for all the spectra with averages and standard deviations. P-values for ANOVA single-factor comparison of treatment groups are indicated for all comparisons

Table 6.1: M_1, M_2, and Δ_2 values for all the spectra shown in **Fig. 6.1A and B** with averages and standard deviations. p-values for ANOVA comparison of selected treatment groups are also included. SK-XX are the sample numbers, and referenced spectra not shown in the main text are in the appendix.

Experiment	$M_1 \times 10^4 (s^{-1})$	$M_2 \times 10^9 (s^{-2})$	Δ_2
30% TP2 SK-71	3.46	2.08	0.30
30% TP2 SK-75	3.47	2.10	0.29
Average ± Standard deviation	3.46 ± 0.01	2.09 ± 0.01	0.29 ± 0.00
p-value (30% MSI-78 vs. 30% TP2)	0.87	0.59	0.11
9.0 mM EDTA+30%TP2 SK-72	4.13	2.89	0.25
9.0 mM EDTA+30%TP2 SK-77	3.53	2.11	0.25
Average ± Standard deviation	3.83 ± 0.42	2.50 ± 0.55	0.25 ± 0.00
p-value (9.0 mM EDTA+30%MSI-78 vs. 9.0 mM EDTA+30% TP2)	0.14	0.23	0.01
p-value (30% TP2 vs. 9.0 mM EDTA+30% TP2)	0.35	0.40	0.03

Discussion

CPPs have been of great interest due to their ability to cross cellular membranes and have been utilized to carry cargo into cells with minimal toxicity [124,168]. Since the discovery of the first CPP, Tat, over 30 years ago, various CPPs, natural and synthetic, have been discovered and utilized for drug transport to enhance the bio-distribution of deliverables [124,168,169]. Although CPPs and AMPs have been studied extensively in recent years, there remains great ambiguity regarding the properties that contribute most to their activity.

This chapter compares the lipid acyl chain disorder induced by MSI-78, which permeabilizes cells to a fluorescent dye, with the effect of a CPP (TP2). This is the first ^{2}H NMR observation of the whole-cell bacteria perturbation by a CPP peptide. MSI-78 and TP2 were found to cause similar changes in the ^{2}H NMR spectra of membrane-deuterated bacteria, which implies similar changes in membrane lipid orientational order (**Fig. 6.1A**).

The AMP-induced reduction in the spectral edges ~ ± 12.5 kHz and the corresponding increase in intensity at narrower splittings were also reflected in the M_1 and Δ_2 values. For both AMP and CPP, there was an increase in Δ_2 and a decrease in M_1, associated with the presence of 30% of AMP. This decrease in M_1 and the increase in Δ_2 indicates a lower mean order parameter and a greater relative mean squared width of the order parameter distribution. These changes are consistent with an increase in the disorder along the whole acyl chain and a disruption in the lipid bilayer of the AMP and CPP-treated samples.

To summarize, MSI-78 and TP2 caused similar perturbations to the lipid acyl chain orientational order in the *E. coli* bacterial membranes despite one having antimicrobial properties and the other being a class of cell-penetrating peptides.

Interestingly, TP2 causes changes in the bacterial membrane of ^{2}H NMR spectra that are similar to those due to MSI-78 but don't permeabilize cells. CPP peptides are known for their endocytic uptake and membrane translocation [170–173]. However, these two mechanisms depend on the physicochemical properties of the peptide in combination with the structural properties of the cell membrane [78]. As shown in our study and one by Wimley et al. [122], spontaneous membrane translocation of TP2 might not require membrane permeabilization in order for the TP2 peptide to cross the lipid bilayer.

Additionally, destabilization of the LPS layer seemed to reduce the effect of TP2 on the bacterial membranes, whereas disrupting the LPS layer increased the extent to which bacterial membranes were affected by MSI-78. This was quite unexpected. It is unclear why this is. One possibility might be the difference in the sequence of the two peptides. For example, TP2 gets its positive charge from arginine residues, while MSI-78 has no arginine but many lysines. Additionally, TP2 is a much shorter peptide than MSI-78, and MSI-78 carries more ring residues in its sequences.

Most of the data available to date for CPPs has been based on the use of fluorescence dyes to understand the membrane-crossing properties of these peptides [123]. However, a study by Hong et.al. on POPE and POPG has shown that ^{2}H NMR spectra TAT a CPP peptides do not cause dynamic heterogeneity but interact with the membrane with a different mechanism [174]. Further study is required to understand if this is a general difference between AMPs and CPPs, or if it is specific to MSI-78 and TP2, as well as to understand the mechanism for the difference. Another study by Vogel et.al. on RW9 and RL9 two arginine rich CPP peptides has shown that POPC/POPG membranes flexibility has slightly increased by both the peptides [188].

Chapter 7. Selectivity of AMPs for bacterial cells versus mammalian cells

AMPs have been shown to exhibit cell selectivity. They selectively kill bacteria at concentrations not significantly toxic to mammalian cells [114,175]. AMPs can be nonhemolytic at concentrations above their minimal inhibitory concentrations (MICs) against many bacterial strains [114]. However, the effect of competition between AMP binding to bacterial and mammalian cells on antimicrobial activity and how interactions between AMPs and mammalian cells might be related to host cell toxicity and cell selectivity have not been well examined.

The study described in this chapter is intended to provide some information about AMP selectivity by examining whether non-bacterial cells (mammalian cells) can compete with bacteria for AMP binding in a mixture of bacteria and mammalian cells. The mammalian cell line used in this study was the Ramos cell line, derived from Burkitt's lymphoma [176]. The first step in this study is to confirm that the presence of Ramos cells does not affect membrane order in deuterated bacteria. To do this, I first had to optimize the cell growth time to produce enough Ramos cells for NMR. I started with a small culture of 50 ml of Ramos cells. After 2 days, cells were counted for a number of cells, and we judged that the pellet was not enough to fill the NMR rotor, so the cells were re-cultured for another 2 weeks. After 2 weeks and 3 days, the total number of cells was 2.9 x 109 cells, which was enough to fill the 3.2 mm NMR rotor.

Then I moved to do deuterium NMR on samples containing a mixture of deuterated *E. coli* and Ramos cells that are not deuterated. Representative spectra shown in **Fig. 7.1** present the ^{2}H NMR spectra of deuterated *E. coli* alone and deuterated *E. coli* cells mixed with Ramos cells. The

NMR spectra show no change in spectral shape for deuterated *E. coli* membranes in the mixture of two cell types compared to just *E. coli* cells.

The spectra display similar characteristics, including the edges at ~ ± 12.5 kHz. The lack of observable difference between the spectra from the membrane-deuterated *E. coli* (in black) and a mixture of membrane-deuterated *E. coli* and Ramos cells (in purple) indicates that, as expected, the presence of Ramos cells does not affect the membrane order in deuterated bacteria. The signal-to-noise ratio for the mixed sample (purple) is roughly half of the membrane-deuterated *E. coli* sample (black), so it is possible that Ramos cells account for about half of the mixed sample.

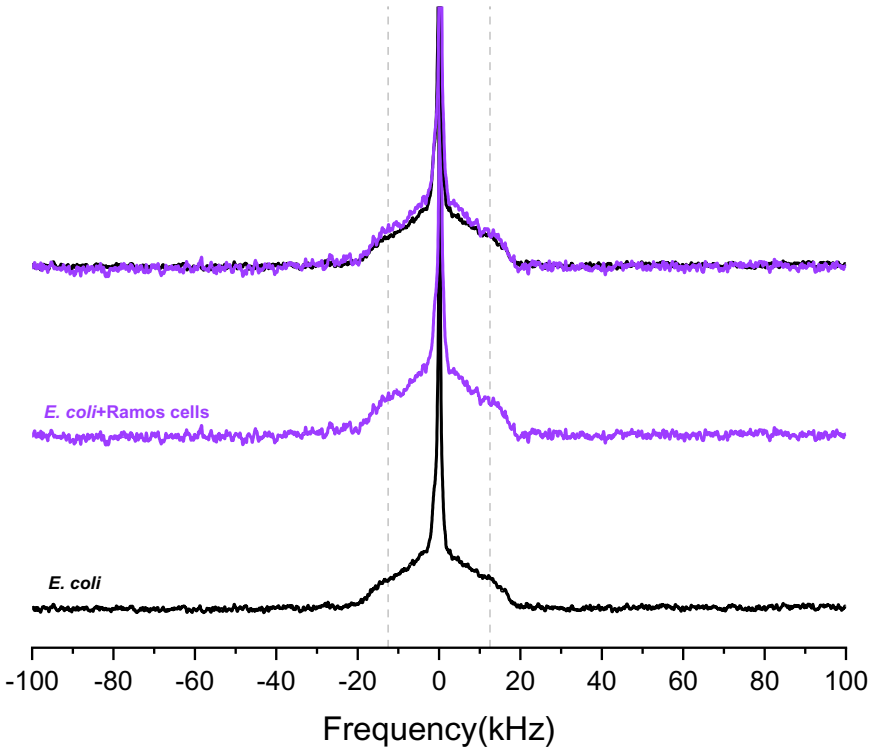

Fig. 7.1: No change in lipid acyl chain order between deuterated *E. coli* and a mixture of non-deuterated Ramos cells and deuterated *E. coli*: ^{2}H NMR spectra of deuterium-enriched *E. coli* that are untreated (black, SK-53); a mixture of deuterated *E. coli* and non-deuterated Ramos cells (purple, SK-76); Dashed lines at ±12.5 kHz are shown to facilitate the comparison of the spectra. Each spectrum is obtained from 110,000 scans recorded over 12 h at 37°C in a 600 MHz NMR spectrometer and normalized by area.

The next objective of this study was to assess the extent to which AMP binds to Ramos cells relative to bacteria. We decided to examine how the presence of Ramos cells affects the response of bacteria to MSI-78. To facilitate comparison, we wanted to use comparable amounts of lipids from bacteria and Ramos cells and a total lipid content similar to that in our study of MSI-78 interacting with bacteria. In section 2.3, we discussed calculating the dry weight of bacteria and the lipid ratio. In order to obtain the lipids ratio in the Ramos cells, we made use of the cell diameter of the Ramos cell. We can calculate the surface area of each cell. Then we looked up the surface area per lipid (0.5 nm^2) [161,177] and used that to estimate how many lipids are in the cytoplasm membrane of the cells (explained in Section 2.11). For the mixed cell NMR sample study, the total number of bacterial lipids was estimated to be 3.61 x 10^{18} lipids, and the total number of Ramos cells membrane lipids was estimated to be 1.45 x 10^{19}. The sample is thus estimated to contain about 4 times as many Ramos cell lipids as bacterial lipids.

Fig. 7.2 shows representative ^2H NMR spectra of the mixture of deuterated *E. coli* and non-deuterated Ramos cells (in black), the sample containing only *E. coli* treated with 30% MSI-78 (in blue), and the mixture of cells (i.e., Ramos cells and *E. coli* cells) treated with 30% MSI-78 in pink. The ^2H NMR spectrum of the bacteria + Ramos cells mixture treated with MSI-78 has a small but noticeable shoulder at ~ ±12.5 kHz compared to the spectrum of *E. coli* alone treated with 30% MSI-78, for which the shoulder is absent.

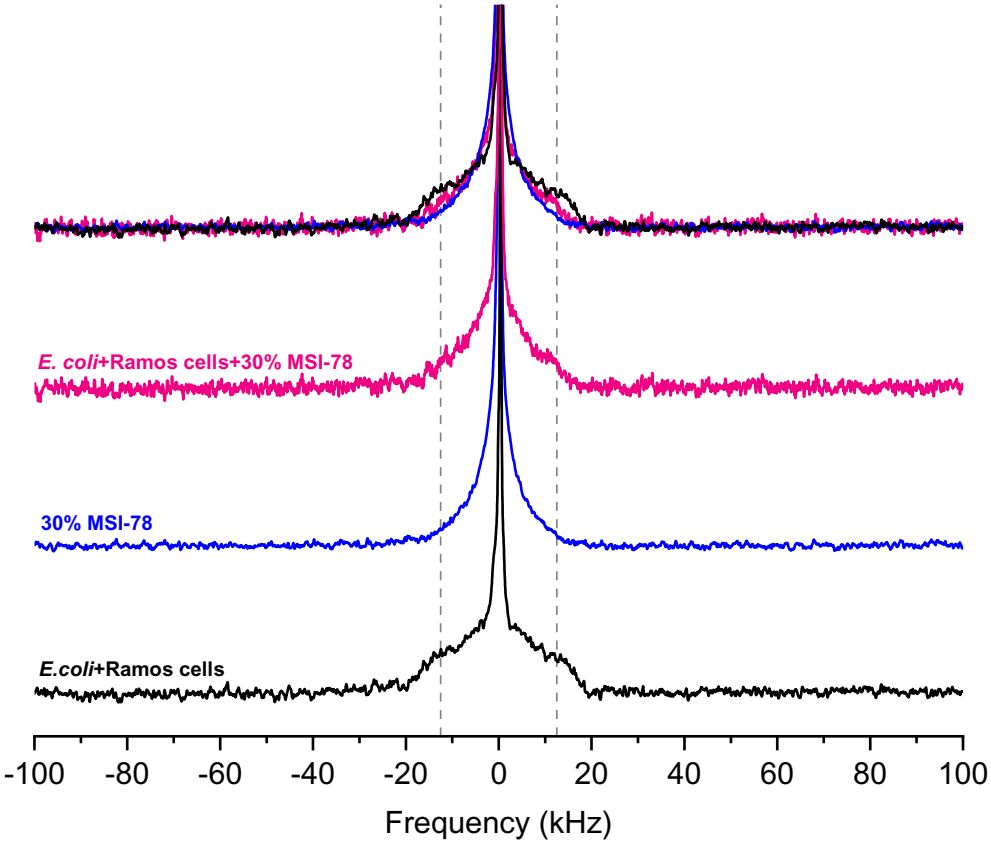

Fig. 7.2: Presence of Ramos cells impacts the effect of MSI-78 on lipid acyl chain order: ^{2}H NMR spectra of deuterated *E. coli* and non-deuterated Ramos cells (black, SK-76); deuterated *E. coli* treated with 30% MSI-78 (blue, SK-78) and deuterated *E. coli* and non-deuterated Ramos cells treated with 30% MSI-78 (pink, SK-79); Dashed lines at ±12.5 kHz are shown to facilitate the comparison of the spectra. Each spectrum is obtained from 110,000 scans recorded over 12 h at 37°C in a 600 MHz NMR spectrometer and normalized by area.

At the same time, the intensity at smaller splittings (between ~± 5 kHz) is smaller in the spectrum of the mixed cell sample treated with MSI-78 than in the sample of *E. coli* alone treated with MSI-78. Together, these observations about the spectra suggest that the presence of Ramos cells slightly reduces the amount of MSI-78 available to interact with *E. coli*. As noted earlier, the spectra of the *E. coli* cells treated with 30% MSI-78 with Ramos cells have a lower signal-to-noise ratio as compared to *E. coli* treated with 30% MSI-78.

We have calculated spectral moments for all the ^{2}H NMR spectra in this thesis but have yet to calculate spectral moments for this chapter. The result shown in this chapter is that replacing a significant fraction of bacteria with mammalian cells did not increase the relative amount of peptide available to interact with the bacteria, so some of the peptides must be taken up by mammalian cells. Therefore, a moment analysis would only be helpful with a more quantitative assessment of the relative amounts of bacterial and Ramos cell membrane lipids.

One approach that could potentially answer many unanswered questions regarding mammalian cells and AMPs would be directly detecting mammalian cell membrane perturbation by AMPs using ^{2}H NMR. This would require developing a method to deuterate the mammalian cells. In the next paragraph, I will discuss how I have attempted to deuterate the Ramos cells and obtain ^{2}H NMR spectra of deuterated Ramos cells.

In an effort to deuterate the Ramos cell, I adapted the protocol from Davis et al. [162], who studied deuterated erythrocyte membranes. First, Ramos cells were grown for two weeks, and the pellet was incubated with deuterated palmitic acid in methanol for 15 minutes at room temperature. The mixture was then centrifuged, and the NMR rotor was packed with the pellet.

Fig. 7.3 shows a spectrum ^{2}H NMR spectrum of deuterated Ramos cells.

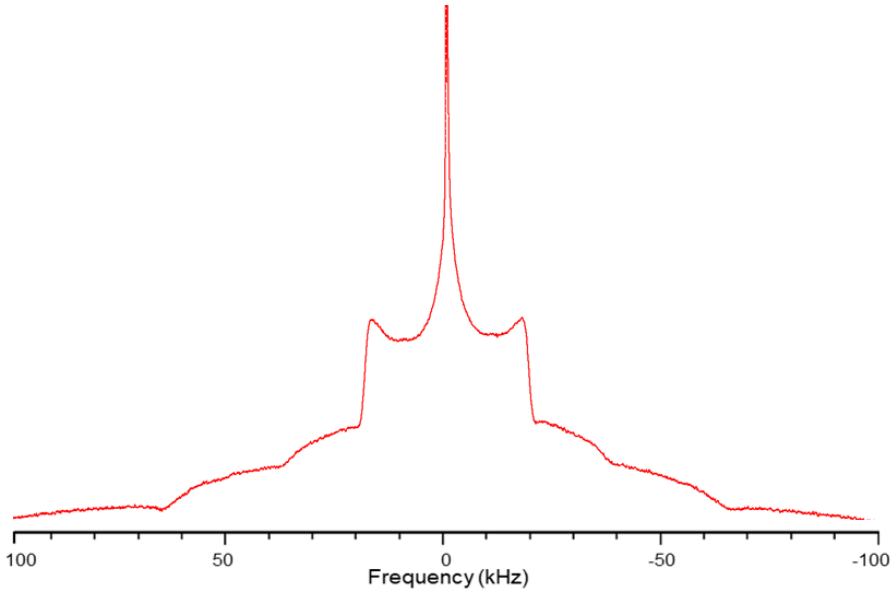

Fig. 7.3: First attempt to deuterate Ramos cells: ^{2}H NMR spectra of untreated deuterium-enriched Ramos cells (red, SK-81). The spectrum is obtained from 110,000 scans recorded over 12 h at 37°C in a 600 MHz NMR spectrometer.

Without an unambiguous assignment of the highly ordered lipid component, it is not possible to interpret the deuterated Ramos cell spectrum meaningfully. However, we can still understand some of the features. There is an intensity to ~ ± 62.5 kHz, meaning the lipid acyl chain motion is highly constrained. This has been seen in the ^{2}H NMR spectrum of gel-phase DPPC-d_{62} at 20°C [129]. Tardy et al. have also seen intensity out to ~± 62.5 kHz in membrane-deuterated *E. coli* ^{2}H NMR spectra, indicating the presence of a phospholipid in the gel-phase [145]. The spectrum in **Fig. 7.3** also has a prominent doublet with edges ~± 17.5 kHz [159]. The presence of a single doublet with this splitting could indicate some lipid in the liquid-ordered phase, or it could be the methyl doublet from a more solid phase.

Discussion

This work addresses an important yet less studied problem concerning the mechanism for the AMPs' cell selectivity for bacterial cells over mammalian cells. While there has been extensive research on the effects of AMPs on bacterial cells, there has still been little study of the interaction of AMPs with mammalian cells. Mammalian cell lines have been examined for cell viability in the presence of AMPs [178–180]. A few studies have examined the AMP selectivity interactions of AMPs with non-bacterial cells. Still, they have focused on red blood cells (RBCs) because it is easy to prepare RBC samples in large quantities, and hemolysis assays can easily be done by monitoring the colour of hemoglobin [111,101].

This study suggests that even without deuterating the Ramos cells, I can still draw some conclusions regarding the relative binding of the AMPs to bacteria and non-bacterial cells and thus learn something about AMP selectivity. In the presence of Ramos cells, the perturbation of the *E. coli* membrane by AMP is reduced relative to the bacteria plus MSI-78 experiments, despite the ratio of peptide to *E. coli* lipid being 4 to 5 times larger than in those experiments. This indicates that the Ramos cell must be binding some AMP. This suggests that the basis for non-bacterial cell resistance to AMP effects is not just a result of AMP being completely unable to bind to non-bacterial cells.

Many review articles have studied and discussed the underlying basis of AMP selectivity for bacterial cells beyond differences in anionic phospholipids content [115,117,175]. One possibility is that the cholesterol in mammalian cells prevents damage from AMPs [175]. On the other hand, Ramamoorthy et al. have discussed the heterogeneous lipid systems of mammalian cells and suggested that the cholesterol-rich domains can be disrupted by AMPs [181]. In a recent study from the Marcotte group, where they tried to deuterate RBC cells, they achieved 25%

deuteration of palmitic chains in the membranes and studied the effect of two AMPs, caerin 1.1 and aurein 1.2. on RBC ghost by ^{2}H NMR and ^{31}P techniques [104].

In order to draw more detailed conclusions about how bacterial and mammalian cells compete for AMP binding, I must repeat these experiments and get reproducible spectra to understand the ^{2}H NMR spectra of deuterated Ramos cells completely. I also must optimize the deuterated palmitic acid concentration used in the preparations of deuterated Ramos cells. I can do mass spectrometry to analyze the lipid composition of Ramos cells, which will help us to understand the lipid environment of Ramos cells. Analysis of the lipid composition of the Ramos cells could be done by firstly separating the fatty acid chains from the lipid headgroups using hydrolysis followed by methylation. Once the fatty acids are extracted from the Ramos cells, It should than be possible to obtain a complete lipid profile using GC-MS. Once a protocol for reproducible preparations of deuterated Ramos cells has been identified, it will be possible to carry out a more detailed analysis of the resulting spectra.

Chapter 8. Conclusions and future directions

Our group and others [137,139,140] have deuterated membrane phospholipid acyl chains in the Gram-negative bacteria *E. coli.* It is interesting to compare the M_1, M_2, and Δ_2 values reported here to corresponding values reported for earlier studies, although we can expect the values to be altered by the *E. coli* strain chosen and the growth protocol used.

Previous studies have been on wild-type *E. coli* prepared and deuterated using the protocol described here [145,156] and on *E. coli* deuterated by taking advantage of a mutation that suppresses total fatty acid synthesis [139]. The M_1, M_2, and Δ_2 for untreated cells found in this study looks smaller than all the other values observed for untreated *E. coli* (**Table 8.1**) in all of these earlier studies [139,145,182]. The average M_1 , M_2, and Δ_2 values were more replicable compare to M_1 , M_2, and Δ_2 values reported in previous work [139,140]. The increase in Δ_2 by 0.16, resulting from treatment with 30% MSI-78 in the present study with *E. coli* JM109s, is comparable to the 0.10 increase seen for the same amount of MSI-78 in the earlier study with mutated *E. coli* [139]. It should be noted that while Santisteban et.al has observed higher values for M_1, M_2, and Δ_2, the values in that study reflected increased spectral intensity out to frequencies of ~ ± 62.5 kHz. Enhanced intensity out to such large splittings indicates the presence of a highly ordered structure in which the deuterated acyl chain movements are more restricted [144]. For splittings close to ± 62.5 kHz, the shape of the DPPC-d_{62} gel phase spectrum (20°C) is similar to the spectral component seen at similar splittings in the spectra of *E. coli* JM109 and *B. subtilis* at 37°C. This suggests that the broad spectral component seen for these samples arises from slow reorientation of highly ordered acyl chains. One possibility that is suggested in Santisteban thesis

would be that the bacteria are retaining and storing lipids in a non-cell- membrane site in a gel-like phase state or that gel-like domains are being formed in the bacterial membrane [134].

Table 8.1 M_1, M_2, and Δ_2 values reported for earlier studies of ^{2}H NMR membrane-deuterated bacteria.

Bacterial Strain	$\boldsymbol{M_1 \times 10^4 (s^{-1})}$	$\boldsymbol{M_2 \times 10^9 (s^{-2})}$	$\boldsymbol{\Delta_2}$
E. coli JM109 this thesis	4.09	2.61	0.14
E. coli JM109 Santisteban et.al [144]	9.00	17.0	0.47
B. subtilis Santisteban et.al [140]	6.00	9.00	0.62
E. coli Ppd117 Tardy et.al [145]	6.30	9.00	0.68
E. coli LA8 Pius et.al [139]	5.00	3.40	0.26

In this study, I have also tried to use another approach, ^{2}H MAS NMR, to characterize deuterated membrane bacteria. In order to establish the reliability of the ^{2}H MAS NMR moments, the information extracted from MAS is compared to the moments from the ^{2}H NMR static samples. The preliminary ^{2}H MAS NMR data sets for untreated deuterated *E. coli* samples obtained with a spinning rate of 10 kHz provide much of the same information obtained from the static ^{2}H NMR spectra but in a shorter experiment. However, more reproducible MAS spectra will need to be recorded for reliable moment calculations. In addition, when I tried to record the MAS spectra of samples treated with AMP, I observed that sidebands were lost. This suggests that MAS might be more suitable for untreated bacterial samples than those treated with AMP.

The major focus of this study was to determine if the lipopolysaccharide layer in the Gram-negative cell envelope impacts the interaction between the lipid membrane and with AMPs and CPPs. This was accomplished by examining EDTA's effect on the stability of LPS. The interaction between the negative charges of Lipid A and the divalent ions Mg^{2+} and Ca^{2+} is essential for the stability of the LPS membrane [164]. We first developed a method to gently destabilize the LPS layer of *E. coli.* We (**Fig. 4.2B** and **4.2C**) confirmed that above a threshold concentration, EDTA

drastically alters the Gram-staining of the bacteria and changes them from rod-shaped to spherical-shaped without killing them. It is thus rather striking that despite these dramatic changes to the bacteria, the lipid chain order remains largely unchanged by treatment with 9.0 mM EDTA (**Fig. 4.2B**). The dramatic changes in the carbohydrate region of the LPS and the cell shape appear to leave the lipid acyl chains of the bacterial membrane largely unperturbed.

The central question posed in this work is the role of the LPS layer in either protecting bacteria from AMPs or in potentiating their activity. As noted in the **Introduction**, if some of the AMP gets bound up in the LPS layer and doesn't reach the membrane, that could explain why the AMP:L ratios needed to see activity are higher in studies with intact bacteria compared to studies of model membrane permeabilization [54,107,108].

In this work, we show that LPS destabilization by EDTA before treatment with the AMP MSI-78 does indeed increase the ability of MSI-78 to perturb the lipid acyl chains. Thus, at least for MSI-78, the LPS layer does help protect the lipid membrane of the bacteria from the AMP. This result can be seen by comparing the NMR spectra of membrane-deuterated bacteria treated with MSI-78 alone to spectra from bacteria first treated with EDTA to destabilize the LPS and then treated with AMP (**Fig. 5.2**). The effect of LPS destabilization on the membrane response to AMP can also be appreciated from parameters that characterize the NMR spectral shape, M_1, M_2 and Δ_2 (**Fig. 5.3**). In particular, M_1 and M_2 both decrease more in the cells treated with both EDTA and MSI-78 than in those treated with AMP alone than in those treated with AMP alone, indicating more AMP-induced acyl chain disruption. Δ_2, which is sensitive to the shape of the spectra and is expected to increase if the AMP alters the distribution of orientational order along the acyl chain, increases more in the doubly treated cells than for AMP treatment alone. Overall, I have shown

that gently destabilizing the LPS layer of *E. coli* bacteria has given a little more access for MSI-78 to reach the lipid bilayer.

This finding has the potential to explain unanswered questions about how AMPs interact with bacteria. It has long been known that it takes a greater AMP:L ratio to permeabilize whole bacteria than to permeabilize model membranes [43,56,58,107,183,184], but the reason for this difference is not understood. We show here that LPS, present in bacteria but not model membranes, protects bacteria to some extent from the AMP MSI-78. LPS protection from AMP membrane permeabilization would explain why model lipid bilayers are more prone to permeabilization by AMP than are bilayers in whole bacteria. Furthermore, since efforts to optimize AMPs as drugs often rely solely on optimizing the AMP's lipid-permeabilizing activities, consideration of other interactions like AMP-LPS interactions may prove helpful in AMP-based drug design.

Another objective of this work was to compare the effect of cell-penetrating peptides (TP2) to antimicrobial peptides (MSI-78) on *E. coli* membranes. This is important since only a few ^{2}H NMR studies of the whole cell have been reported [103,137,139,140,145,146,155,156,182], and only a few of them investigated the effects of AMPs on the structure and dynamics of the lipid bilayer [137,139,140,156]. In addition, no whole cell ^{2}H-NMR studies of a CPP have been reported before this work.

We find it fascinating that while one peptide, the AMP MSI-78, permeabilizes the bilayer to a fluorescent dye and the other, the CPP TP2, does not (**Fig. 6.1B, 6.1C**) [135], the two peptides have much the same effect at the level of the membrane lipid orientational order as reflected by ^{2}H NMR spectra (**Fig. 6.1A**). Possible explanations for why the changes in lipid membrane order are not sensitive to the difference in mechanism between these two peptide types might relate to the timescale of the peptide-induced lipid perturbations (which our NMR data probe on the ~100

μs timescale) or the diameter of the defects induced by the peptides. Whatever the explanation, it is intriguing to find such a fundamental property, i.e., membrane acyl chain disruption, shared by two peptides that have different effects on membrane permeabilization.

To understand in more detail of timescale of the peptide-induced lipid perturbations or the diameter of the defects induced by the MSI-78 and CPP. Atomic force microscopy (AFM) can be used for nanoscale accuracy. AFM imaging has enabled fundamentally new insights into pore formation's architecture, abundance and dynamics [135].

Another thought-provoking aspect of comparing the lipid interactions of MSI-78 and TP2 was the effect of LPS destabilization on the peptide-induced lipid disruptions. It was quite unexpected that LPS appeared to protect bacteria from MSI-78 but sensitize bacteria to TP2, as judged by the changes in Δ_2 values calculated from the NMR spectra (**Fig. 6.2**) unclear why this is. Still, one possibility might be the difference in the sequence of the two peptides. For example, TP2 gets its positive charge from arginine residues, while MSI-78 (GIGKFLKKAKKFGKAFVKILKK-NH_2) has no arginine but many lysines. TP2 (PLIYLRLLRGQWC-NH_2) is a much shorter peptide than MSI-78, and MSI-78 carries more ring residues in its sequence. The result further underlines the need to consider interactions beyond peptide-lipid interactions in understanding the mechanisms by which surface-active peptides affect bacteria. Also, this approach can be implemented to other strain of bacteria and different class of AMPs or CPPs that will help us compare how the different class of peptides behaves on bacterial membrane.

The final part of this thesis (Chapter 7) addresses an important question that very few studies have reported till now. AMPs potency is assessed, in part by AMPs selectivity

[115,185,186]. The concept of peptide selectivity (defined as MHC/MIC) has been widely used in the literature as a standard "ruler" for assessing their potency as therapeutic agents [107,175].

We have provided some information about AMP selectivity by examining whether non-bacterial cells can compete with bacteria for AMP binding in a mixture of bacteria and mammalian cells (Ramos cells. In our study to assess the extent to which AMP (MSI-78) binds to Ramos cells relative to bacteria, we decided to examine how the presence of Ramos cells affects the response of bacteria to MSI-78. To facilitate comparison, we chose to use the comparable peptide-to-bacterial lipid ratio in the mixed cell samples as in our study of MSI-78 interacting with bacteria. We first confirmed that the presence of Ramos cells does not affect membrane order in deuterated bacteria. Interestingly, when the MSI-78 was added to the mixture of cells, i.e., membrane-deuterated *E. coli* and Ramos cells, we found that the presence of Ramos cells slightly reduced the amount of MSI-78 available to interact with the *E. coli*, presumably due to some binding of MSI-78 by the Ramos cells.

The last piece of this study was trying to deuterate the mammalian (Ramos cells). The resulting spectrum, shown in **Fig. 7.3**, does not appear to be characteristic of liquid-crystalline membrane lipids, suggesting that most deuterated fatty acids ended up in non-liquid-crystalline membrane environments. It is possible that some of the deuterated palmitic acids formed crystals and didn't deuterate the Ramos cell membrane. Further work will be needed in order to establish a protocol for reproducible deuteration of mammalian cells like Ramos cells.

8.1 Directions for future work

The work reported in this thesis focuses on LPS role in determining how antimicrobial peptides and cell-penetrating peptides membrane interact. In this study, I have shown that LPS, present in bacteria but not model membranes, protects bacteria from the AMP MSI-78. Protection

from AMP membrane permeabilization by LPS could explain why model lipid bilayers are more prone to permeabilization by AMP than bilayers in whole bacteria.

As discussed in this thesis, before AMPs can interact with the cytoplasmic membrane in Gram-negative bacteria, it has to traverse the outer membrane of the LPS layer. In Gram-positive bacteria, before AMPs can interact with the cytoplasmic membrane, they must cross the cell wall composed of teichoic acids and peptidoglycan [112]. It would thus be valuable to the extent to the current study to a similar study of AMP-bacterial interactions with Gram-positive bacteria. For example, it would be interesting to investigate, in Gram-positive bacteria, how destabilizing the teichoic acid (TA) will affect the level of membrane disruption by one of the AMPs (MSI-78) or CPPs (i.e., TP2) by ^{2}H NMR. Koprivnjak et al. [187] showed how the *S. aureus tagO* mutant was selectively resistant to two AMPs, the mammalian group II phospholipase A2 (gIIA PLA2) and the human β-defensin 3. Since the *tagO* mutant of *S. aureus* lacks teichoic wall acid (WTA), Koprivnjak et al. suggested that the AMPs lacked the initial rung of the poly-anionic ladder, which would prevent the AMPs from reaching the cell membrane. Using ^{2}H NMR to observe peptide-induced membrane disruption of a membrane-deuterated mutant strain of *S. aureus* that lacks the WTA could provide useful insight into interaction with anionic teichoic acids that may act as either a trap for AMPs or a source for a route to the cytoplasmic membrane.

Next, in order to look for an intracellular target of CPP-TP2, differential scanning calorimetry (DSC) experiments could be performed. DSC has already been used in our lab group to understand the intracellular target for MSI-78, and this study has shown that ribosomes are an intracellular target of MSI-78 [184].

In addition, it would also be interesting to do a mass spectrometry analysis after pelleting the CPP treatment cells. It would help us understand how much peptide is bound and how much

is left on the supernatant. We should do a mass spectrometry of the supernatant and analyze the data to estimate how much unbound peptide is left in the supernatant.

Furthermore, one interesting observation Wimley et al. [120] reported is that TP2 has an interesting behaviour; increasing the peptide-to-lipid ratio causes decreased translocation rates. So, it would be exciting to observe the level of membrane disruption by ^{2}H NMR of membrane-deuterated bacteria by reducing the P/L ratio. In my study, I have used 30% TP2, we can use 10% and 20% TP2 and compare them with the effects of 30% TP2 on the ^{2}H NMR spectra of membrane-deuterated bacteria.

A potentially exciting follow-up to this study would be to deuterate the mammalian cells. Firstly, we may have to optimize the protocol to ensure that the deuterated material is primarily incorporated into the mammalian cell membranes. Dr. Robert Brown (Biochemistry Dept. MUN) has suggested that we can feed the Ramos cells with deuterated palmitic acid complexed with BSA (Bovine serum Albumin). This is expected to help the cell membrane uptake of the deuterated palmitic acid, which will be a prerequisite for observing reproducible ^{2}H NMR spectra of mammalian cells. Observing mammalian cell membrane order using ^{2}H NMR will eventually help us understand how mammalian cells are affected by the AMPs [105]. This work would bridge model membranes and in vitro studies and help us understand AMP drug toxicity toward mammalian cells.

Bibliography

1. Bone, T.H.; Nubia, S.; Bassett, E.J.; Keith, M.S.; Armelagos, G.J.; Martin, D.L.; Villanueva, A.R. Tetracycline-Labeled Human Bone from Ancient Sudanese Nubia (A . D . 350). *Adv. Sci.* **2008**, *209*, 1532–1534.

2. Henderson, J.W.; Warren, J. The Yellow Brick Road to Penicillin: A Story of Serendipity. *Mayo Clin. Proc.* **1997**, *72*, 683–687, doi:10.1016/s0025-6196(11)63577-5.

3. Cabeen, M.T.; Jacobs-Wagner, C. Bacterial Cell Shape. *Nat. Rev. Microbiol.* **2005**, *3*, 601–610, doi:10.1038/nrmicro1205.

4. Shockman, G.D.; Barrett, J.F. Structure, Function, and Assembly of Cell Walls of Gram-Positive Bacteria. *Annu. Rev. Microbiol.* **1983**, *37*, 501–527, doi:10.1146/annurev.mi.37.100183.002441.

5. Gehman, J.D.; Luc, F.; Hall, K.; Lee, T.H.; Boland, M.P.; Pukala, T.L.; Bowie, J.H.; Aguilar, M.I.; Separovic, F. Effect of Antimicrobial Peptides from Australian Tree Frogs on Anionic Phospholipid Membranes. *Biochemistry* **2008**, *47*, 8557–8565, doi:10.1021/bi800320v.

6. Nikaido, H.; Vaara, M. Molecular Basis of Bacterial Outer Membrane Permeability. *Microbiol. Rev.* **1985**, *49*, 1–32, doi:10.1128/mmbr.49.1.1-32.1985.

7. Raetz, C.R.H.; Whitfield, C. Lipopolysaccharide Endotoxins. *Annu. Rev. Biochem.* **2002**, *71*, 635–700, doi:10.1146/annurev.biochem.71.110601.135414.

8. Alexander, C.; Rietschel, E.T. Bacterial Lipopolysaccharides and Innate Immunity. *J.*

Endotoxin Res. **2001**, *7*, 167–202, doi:10.1179/096805101101532675.

9. Trent, M.S.; Stead, C.M.; Tran, A.X.; Hankins, J. V. Invited Review: Diversity of Endotoxin and Its Impact on Pathogenesis. *J. Endotoxin Res.* **2006**, *12*, 205–223, doi:10.1179/096805106X118825.

10. Gronow, S.; Brade, H. Lipopolysaccharide Biosynthesis: Which Steps Do Bacteria Need to Survive? *J. Endotoxin Res.* **2001**, *7*, 3–23, doi:10.1179/096805101101532468.

11. Vaara, M. Agents That Increase the Permeability of the Outer Membrane. *Microbiol. Rev.* **1992**, *56*, 395–411, doi:10.1128/mmbr.56.3.395-411.1992.

12. Erridge, C.; Bennett-Guerrero, E.; Poxton, I.R. Structure and Function of Lipopolysaccharides. *Microbes Infect.* **2002**, *4*, 837–851, doi:10.1016/S1286-4579(02)01604-0.

13. Frirdich, E.; Whitfield, C. Lipopolysaccharide Inner Core Oligosaccharide Structure and Outer Membrane Stability in Human Pathogens Belonging to the Enterobacteriaceae. *J. Endotoxin Res.* **2005**, *11*, 133–144, doi:10.1179/096805105X46592.

14. Nikaido, H. Preventing Drug Access to Targets: Cell Surface Permeability Barriers and Active Efflux in Bacteria. *Semin. Cell Dev. Biol.* **2001**, *12*, 215–223, doi:10.1006/scdb.2000.0247.

15. Szafranek, J.; Kumirska, J.; Czerwicka, M.; Kunikowska, D.; Dziadziuszko, H.; Głośnicka, R. Structure and Heterogeneity of the O-Antigen Chain of Salmonella Agona Lipopolysaccharide. *FEMS Immunol. Med. Microbiol.* **2006**, *48*, 223–236, doi:10.1111/j.1574-695X.2006.00141.x.

16. Venter, P.; Abraham, M.; Lues, J.F.R.; Ivanov, I. The Influence of Sanitizers on the Lipopolysaccharide Composition of *Escherichia Coli* O111. *Int. J. Food Microbiol.* **2006**, *111*, 221–227, doi:10.1016/j.ijfoodmicro.2006.05.009.

17. Skurnik, M.; Bengoechea, J.A. The Biosynthesis and Biological Role of Lipopolysaccharide O-Antigens of Pathogenic Yersiniae. *Carbohydr. Res.* **2003**, *338*, 2521–2529, doi:10.1016/S0008-6215(03)00305-7.

18. Yocum, R.R.; Rasmussen, J.R.; Strominger, J.L. The Mechanism of Action of Penicillin. Penicillin Acylates the Active Site of *Bacillus Stearothermophilus* D-Alanine Carboxypeptidase. *J. Biol. Chem.* **1980**, *255*, 3977–3986, doi:10.1016/s0021-9258(19)85621-1.

19. Hu, Y.; Liu, A.; Vaudrey, J.; Vaiciunaite, B.; Moigboi, C.; McTavish, S.M.; Kearns, A.; Coates, A. Combinations of β-Lactam or Aminoglycoside Antibiotics with Plectasin Are Synergistic against Methicillin-Sensitive and Methicillin-Resistant *Staphylococcus Aureus*. *PLoS One* **2015**, *10*, 1–15, doi:10.1371/journal.pone.0117664.

20. Ovung, A.; Bhattacharyya, J. Sulfonamide Drugs: Structure, Antibacterial Property, Toxicity, and Biophysical Interactions. *Biophys. Rev.* **2021**, *13*, 259–272, doi:10.1007/s12551-021-00795-9.

21. Kumar S.; Singh. B.R. An Overview of Mechanisms and Emergence of Antimicrobials Drug Resistance. *Adv. Anim. Vet. Sci.* **2013**, *1*, 7 – 14.

22. Fàbrega, A.; Madurga, S.; Giralt, E.; Vila, J. Mechanism of Action of and Resistance to Quinolones. *Microb. Biotechnol.* **2009**, *2*, 40–61, doi:10.1111/j.1751-7915.2008.00063.x.

23. Wehrli, W. Rifampin : Mechanisms of Action and Resistance The Use of Rifampin in the Treatment of Nontuberculous Infections. *Rev. Infect. Dis.* **1983**, *5*, S407–S411.

24. Bhattacharjee, M.K. *Chemistry of Antibiotics and Related Drugs*; 2016; ISBN 9783319407463.

25. Blair, J.M.A.; Webber, M.A.; Baylay, A.J.; Ogbolu, D.O.; Piddock, L.J.V. Molecular Mechanisms of Antibiotic Resistance. *Nat. Rev. Microbiol.* **2015**, *13*, 42–51, doi:10.1038/nrmicro3380.

26. Abedeji, W.A. The Treasure Called Antibiotics. *Ann. Ibadan Postgrad. Med.* **2016**, *14*, 56–57.

27. Abraham, E.P. The Antibiotics. *Compr. Biochem.* **1963**, *11*, 181–224, doi:10.1016/B978-1-4831-9711-1.50022-3.

28. World Health Organization (WHO), Global Priority List of Antibiotic-Resistant Bacteria to Guide Research, Discovery and Development of New Antibiotic.Geneva, Switzerland. 2021.

29. World Health Organization (WHO), Antimicrobial Resistance Global Report on Surveillance : 2014 Summary.

30. Prestinaci, F.; Pezzotti, P.; Pantosti, A. Antimicrobial Resistance: A Global Multifaceted Phenomenon. *Pathog. Glob. Health* **2015**, *109*, 309–318, doi:10.1179/2047773215Y.0000000030.

31. Bahar, A.A.; Ren, D. Antimicrobial Peptides. *Pharmaceuticals* **2013**, *6*, 1543–1575, doi:10.3390/ph6121543.

32. Moravej, H.; Moravej, Z.; Yazdanparast, M.; Heiat, M.; Mirhosseini, A.; Moosazadeh Moghaddam, M.; Mirnejad, R. Antimicrobial Peptides: Features, Action, and Their Resistance Mechanisms in Bacteria. *Microb. Drug Resist.* **2018**, *24*, 747–767, doi:10.1089/mdr.2017.0392.

33. Steiner, H.; Hultmark, D.; Engström, Å.; Bennich, H.; Boman, H.G. Sequence and Specificity of Two Antibacterial Proteins Involved in Insect Immunity. *Nature* **1981**, *292*, 246–248, doi:10.1038/292246a0.

34. Hani, K.; Zairi, A.; Tangy, F.; Bouassida, K. Dermaseptins and Magainins: Antimicrobial Peptides from Frogs' Skin-New Sources for a Promising Spermicides Microbicides-a Mini Review. *J. Biomed. Biotechnol.* **2009**, *2009*, doi:10.1155/2009/452567.

35. Ge, Y.; MacDonald, D.L.; Holroyd, K.J.; Thornsberry, C.; Wexler, H.; Zasloff, M. In Vitro Antibacterial Properties of Pexiganan, an Analog of Magainin. *Antimicrob. Agents Chemother.* **1999**, *43*, 782–788, doi:10.1128/aac.43.4.782.

36. Jenssen, H.; Hamill, P.; Hancock, R.E.W. Peptide Antimicrobial Agents. *Clin. Microbiol. Rev.* **2006**, *19*, 491–511, doi:10.1128/CMR.00056-05.

37. Ting, D.S.J.; Beuerman, R.W.; Dua, H.S.; Lakshminarayanan, R.; Mohammed, I. Strategies in Translating the Therapeutic Potentials of Host Defense Peptides. *Front. Immunol.* **2020**, *11*, 1–16, doi:10.3389/fimmu.2020.00983.

38. Lindsey M. Gottler and Ayyalusamy Ramamoorthy Structure, Membrane Orientation, Mechanism, and Function of Pexiganan – A Highly Potent Antimicrobial Peptide Designed From Magainin. *Biochim Biophys Acta. 2009* **2009**, *83*, 1–11, doi:doi:10.1016/j.bbamem.2008.10.009. Structure,.

39. Zasloff, M. Antimicrobial Peptides of Multicellular Organisms. *Nature*. **2002**, *415*, 389-395.

40. Ganz, T. Defensins : Antimicrobial Peptides of Innate Immunity. *Nat Rev Immunol*, **2003**, *3*, 710–721, doi:10.1038/nri1180.

41. Xhindoli, D.; Pacor, S.; Benincasa, M.; Scocchi, M.; Gennaro, R.; Tossi, A. The Human Cathelicidin LL-37 - A Pore-Forming Antibacterial Peptide and Host-Cell Modulator. *Biochim. Biophys. Acta - Biomembr.* **2016**, *1858*, 546–566, doi:10.1016/j.bbamem.2015.11.003.

42. Murakami, M.; Ohtake, T.; Dorschner, R.A.; Schittek, B.; Garbe, C.; Gallo, R.L. Cathelicidin Anti-Microbial Peptide Expression in Sweat, an Innate Defense System for the Skin. *J. Invest. Dermatol.* **2002**, *119*, 1090–1095, doi:10.1046/j.1523-1747.2002.19507.x.

43. Gazit, E.; Miller, I.R.; Biggin, P.C.; Sansom, M.S.P.; Shai, Y. Structure and Orientation of the Mammalian Antibacterial Peptide Cecropin P1 within Phospholipid Membranes. *J. Mol. Biol.* **1996**, *258*, 860–870, doi:10.1006/jmbi.1996.0293.

44. Falla, T.J.; Nedra Karunaratne, D.; Hancock, R.E.W. Mode of Action of the Antimicrobial Peptide Indolicidin. *J. Biol. Chem.* **1996**, *271*, 19298–19303, doi:10.1074/jbc.271.32.19298.

45. Rozek, A.; Friedrich, C.L.; Hancock, R.E.W. Structure of the Bovine Antimicrobial Peptide Indolicidin Bound to Dodecylphosphocholine and Sodium Dodecyl Sulfate Micelles. *Biochemistry* **2000**, *39*, 15765–15774, doi:10.1021/bi000714m.

46. Gagnon, M.C.; Strandberg, E.; Grau-Campistany, A.; Wadhwani, P.; Reichert, J.; Bürck, J.; Rabanal, F.; Auger, M.; Paquin, J.F.; Ulrich, A.S. Influence of the Length and Charge on the Activity of α-Helical Amphipathic Antimicrobial Peptides. *Biochemistry* **2017**, *56*, 1680–1695, doi:10.1021/acs.biochem.6b01071.

47. Dathe, M.; Nikolenko, H.; Meyer, J.; Beyermann, M.; Bienert, M. Optimization of the Antimicrobial Activity of Magainin Peptides by Modification of Charge. *FEBS Lett.* **2001**, *501*, 146–150, doi:10.1016/s0014-5793(01)02648-5.

48. Nakajima, Y. Mode of Action and Resistance Mechanisms of Antimicrobial Macrolides. *Macrolide Antibiot. Chem. Biol. Pract. Second Ed.* **2003**, *55*, 453–499, doi:10.1016/B978-012526451-8/50011-4.

49. Dathe, M.; Wieprecht, T. Structural Features of Helical Antimicrobial Peptides: Their Potential to Modulate Activity on Model Membranes and Biological Cells. *Biochim. Biophys. Acta - Biomembr.* **1999**, *1462*, 71–87, doi:10.1016/S0005-2736(99)00201-1.

50. Chen, Y.; Mant, C.T.; Farmer, S.W.; Hancock, R.E.W.; Vasil, M.L.; Hodges, R.S. Rational Design of α-Helical Antimicrobial Peptides with Enhanced Activities and Specificity/Therapeutic Index. *J. Biol. Chem.* **2005**, *280*, 12316–12329, doi:10.1074/jbc.M413406200.

51. Perumal, P.; Pandey, V.P. Antimicrobial Peptides: The Role of Hydrophobicity in the Alpha Helical Structure. *J. Pharm. Pharmacogn. Res.* **2013**, *1*, 39–53.

52. Yin, L.M.; Edwards, M.A.; Li, J.; Yip, C.M.; Deber, C.M. Roles of Hydrophobicity and Charge Distribution of Cationic Antimicrobial Peptides in Peptide-Membrane Interactions. *J. Biol. Chem.* **2012**, *287*, 7738–7745, doi:10.1074/jbc.M111.303602.

53. Chen, Y.; Guarnieri, M.T.; Vasil, A.I.; Vasil, M.L.; Mant, C.T.; Hodges, R.S. Role of Peptide Hydrophobicity in the Mechanism of Action of α-Helical Antimicrobial Peptides. *Antimicrob. Agents Chemother.* **2007**, *51*, 1398–1406, doi:10.1128/AAC.00925-06.

54. Wimley, W.C. Describing the Mechanism of Antimicrobial Peptide Action with the Interfacial Activity Model. *ACS Chem. Biol.* **2010**, 905-917.

55. Kang, H.; Kim, C.; Seo, C.H.; Park, Y. The Therapeutic Applications of Antimicrobial Peptides (AMPs): A Patent Review. **2017**, *55*, 1–12, doi:10.1007/s12275-017-6452-1.

56. Nguyen, L.T.; Haney, E.F.; Vogel, H.J. The Expanding Scope of Antimicrobial Peptide Structures and Their Modes of Action. *Trends Biotechnol.* **2011**, *29*, 464–472, doi:10.1016/j.tibtech.2011.05.001.

57. Rapaport, D.; Shai, Y. Interaction of Fluorescently Labeled Pardaxin and Its Analogues with Lipid Bilayers. *J. Biol. Chem.* **1991**, *266*, 23769–23775, doi:10.1016/s0021-9258(18)54349-0.

58. Brogden, K.A. Antimicrobial Peptides: Pore Formers or Metabolic Inhibitors in Bacteria? *Nat. Rev. Microbiol.* **2005**, 238-250.

59. Shai, Y. Mechanism of the Binding, Insertion and Destabilization of Phospholipid Bilayer Membranes by α-Helical Antimicrobial and Cell Non-Selective Membrane-Lytic Peptides. *Biochim. Biophys. Acta - Biomembr.* **1999**, *1462*, 55–70, doi:10.1016/S0005-2736(99)00200-X.

60. Matsuzaki, K. Membrane Permeabilization Mechanisms. *Adv Exp Med Biol*, 2019.9-16.

61. Kabelka, I.; Vácha, R. Advances in Molecular Understanding of α-Helical Membrane-

Active Peptides. *Acc. Chem. Res.* **2021**, *54*, 2196–2204, doi:10.1021/acs.accounts.1c00047.

62. Cheng, J.T.J.; Hale, J.D.; Elliot, M.; Hancock, R.E.W.; Straus, S.K. Effect of Membrane Composition on Antimicrobial Peptides Aurein 2.2 and 2.3 from Australian Southern Bell Frogs. *Biophys. J.* **2009**, *96*, 552–565, doi:10.1016/j.bpj.2008.10.012.

63. Sengupta, D.; Leontiadou, H.; Mark, A.E.; Marrink, S.J. Toroidal Pores Formed by Antimicrobial Peptides Show Significant Disorder. *Biochim. Biophys. Acta - Biomembr.* **2008**, *1778*, 2308–2317, doi:10.1016/j.bbamem.2008.06.007.

64. Shai, Y. Active Antimicrobial Peptides. *Biopolymers* **2002**, 236–248.

65. Chen, C.H.; Starr, C.G.; Troendle, E.; Wiedman, G.; Wimley, W.C.; Ulmschneider, J.P.; Ulmschneider, M.B. Simulation-Guided Rational de Novo Design of a Small Pore-Forming Antimicrobial Peptide. *J. Am. Chem. Soc.* **2019**, *141*, 4839–4848, doi:10.1021/jacs.8b11939.

66. Epand, R.M.; Walker, C.; Epand, R.F.; Magarvey, N.A. Molecular Mechanisms of Membrane Targeting Antibiotics. *Biochim. Biophys. Acta - Biomembr.* **2016**, doi:10.1016/j.bbamem.2015.10.018.

67. Andersson, D.I.; Hughes, D.; Kubicek-Sutherland, J.Z. Mechanisms and Consequences of Bacterial Resistance to Antimicrobial Peptides. *Drug Resist. Updat.* **2016**, *26*, 43–57, doi:10.1016/j.drup.2016.04.002.

68. Huang, H.W. Action of Antimicrobial Peptides: Two-State Model. *Biochemistry* **2000**, *39*, 8347–8352, doi:10.1021/bi000946l.

69. Matsuzaki, K. Magainins as Paradigm for the Mode of Action of Pore Forming Polypeptides. *Biochim. Biophys. Acta - Rev. Biomembr.* **1998**, *1376*, 391–400, doi:10.1016/S0304-4157(98)00014-8.

70. Scocchi, M.; Mardirossian, M.; Runti, G.; Benincasa, M. Non-Membrane Permeabilizing Modes of Action of Antimicrobial Peptides on Bacteria. *Curr. Top. Med. Chem.* **2015**, doi:10.2174/1568026615666150703121009.

71. Friedrich, C.L.; Rozek, A.; Patrzykat, A.; Hancock, R.E.W. Structure and Mechanism of Action of an Indolicidin Peptide Derivative with Improved Activity against Gram-Positive Bacteria *. *J. Biol. Chem.* **2001**, *276*, 24015–24022, doi:10.1074/jbc.M009691200.

72. Lan, Y.; Ye, Y.; Kozlowska, J.; Lam, J.K.W.; Drake, A.F.; Mason, A.J. Structural Contributions to the Intracellular Targeting Strategies of Antimicrobial Peptides. *BBA - Biomembr.* **2010**, *1798*, 1934–1943, doi:10.1016/j.bbamem.2010.07.003.

73. Haney, E.F.; Straus, S.K.; Hancock, R.E.W. Reassessing the Host Defense Peptide Landscape. *Front. Chem.* **2019**, *7*, 1–22, doi:10.3389/fchem.2019.00043.

74. Marks, J.R.; Placone, J.; Hristova, K.; Wimley, W.C. Spontaneous Membrane-Translocating Peptides by Orthogonal High-Throughput Screening. *J. Am. Chem. Soc.* **2011**, *133*, 8995–9004, doi:10.1021/ja2017416.

75. Kauffman, W.B.; Guha, S.; Wimley, W.C. Synthetic Molecular Evolution of Hybrid Cell Penetrating Peptides. *Nat. Commun.* **2018**, *9*, doi:10.1038/s41467-018-04874-6.

76. Henriques, S.T.; Melo, M.N.; Castanho, M.A.R.B. Cell-Penetrating Peptides and Antimicrobial Peptides: How Different Are They? *Biochem. J.* **2006**, *399*, 1–7,

doi:10.1042/BJ20061100.

77. Kalafatovic, D.; Giralt, E. *Cell-Penetrating Peptides: Design Strategies beyond Primary Structure and Amphipathicity*; 2017; Vol. 22; ISBN 3493403712.

78. Ruseska, I.; Zimmer, A. Internalization Mechanisms of Cell-Penetrating Peptides. *Beilstein J. Nanotechnol.* **2020**, *11*, 101–123, doi:10.3762/bjnano.11.10.

79. Ezzat, K.; Helmfors, H.; Tudoran, O.; Juks, C.; Lindberg, S.; Padari, K.; El-Andaloussi, S.; Pooga, M.; Langel, Ü. Scavenger Receptor-mediated Uptake of Cell-penetrating Peptide Nanocomplexes with Oligonucleotides. *FASEB J.* **2012**, *26*, 1172–1180, doi:10.1096/fj.11-191536.

80. Wang, G.; Li, X.; Wang, Z. APD3: The Antimicrobial Peptide Database as a Tool for Research and Education. *Nucleic Acids Res.* **2016**, *44*, D1087–D1093, doi:10.1093/nar/gkv1278.

81. Gordon, Y.J.; Romanowski, E.G.; McDermott, A.M. Mini Review: A Review of Antimicrobial Peptides and Their Therapeutic Potential as Anti-Infective Drugs. *Curr. Eye Res.* **2005**, *30*, 505–515, doi:10.1080/02713680590968637.

82. Huanbo Tan, Wencheng Su, Wenyu Zhang, Pengju Wang, M.S. and P.Z. Recent Advances in Half-Life Extension Strategies for Therapeutic Peptides and Proteins. *Curr. Pharm. Des. 24*, *Issue*, 4932–4946.

83. Erak, M.; Bellmann-Sickert, K.; Els-Heindl, S.; Beck-Sickinger, A.G. Peptide Chemistry Toolbox – Transforming Natural Peptides into Peptide Therapeutics. *Bioorganic Med. Chem.* **2018**, *26*, 2759–2765, doi:10.1016/j.bmc.2018.01.012.

84. Nijnik, A.; Hancock, R.E.W. The Roles of Cathelicidin LL-37 in Immune Defences and Novel Clinical Applications. *Curr. Opin. Hematol.* **2009**, *16*, 41–47, doi:10.1097/MOH.0b013e32831ac517.

85. Mangoni, M.L.; Mcdermott, A.M.; Zasloff, M. Antimicrobial Peptides and Wound Healing: Biological and Therapeutic Considerations. *Exp. Dermatol.* **2016**, *25*, 167–173, doi:10.1111/exd.12929.

86. Hamamoto, K.; Kida, Y.; Zhang, Y.; Shimizu, T.; Kuwano, K. Antimicrobial Activity and Stability to Proteolysis of Small Linear Cationic Peptides with D-Amino Acid Substitutions. *Microbiol. Immunol.* **2002**, *46*, 741–749, doi:10.1111/j.1348-0421.2002.tb02759.x.

87. Nguyen, L.T.; Chau, J.K.; Perry, N.A.; Boer, L. De; Zaat, S.A.J.; Hans, J. Serum Stabilities of Short Tryptophan- and Arginine-Rich Antimicrobial Peptide Analogs. **2010**, *5*, 11–18, doi:10.1371/journal.pone.0012684.

88. Wang, J.; Yadav, V.; Smart, A.L.; Tajiri, S.; Basit, A.W. Toward Oral Delivery of Biopharmaceuticals: An Assessment of the Gastrointestinal Stability of 17 Peptide Drugs. *Mol. Pharm.* **2015**, *12*, 966–973, doi:10.1021/mp500809f.

89. Wang, J.; Yadav, V.; Smart, A.L.; Tajiri, S.; Basit, A.W. Stability of Peptide Drugs in the Colon. *Eur. J. Pharm. Sci.* **2015**, *78*, 31–36, doi:10.1016/j.ejps.2015.06.018.

90. Fosgerau, K.; Hoffmann, T. Peptide Therapeutics : Current Status and Future Directions §. *Drug Discov. Today* **2015**, *20*, 122–128, doi:10.1016/j.drudis.2014.10.003.

91. Menacho-melgar, R.; Decker, J.S.; Hennigan, J.N.; Lynch, M.D. A Review of Lipidation

in the Development of Advanced Protein and Peptide Therapeutics. *J. Control. Release* **2019**, *295*, 1–12, doi:10.1016/j.jconrel.2018.12.032.

92. Zaman, R.; Islam, R.A.; Ibnat, N.; Othman, I.; Zaini, A. Current Strategies in Extending Half-Lives of Therapeutic Proteins. *J. Control. Release* **2019**, *301*, 176–189, doi:10.1016/j.jconrel.2019.02.016.

93. H Raghuraman, A.C. Melittin: A Membrane-Active Peptide with Diverse Functions. *Biosci. Rep.* **2007**, *27*, 189–223.

94. B.Bechinger Structure and Functions of Channel-Forming Peptides: Magainins, Cecropins, Melittin and Alamethicin. **1997**, *211*, 197–211.

95. Leitgeb, Balazs, Andras Szekeres, Laszlo Manczinger, Csaba Vagvolgyi, and L.K. The History of Alamethicin : A Review of the Most Extensively Studied Peptaibol. **2007**, *4*, 1027–1051.

96. Etayash, H.; Pletzer, D.; Kumar, P.; Straus, S.K.; Hancock, R.E.W. Cyclic Derivative of Host-Defense Peptide IDR-1018 Improves Proteolytic Stability, Suppresses In Fl Ammation, and Enhances In Vivo Activity. **2020**, doi:10.1021/acs.jmedchem.0c00303.

97. Zhao, Y.; Zhang, M.; Qiu, S.; Wang, J.; Peng, J.; Zhao, P.; Zhu, R.; Wang, H.; Li, Y.; Wang, K.; et al. Antimicrobial Activity and Stability of the d - Amino Acid Substituted Derivatives of Antimicrobial Peptide Polybia - MPI. *AMB Express* **2016**, doi:10.1186/s13568-016-0295-8.

98. Witteloostuijn, S.B. Van; Pedersen, S.L.; Jensen, K.J. Half-Life Extension of Biopharmaceuticals Using Chemical Methods : Alternatives to PEGylation. **2016**, 2474–

2495, doi:10.1002/cmdc.201600374.

99. Chen, C.H.; Lu, T.K. Development and Challenges of Antimicrobial Peptides for Therapeutic Applications. *Antibiotics* **2020**, *9*, doi:10.3390/antibiotics9010024.

100. Wijesinghe, A.; Kumari, S.; Booth, V. Conjugates for Use in Peptide Therapeutics: A Systematic Review and Meta-Analysis. *PLoS One* **2022**, *17*, 1–19, doi:10.1371/journal.pone.0255753.

101. Battista, F.; Oliva, R.; Vecchio, P. Del; Winter, R.; Petraccone, L. Insights into the Action Mechanism of the Antimicrobial Peptide Lasioglossin Iii. *Int. J. Mol. Sci.* **2021**, *22*, 1–18, doi:10.3390/ijms22062857.

102. Orädd, G.; Schmidtchen, A.; Malmsten, M. Effects of Peptide Hydrophobicity on Its Incorporation in Phospholipid Membranes - An NMR and Ellipsometry Study. *Biochim. Biophys. Acta - Biomembr.* **2011**, *1808*, 244–252, doi:10.1016/j.bbamem.2010.08.015.

103. Kumari, S.; Booth, V. Antimicrobial Peptide Mechanisms Studied by Whole - Cell Deuterium NMR. *Int. J Mol Sci.* **2022**.

104. Savini, F.; Bobone, S.; Roversi, D.; Mangoni, M.L.; Stella, L. From Liposomes to Cells: Filling the Gap between Physicochemical and Microbiological Studies of the Activity and Selectivity of Host-Defense Peptides. *Pept. Sci.* **2020**, 1–15, doi:10.1002/pep2.24041.

105. Kumar, K.; Sebastiao, M.; Arnold, A.A.; Bourgault, S.; Warschawski, D.E.; Marcotte, I. In Situ Solid-State NMR Study of Antimicrobial Peptide Interactions with Erythrocyte Membranes. *Biophys. J.* **2022**, *121*, 1512–1524, doi:10.1016/j.bpj.2022.03.009.

106. Wimley, W.C. Describing the Mechanism of Antimicrobial Peptide Action with the

Interfacial Activity Model. **2013**, *14*, 799–811, doi:10.1503/cmaj.060803.

107. Melo, M.N.; Ferre, R.; Castanho, M.A.R.B. Antimicrobial Peptides: Linking Partition, Activity and High Membrane-Bound Concentrations. *Nat. Rev. Microbiol.* **2009**, *7*, 245–250, doi:10.1038/nrmicro2095.

108. Roversi, D.; Luca, V.; Aureli, S.; Park, Y.; Mangoni, M.L.; Stella, L. How Many Antimicrobial Peptide Molecules Kill a Bacterium? The Case of PMAP-23. *ACS Chem. Biol.* **2014**, *9*, 2003–2007, doi:10.1021/cb500426r.

109. Ebbensgaard, A.; Mordhorst, H.; Aarestrup, F.M.; Hansen, E.B. The Role of Outer Membrane Proteins and Lipopolysaccharides for the Sensitivity of *Escherichia Coli* to Antimicrobial Peptides. *Front. Microbiol.* **2018**, *9*, 1–13, doi:10.3389/fmicb.2018.02153.

110. Separovic, F.; Keizer, D.W.; Sani, M.-A. In-Cell Solid-State NMR Studies of Antimicrobial Peptides. *Front. Med. Technol.* **2020**, *2*, 1–8, doi:10.3389/fmedt.2020.610203.

111. Torrent, M.; Navarro, S.; Moussaoui, M.; Nogués, M.V.; Boix, E. Eosinophil Cationic Protein High-Affinity Binding to Bacteria-Wall Lipopolysaccharides and Peptidoglycans. *Biochemistry* **2008**, *47*, 3544–3555, doi:10.1021/bi702065b.

112. Malanovic, N.; Lohner, K. Antimicrobial Peptides Targeting Gram-Positive Bacteria; *Pharmaceuticals*. **2016**; Vol. 9; ISBN 4331638049.

113. Hancock, R.E.W.; Sahl, H.G. Antimicrobial and Host-Defense Peptides as New Anti-Infective Therapeutic Strategies. *Nat. Biotechnol.* **2006**, *24*, 1551–1557, doi:10.1038/nbt1267.

114. Matsuzaki, K.; Sugishita, K.I.; Fujii, N.; Miyajima, K. Molecular Basis for Membrane Selectivity of an Antimicrobial Peptide, Magainin 2. *Biochemistry* **1995**, *34*, 3423–3429, doi:10.1021/bi00010a034.

115. Schefter, B.R.; Nourbakhsh, S.; Taheri-Araghi, S.; Ha, B.-Y. Modeling Cell Selectivity of Antimicrobial Peptides: How Is the Selectivity Influenced by Intracellular Peptide Uptake and Cell Density. *Front. Med. Technol.* **2021**, *3*, 1–9, doi:10.3389/fmedt.2021.626481.

116. Hawrani, A.; Howe, R.A.; Walsh, T.R.; Dempsey, C.E. Origin of Low Mammalian Cell Toxicity in a Class of Highly Active Antimicrobial Amphipathic Helical Peptides. *J. Biol. Chem.* **2008**, *283*, 18636–18645, doi:10.1074/jbc.M709154200.

117. Oren, Z.; Shai, Y. Selective Lysis of Bacteria but Not Mammalian Cells by Diastereomers of Melittin: Structure-Function Study. *Biochemistry* **1997**, *36*, 1826–1835, doi:10.1021/bi962507l.

118. Oren, Z.; Shai, Y. Cyclization of a Cytolytic Amphipathic α-Helical Peptide and Its Diastereomer: Effect on Structure, Interaction with Model Membranes, and Biological Function. *Biochemistry* **2000**, *39*, 6103–6114, doi:10.1021/bi992408i.

119. Imura, Y.; Choda, N.; Matsuzaki, K. Magainin 2 in Action: Distinct Modes of Membrane Permeabilization in Living Bacterial and Mammalian Cells. *Biophys. J.* **2008**, *95*, 5757–5765, doi:10.1529/biophysj.108.133488.

120. Ferro-Flores, G.; Arteaga De Murphy, C.; Pedraza-López, M.; Meléndez-Alafort, L.; Zhang, Y.M.; Rusckowski, M.; Hnatowich, D.J. In Vitro and in Vivo Assessment of 99mTc-UBI Specificity for Bacteria. *Nucl. Med. Biol.* **2003**, *30*, 597–603, doi:10.1016/S0969-8051(03)00054-4.

121. Derossi, D.; Calvet, S.; Trembleau, A.; Brunissen, A.; Chassaing, G.; Prochiantz, A. Cell Internalization of the Third Helix of the Antennapedia Homeodomain Is Receptor-Independent. *J. Biol. Chem.* **1996**, *271*, 18188–18193, doi:10.1074/jbc.271.30.18188.

122. Vivès, E.; Brodin, P.; Lebleu, B. A Truncated HIV-1 Tat Protein Basic Domain Rapidly Translocates through the Plasma Membrane and Accumulates in the Cell Nucleus. *J. Biol. Chem.* **1997**, *272*, 16010–16017, doi:10.1074/jbc.272.25.16010.

123. W. Berkeley Kauffman, Taylor Fuselier, Jing He, and W.C.W. Mechanism Matters: A Taxonomy of Cell Penetrating Peptides W. *Trends Biochem Sci. 2015* **2015**, *40*, 749–764, doi:10.1016/j.tibs.2015.10.004.Mechanism.

124. Bechara, C.; Sagan, S. Cell-Penetrating Peptides: 20 Years Later, Where Do We Stand? *FEBS Lett.* **2013**, *587*, 1693–1702, doi:10.1016/j.febslet.2013.04.031.

125. Ouellet, M.; Bernard, G.; Voyer, N.; Auger, M. Insights on the Interactions of Synthetic Amphipathic Peptides with Model Membranes as Revealed by 31P and 2H Solid-State NMR and Infrared Spectroscopies. *Biophys. J.* **2006**, doi:10.1529/biophysj.105.077339.

126. Simeoni, F.; Morris, M.C.; Heitz, F.; Divita, G. Insight into the Mechanism of the Peptide-Based Gene Delivery System MPG: Implications for Delivery of SiRNA into Mammalian Cells. *Nucleic Acids Res.* **2003**, *31*, 2717–2724, doi:10.1093/nar/gkg385.

127. A. Ziegler, P.Nervi, M.Durrenberger, J.Seelig. The cationic cell-penetrating peptide CPP(TAT) derived from the HIV-1 protein TAT is rapidly transported into living fibroblasts: optical, biophysical, and metabolic evidence. *Biochemistry.* **2005**. *11,* 138-140.

128. Hallock, K.J.; Lee, D.K.; Ramamoorthy, A. MSI-78, an Analogue of the Magainin Antimicrobial Peptides, Disrupts Lipid Bilayer Structure via Positive Curvature Strain.

Biophys. J. **2003**, *84*, 3052–3060, doi:10.1016/S0006-3495(03)70031-9.

129. Fuchs, P.C.; Barry, A.L.; Brown, S.D. In Vitro Antimicrobial Activity of MSI-78, a Magainin Analog. *Antimicrob. Agents Chemother.* **1998**, *42*, 1213–1216, doi:10.1128/aac.42.5.1213.

130. Lipsky, B.A.; Holroyd, K.J.; Zasloff, M. Topical versus Systemic Antimicrobial Therapy for Treating Mildly Infected Diabetic Foot Ulcers: A Randomized, Controlled, Double-Blinded, Multicenter Trial of Pexiganan Cream. *Clin. Infect. Dis.* **2008**, *47*, 1537–1545, doi:10.1086/593185.

131. Monteiro, C.; Pinheiro, M.; Fernandes, M.; Maia, S.; Seabra, C.L.; Ferreira-Da-Silva, F.; Reis, S.; Gomes, P.; Martins, M.C.L. A 17-Mer Membrane-Active MSI-78 Derivative with Improved Selectivity toward Bacterial Cells. *Mol. Pharm.* **2015**, *12*, 2904–2911, doi:10.1021/acs.molpharmaceut.5b00113.

132. Maloy, W.L.; Kari, U.P. Structure–Activity Studies on Magainins and Other Host Defense Peptides. *Biopolymers* **1995**, *37*, 105–122, doi:10.1002/bip.360370206.

133. Leontiadou, H.; Mark, A.E.; Marrink, S.J. Antimicrobial Peptides in Action. *J. Amer. Chem. Soc* **2006**, 12156–12161.

134. Marassi, F.M.; Opella, S.J. A Solid-State NMR Index of Helical Membrane Protein Structure and Topology. *J. Magn. Reson.* **2000**, *144*, 150–155, doi:10.1006/jmre.2000.2035.

135. Fuselier, T.; Wimley, W.C. Spontaneous Membrane Translocating Peptides: The Role of Leucine-Arginine Consensus Motifs. *Biophys. J.* **2017**, *113*, 835–846,

doi:10.1016/j.bpj.2017.06.070.

136. Lee, H.; Lim, S.I.; Shin, S.H.; Lim, Y.; Koh, J.W.; Yang, S. Conjugation of Cell-Penetrating Peptides to Antimicrobial Peptides Enhances Antibacterial Activity. *ACS Omega* **2019**, *4*, 15694–15701, doi:10.1021/acsomega.9b02278.

137. Laadhari, M.; Arnold, A.A.; Gravel, A.E.; Separovic, F.; Marcotte, I. Interaction of the Antimicrobial Peptides Caerin 1.1 and Aurein 1.2 with Intact Bacteria by ^{2}H Solid-State NMR. *Biochim. Biophys. Acta - Biomembr.* **2016**, doi:10.1016/j.bbamem.2016.09.009.

138. Salnikov, E.S.; Mason, A.J.; Bechinger, B. Membrane Order Perturbation in the Presence of Antimicrobial Peptides by 2H Solid-State NMR Spectroscopy. *Biochimie* **2009**, *91*, 734–743, doi:10.1016/j.biochi.2009.01.002.

139. Pius, J.; Morrow, M.R.; Booth, V. 2H Solid-State Nuclear Magnetic Resonance Investigation of Whole *Escherichia Coli* Interacting with Antimicrobial Peptide MSI-78. *Biochemistry* **2012**, *51*, 118–125, doi:10.1021/bi201569t.

140. Santisteban, N.P.; Morrow, M.R.; Booth, V. Effect of AMPs MSI-78 and BP100 on the Lipid Acyl Chains of 2H-Labeled Intact Gram Positive Bacteria. *Biochim. Biophys. Acta - Biomembr.* **2020**, *1862*, 183199, doi:10.1016/j.bbamem.2020.183199.

141. Bloom, M. “NMR Studies of Membranes and Whole Cells". *Zeitschrift f˙ur Phys. Chemie* **1987**, *153*, 67–67.

142. McCabe, M.A.; Wassall, S.R. Fast-Fourier-Transform DePaking. *J. Magn. Reson. Ser. B* 1995, *106*, 80–82.

143. Lafleur, M.; Fine, B.; Sternin, E.; Cullis, P.R.; Bloomt, M. Smoothed Orientational Order

Profile of Lipid Bilayers by 2H-Nuclear Magnetic Resonance. **1989**, *56*, 1037–1041.

144. Santisteban, N.P. Interaction of Antimicrobial Peptides with Bacterial Cell Envelopes, Memorial University of Newfoundland, 2019.

145. Tardy-Laporte, C.; Arnold, A.A.; Genard, B.; Gastineau, R.; Morançais, M.; Mouget, J.L.; Tremblay, R.; Marcotte, I. A 2H Solid-State NMR Study of the Effect of Antimicrobial Agents on Intact *Escherichia Coli* without Mutating. *Biochim. Biophys. Acta - Biomembr.* **2013**, *1828*, 614–622, doi:10.1016/j.bbamem.2012.09.011.

146. Davis,J.H.; C P Nichol, G Weeks, M.B. Study of the Cytoplasmic and Outer Membranes of *Escherichia Coli* by Deuterium Magnetic Resonance. *Biochemistry* **1979**, *18*, doi:10.1021/bi00577a041.

147. Booth, V. Deuterium Solid State NMR Studies of Intact Bacteria Treated With Antimicrobial Peptides. *Front. Med. Technol.* **2021**, *2*, 1–9, doi:10.3389/fmedt.2020.621572.

148. Maricq, M.M.; Waugh, J.S. NMR in Rotating Solids. *J. Chem. Phys.* **1979**, *70*, 3300–3316, doi:10.1063/1.437915.

149. Ackerman, J.L.; Eckman, R.; Pines, A. Experimental Results on Deuterium NMR in the Solid State by Magic Angle Sample Spinning. *Chem. Phys.* **1979**, *42*, 423–428, doi:10.1016/0301-0104(79)80092-0.

150. Clayden, N.J. Computer Simulations of 2H MAS NMR Spinning Sideband Spectra. *Chem. Phys. Lett.* **1986**, *131*, 517–521, doi:10.1016/0009-2614(86)80575-9.

151. Duer, M.J.; Stourton, C. 2H Double-Quantum NMR Spectroscopy for the Study of

Molecular Motion in Solids. **1997**, *52*, 44–52.

152. Cutajar, M.; Ashbrook, S.E.; Wimperis, S. 2H Double-Quantum MAS NMR Spectroscopy as a Probe of Dynamics on the Microsecond Timescale in Solids. *Chem. Phys. Lett.* **2006**, *423*, 276–281, doi:10.1016/j.cplett.2006.03.065.

153. Davis, J.H.; Ziani, L.; Schmidt, M.L. Critical Fluctuations in DOPC/DPPC-D62/Cholesterol Mixtures: 2H Magnetic Resonance and Relaxation. *J. Chem. Phys.* **2013**, *139*, doi:10.1063/1.4816366.

154. Veatch, S.L.; Soubias, O.; Keller, S.L.; Gawrisch, K. Critical Fluctuations in Domain-Forming Lipid Mixtures. *Proc. Natl. Acad. Sci. U. S. A.* **2007**, *104*, 17650–17655, doi:10.1073/pnas.0703513104.

155. Warnet, X.L.; Laadhari, M.; Arnold, A.A.; Marcotte, I.; Warschawski, D.E. Biochimica et Biophysica Acta A 2 H Magic-Angle Spinning Solid-State NMR Characterisation of Lipid Membranes in Intact Bacteria. *BBA - Biomembr.* **2016**, *1858*, 146–152, doi:10.1016/j.bbamem.2015.10.020.

156. N.P. Santisteban, M.R. Morrow, V.B. Protocols for Studying the Interaction of MSI-78 with the Membranes of Whole Gram-Positive and Gram-Negative Bacteria by NMR, in: Antimicrobial Peptides:; Methods and Protocols, Springer New York, New York, NY, 2017;

157. Davis, J. H., Jeffrey, K. R., Bloom, M., Valic, M. I., & Higgs, T.P. Quadrupolar Echo Deuteron Magnetic Resonance Spectroscopy in Ordered Hydrocarbon Chains. *Chem. Phys. Lett.* **1976**, *42(2)*, 390–394.

158. Davis, J.H. The Description of Membrane Lipid Conformation, Order and Dynamics by 2H-NMR. *BBA - Rev. Biomembr.* **1983**, *737*, 117–171, doi:10.1016/0304-4157(83)90015-1.

159. Davis, J.H. Deuterium Magnetic Resonance Study of the Gel and Liquid Crystalline Phases of Dipalmitoyl Phosphatidylcholine. *Biophys. J.* **1979**, 339–358.

160. Bishop, D.G.; Rutberg, L.; Samuelsson, B. The Chemical Composition of the Cytoplasmic Membrane of Bacillus Subtilis. *Eur. J. Biochem.* **1967**, *2*, 448–453, doi:10.1111/j.1432-1033.1967.tb00158.x.

161. Milo, R.; Jorgensen, P.; Moran, U.; Weber, G.; Springer, M. BioNumbers The Database of Key Numbers in Molecular and Cell Biology. *Nucleic Acids Res.* **2009**, *38*, 750–753, doi:10.1093/nar/gkp889.

162. Davis, J.H.; Maraviglia, B.; Weeks, G.; Godin, D. V. Bilayer Rigidity of the Erythrocyte Membrane 2H-NMR of a Perdeuterated Palmitic Acid Probe. *BBA - Biomembr.* **1979**, *550*, 362–366, doi:10.1016/0005-2736(79)90222-0.

163. Laydevant, F.; Mahabadi, M.; Llido, P.; Bourgouin, J.P.; Caron, L.; Arnold, A.A.; Marcotte, I.; Warschawski, D.E. Growth-Phase Dependence of Bacterial Membrane Lipid Profile and Labeling for in-Cell Solid-State NMR Applications. *Biochim. Biophys. Acta - Biomembr.* **2022**, *1864*, 183819, doi:10.1016/j.bbamem.2021.183819.

164. Leive, L. Release of Lipopolysaccharide by EDTA Treatment of *E. coli. Biochem. Biophys. Res. Commun.* **1965**, *21*, 290–296.

165. Vaara, M. Increased Outer Membrane Resistance to Ethylenediaminetetraacetate and

Cations in Novel Lipid A Mutants. *J. Bacteriol.* **1981**, *148*, 426–434, doi:10.1128/jb.148.2.426-434.1981.

166. Prachayasittikul, V.; Isarankura-Na-Ayudhya, C.; Tantimongcolwat, T.; Nantasenamat, C.; Galla, H.J. EDTA-Induced Membrane Fluidization and Destabilization: Biophysical Studies on Artificial Lipid Membranes. *Acta Biochim. Biophys. Sin. (Shanghai).* **2007**, *39*, 901–913, doi:10.1111/j.1745-7270.2007.00350.x.

167. Smith, A.; Hussey, M. American Society for Microbiology: Gram Stain Protocols. **2005**, 1–9.

168. Kristensen, M.; Birch, D.; Nielsen, H.M. Applications and Challenges for Use of Cell-Penetrating Peptides as Delivery Vectors for Peptide and Protein Cargos. *Int. J. Mol. Sci.* **2016**, *17*, doi:10.3390/ijms17020185.

169. Anna Brezden, Mohamed F. Mohamed‡, Manish Nepal†, John S. Harwood,§, Jerrin Kuriakose, Mohamed N. Seleem, and J.C. Dual Targeting of Intracellular Pathogenic Bacteria with a Cleavable Conjugate of Kanamycin and an Antibacterial, Cell Penetrating Peptide. *J Am Chem Soc* **2017**, *176*, 139–148, doi:10.1021/jacs.6b04831.Dual.

170. Morris, M.C.; Deshayes, S.; Heitz, F.; Divita, G. Cell-Penetrating Peptides: From Molecular Mechanisms to Therapeutics. *Biol. Cell* **2008**, *100*, 201–217, doi:10.1042/bc20070116.

171. Lundberg, P.; El-Andaloussi, S.; Sütlü, T.; Johansson, H.; Langel, Ü. Delivery of Short Interfering RNA Using Endosomolytic Cell-penetrating Peptides. *FASEB J.* **2007**, *21*, 2664–2671, doi:10.1096/fj.06-6502com.

172. Nakase, I.; Niwa, M.; Takeuchi, T.; Sonomura, K.; Kawabata, N.; Koike, Y.; Takehashi, M.; Tanaka, S.; Ueda, K.; Simpson, J.C. Cellular Uptake of Arginine-Rich Peptides: Roles for Macropinocytosis and Actin Rearrangement. *Mol. Ther.* **2004**, *10*, 1011–1022, doi:10.1016/j.ymthe.2004.08.010.

173. Wadia, J.S.; Stan, R. V.; Dowdy, S.F. Transducible TAT-HA Fusogenic Peptide Enhances Escape of TAT-Fusion Proteins after Lipid Raft Macropinocytosis. *Nat. Med.* **2004**, *10*, 310–315, doi:10.1038/nm996.

174. Kwon, B.; Waring, A.J.; Hong, M. A 2h Solid-State Nmr Study of Lipid Clustering by Cationic Antimicrobial and Cell-Penetrating Peptides in Model Bacterial Membranes. *Biophys. J.* **2013**, *105*, 2333–2342, doi:10.1016/j.bpj.2013.08.020.

175. Matsuzaki, K. Control of Cell Selectivity of Antimicrobial Peptides. *Biochim. Biophys. Acta - Biomembr.* **2009**, *1788*, 1687–1692, doi:10.1016/j.bbamem.2008.09.013.

176. Jara, P.; Spies, J.; Cárcamo, C.; Arancibia, Y.; Vargas, G.; Martin, C.; Salas, M.; Otth, C.; Zambrano, A. The Effect of Resveratrol on Cell Viability in the Burkitt's Lymphoma Cell Line Ramos. *Molecules* **2018**, *23*, doi:10.3390/molecules23010014.

177. R. B. Montgomery, G. Singer, A.T.P. Surface Area per Lipid Molecule in the Intact Membrane of the Human Red Cell. *Nature* **1969**, *223*, 1–2.

178. Swithenbank, L.; Cox, P.; Harris, L.G.; Dudley, E.; Sinclair, K.; Lewis, P.; Cappiello, F.; Morgan, C. Temporin A and Bombinin H2 Antimicrobial Peptides Exhibit Selective Cytotoxicity to Lung Cancer Cells. *Scientifica (Cairo).* **2020**, doi:10.1155/2020/3526286.

179. Soundrarajan, N.; Park, S.; Le Van Chanh, Q.; Cho, H. sun; Raghunathan, G.; Ahn, B.;

Song, H.; Kim, J.H.; Park, C. Protegrin-1 Cytotoxicity towards Mammalian Cells Positively Correlates with the Magnitude of Conformational Changes of the Unfolded Form upon Cell Interaction. *Sci. Rep.* **2019**, *9*, 1–12, doi:10.1038/s41598-019-47955-2.

180. Larsson, P.; Engqvist, H.; Biermann, J.; Werner Rönnerman, E.; Forssell-Aronsson, E.; Kovács, A.; Karlsson, P.; Helou, K.; Parris, T.Z. Optimization of Cell Viability Assays to Improve Replicability and Reproducibility of Cancer Drug Sensitivity Screens. *Sci. Rep.* **2020**, *10*, 1–12, doi:10.1038/s41598-020-62848-5.

181. Brender, J.R.; McHenry, A.J.; Ramamoorthy, A. Does Cholesterol Play a Role in the Bacterial Selectivity of Antimicrobial Peptides? *Front. Immunol.* **2012**, *3*, 1–4, doi:10.3389/fimmu.2012.00195.

182. Booth, V.; Warschawski, D.E.; Santisteban, N.P.; Laadhari, M.; Marcotte, I. Recent Progress on the Application of ^{2}H Solid-State NMR to Probe the Interaction of Antimicrobial Peptides with Intact Bacteria. *Biochim. Biophys. Acta - Proteins Proteomics* **2017**, *1865*, 1500–1511, doi:10.1016/j.bbapap.2017.07.018.

183. Huang, H.W. Molecular Mechanism of Antimicrobial Peptides: The Origin of Cooperativity. *Biochim. Biophys. Acta - Biomembr.* 2006.

184. Brannan, A.M.; Whelan, W.A.; Cole, E.; Booth, V. Differential Scanning Calorimetry of Whole *Escherichia Coli* Treated with the Antimicrobial Peptide MSI-78 Indicate a Multi-Hit Mechanism with Ribosomes as a Novel Target. *PeerJ* **2015**, *3*, e1516, doi:10.7717/peerj.1516.

185. Nourbakhsh, S.; Taheri-Araghi, S.; Ha, B.Y. Toward Building a Physical Model for Membrane Selectivity of Antimicrobial Peptides: Making a Quantitative Sense of the

Selectivity. *Soft Matter* **2019**, *15*, 7509–7526, doi:10.1039/c9sm00930b.

186. Bagheri, A.; Taheri-Araghi, S.; Ha, B.Y. How Cell Concentrations Are Implicated in Cell Selectivity of Antimicrobial Peptides. *Langmuir* **2015**, *31*, 8052–8062, doi:10.1021/acs.langmuir.5b01533.

187. Koprivnjak, T.; Weidenmaier, C.; Peschel, A.; Weiss, J.P. Wall Teichoic Acid Deficiency in *Staphylococcus Aureus* Confers Selective Resistance to Mammalian Group IIA Phospholipase A2 and Human β-Defensin 3 ∇. *Infect. Immun.* **2008**, *76*, 2169–2176, doi:10.1128/IAI.01705-07.

188. Witte, K.; Olausson, B.; Walrant, A.; Alves, I.; Vogel, A. Structure and dynamics of the two amphipathic arginine-rich peptides RW9 and RL9 in a lipid environment investigated by solid-state NMR and MD simulations. *Biochim Biophys Acta.* 2013.1828, 824-33, doi: 10.1016/j.bbamem.2012.11.014.

Appendix A

Replicates ^{2}H NMR experiments

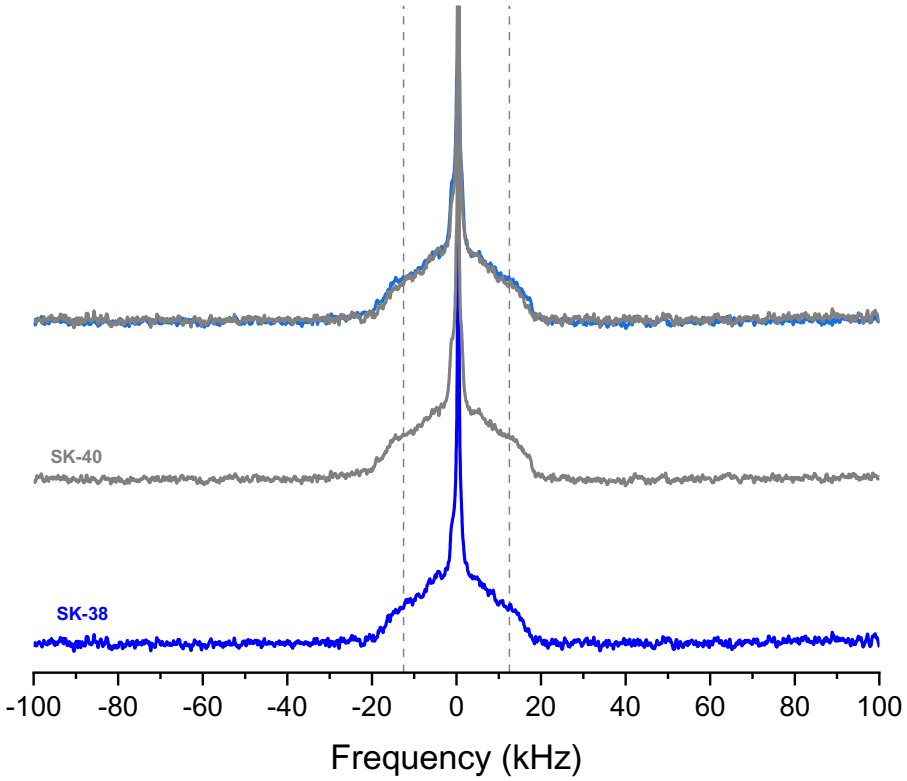

Figure A1: Duplicate spectra of 2.5 mM EDTA treated *E. coli*. ^{2}H NMR of *E. coli* enriched with deuterated acyl chains treated with 2.5 mM EDTA. Dashed lines at ~± 12.5 kHz are included to facilitate the comparison of the spectra. Each spectrum represents 110,000 scans recorded over 12 h at 37°C in a 600 MHz NMR spectrometer and normalized by area. The top panel shows the stacked spectra.

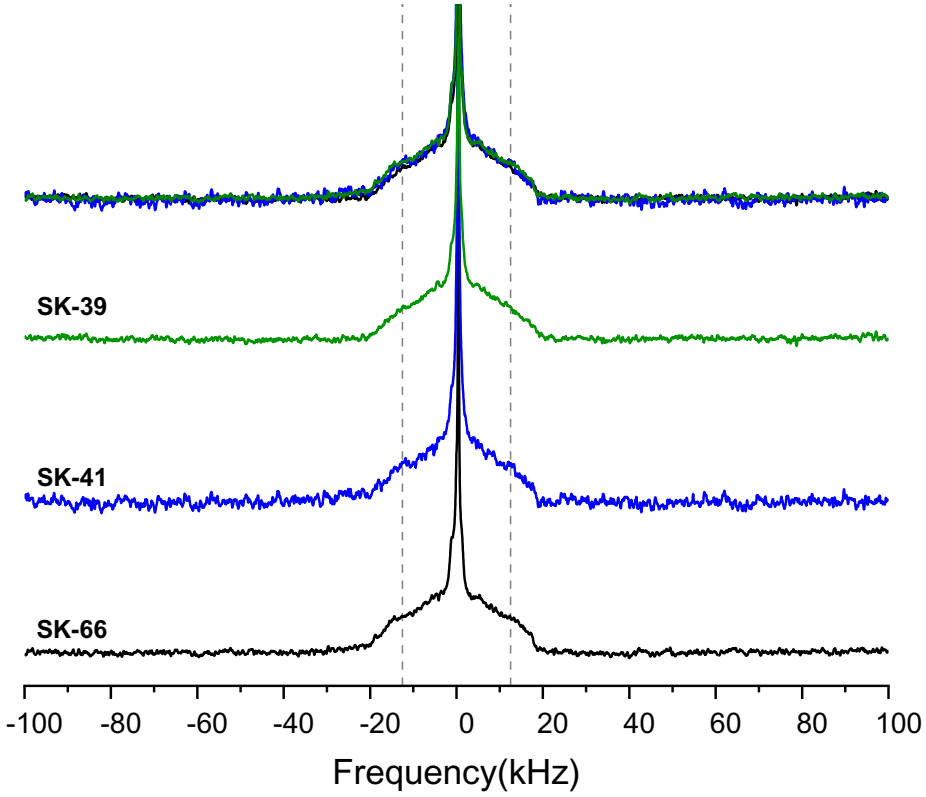

Figure A2: Triplicate spectra of 9.0 mM EDTA treated *E. coli*. ^{2}H NMR of *E. coli* enriched with deuterated acyl chains treated with 9.0mM EDTA. Dashed lines at ~ ±12.5 kHz are included to facilitate comparison of the spectra. Each spectrum represents 110,000 scans recorded over 12 h at 37°C in a 600 MHz NMR spectrometer and normalized by area. The top panel shows the stacked spectra.

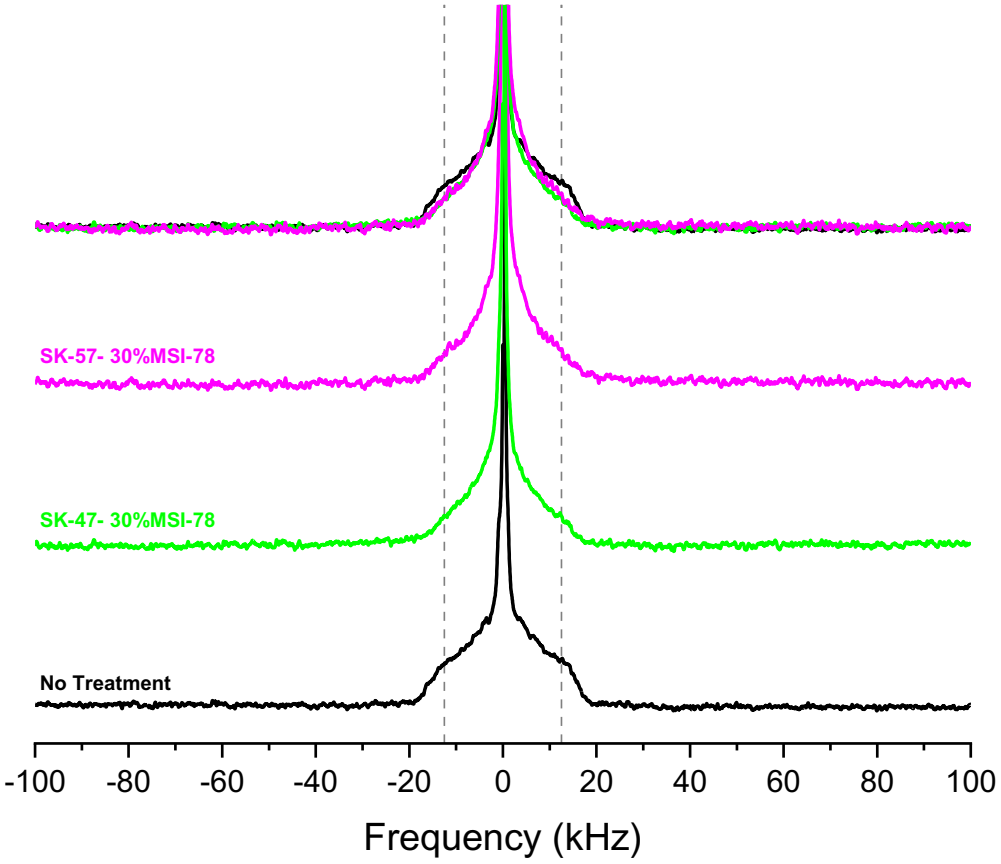

Figure A3: Duplicate spectra of 30% MSI-78 AMP treatment alone. ^{2}H NMR spectra of deuterium-enriched *E. coli*. Dashed lines at ~ ±12.5 kHz are included to facilitate comparison of the spectra. Each spectrum represents 110,000 scans recorded over 12 h at 37°C in a 600 MHz NMR spectrometer and normalized by area. The top panel shows the stacked spectra**.**

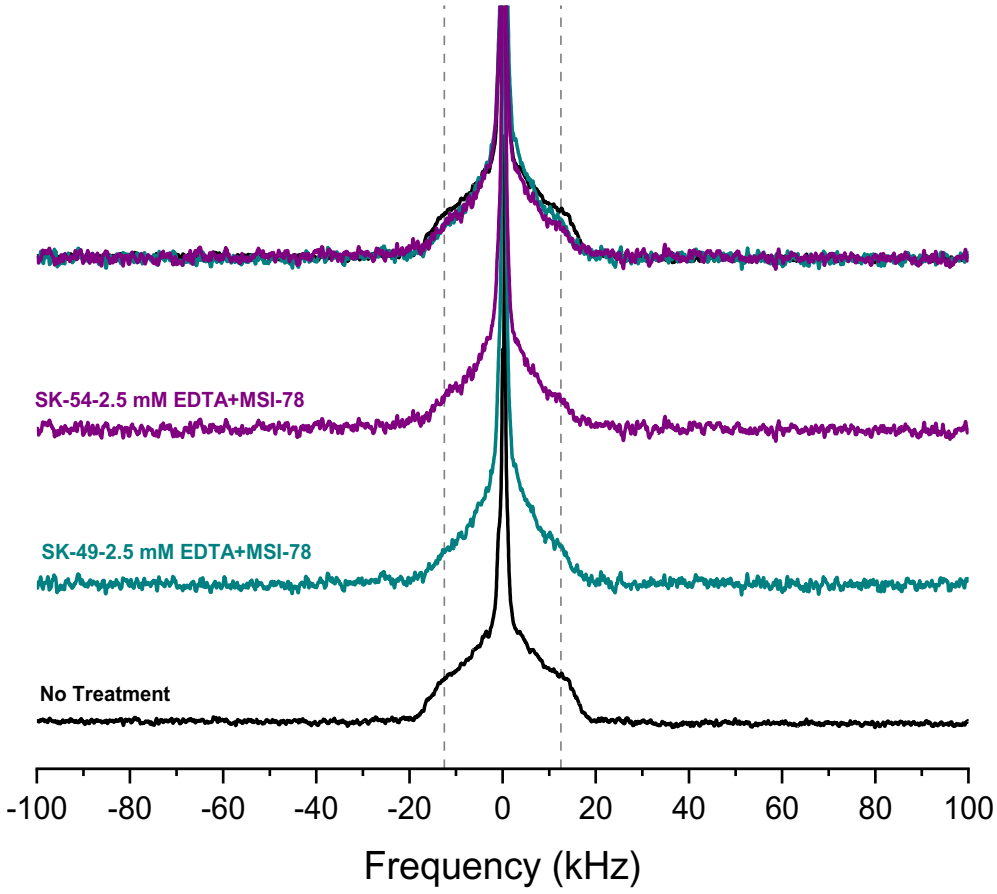

Figure A4: Duplicate spectra of 2.5 mM EDTA and AMP treatment. ^{2}H NMR spectra of deuterium-enriched *E. coli* treated with 2.5 mM EDTA and 30% MSI-78. Dashed lines at ~± 12.5 kHz are included to facilitate the comparison of the spectra. Each spectrum represents 110,000 scans recorded over 12 h at 37°C in a 600 MHz NMR spectrometer and normalized by area. The top panel shows the stacked spectra**.**

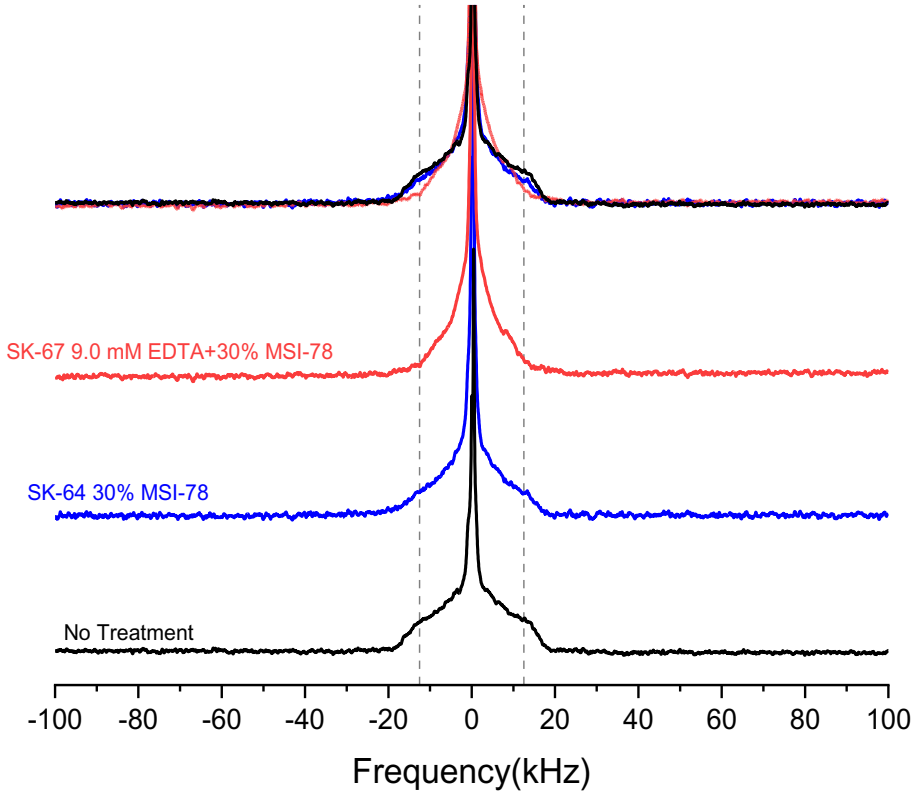

Figure A5: ^{2}H NMR spectra of deuterium-enriched *E.coli* treated with 9.0 mM EDTA and 30% MSI-78. Dashed lines at ~ ± 12.5 kHz are shown to facilitate comparison of the spectra. Each spectrum represents 110,000 scans recorded over 12 h at 37°C in a 600 MHz NMR spectrometer and normalized by area.

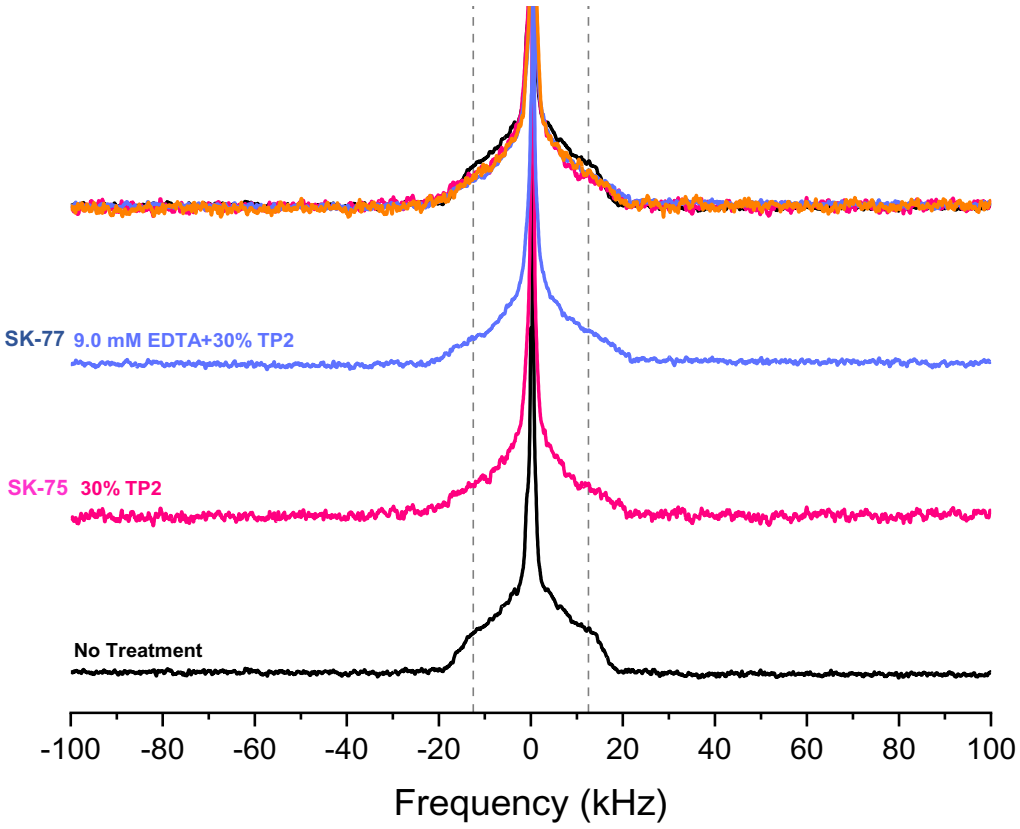

Figure A6: Duplicate ^{2}H NMR spectra of deuterium-enriched *E. coli* treated with 9.0 mM and 30% TP2. Dashed lines at ~ ±12.5 kHz are shown to facilitate comparison of the spectra. Each spectrum represents 100,000 scans recorded over 12 h at 37°C in a 600 MHz NMR spectrometer and normalized by area.

Appendix B

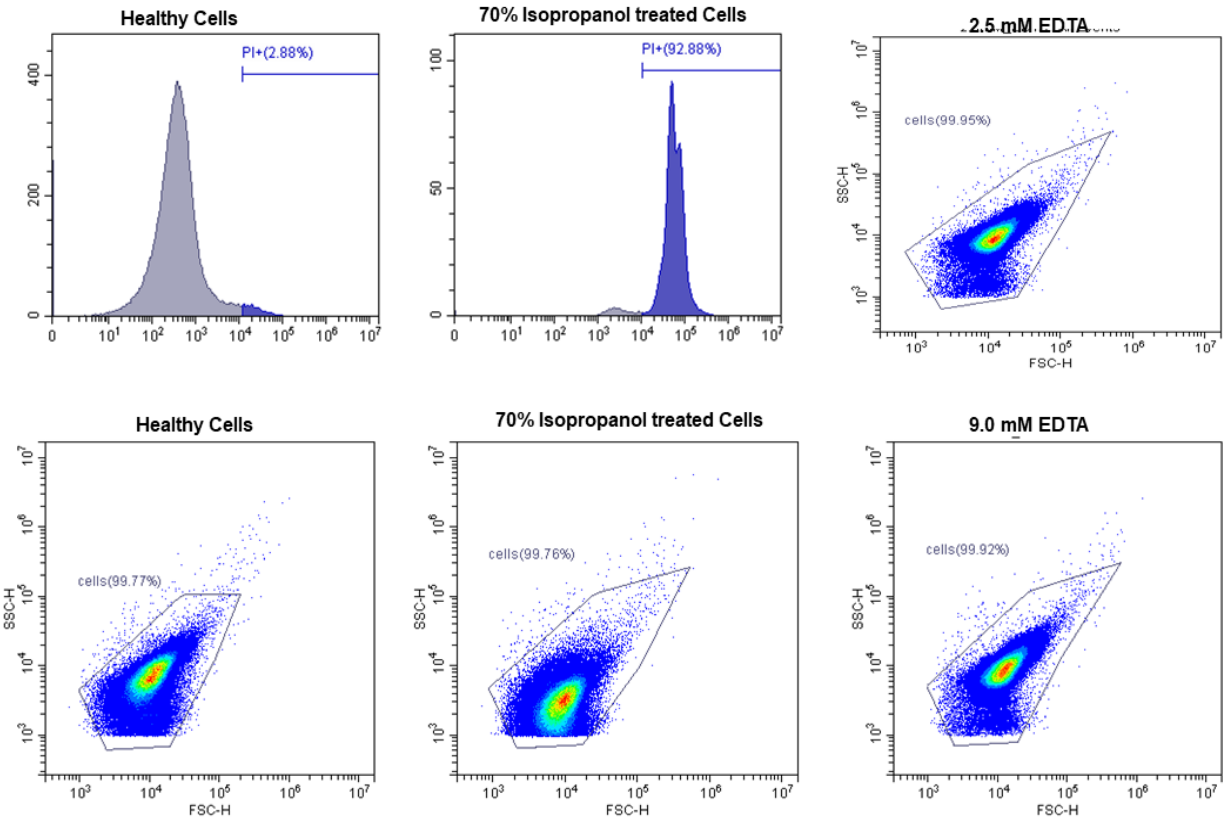

Figure B1: Representative sort plots from flow cytometry: Forward scatter vs. side scatter sort plots for healthy controls, isopropanol-killed cells, 2.5 mM and 9.0 mM EDTA concentrations

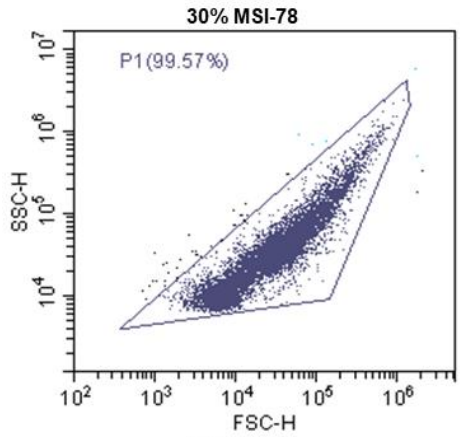
30% MSI-78
P1(99.57%)
SSC-H
FSC-H

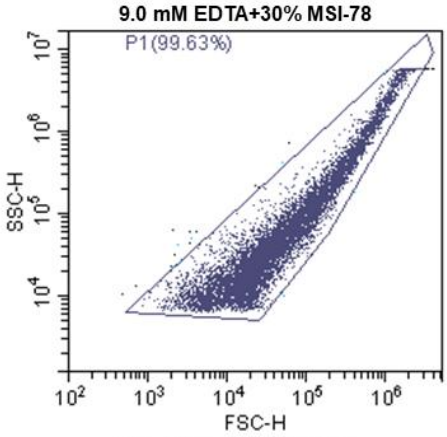
9.0 mM EDTA+30% MSI-78
P1(99.63%)
SSC-H
FSC-H

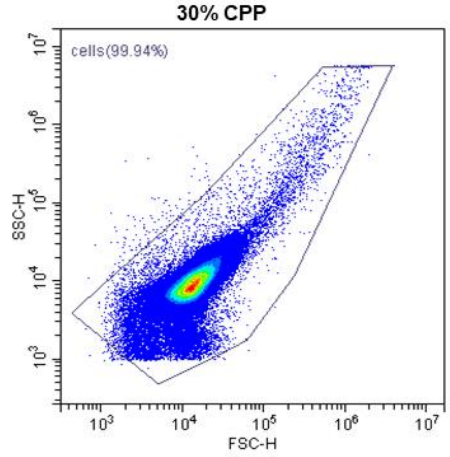
30% CPP
cells(99.94%)
SSC-H
FSC-H

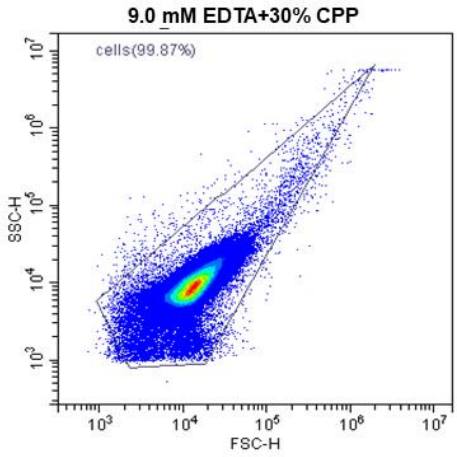
9.0 mM EDTA+30% CPP
cells(99.87%)
SSC-H
FSC-H

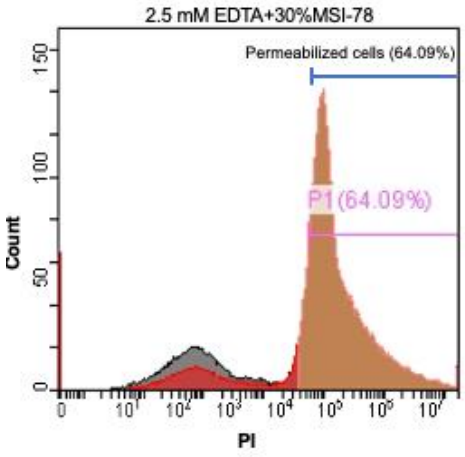
2.5 mM EDTA+30%MSI-78
Permeabilized cells (64.09%)
P1(64.09%)
Count
PI

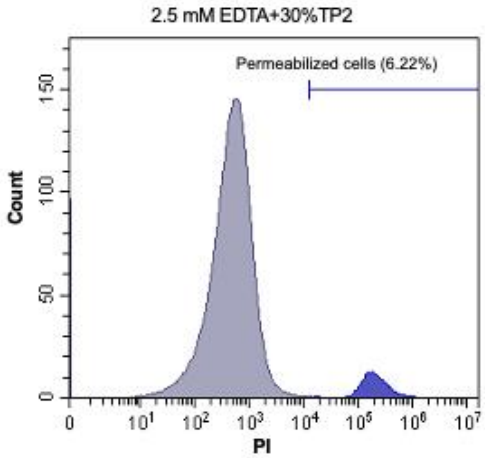
2.5 mM EDTA+30%TP2
Permeabilized cells (6.22%)
Count
PI

Figure B2: Representative sort plots from flow cytometry: Forward scatter vs side scatter sort plots for cells treated with EDTA treated followed by MSI-78 or CPP (TP2) treated cells.

Appendix C

MATLAB code for static ^{2}H NMR moment calculations

```
clc
clear all
%%%format compact is to reduce the space in command window

format compact;
msat=xlsread('2H Raw Data.xlsx','NewIntegral','A2:A8193');
dsat=xlsread('2H Raw Data.xlsx','NewIntegral','AQ2:AQ8193');
figure(1)
plot(msat,dsat)
%
%%%Part
A================================================================================

% % % Freq_kHz is frequency in kHz
% % Intensity is raw intensity
Freq_kHz=msat(:,1);
Intensity=dsat(:,1);

% to find number of data points.
n=numel(Intensity);

%%%% Moving Positive Side of Spectra from 0kHz to 100kHz
I = find(Freq_kHz== -1.129147500000000) %%First Point of the Positive Spectra Start from
0kH
I2 = find(Freq_kHz==0)
Lastpoint = Freq_kHz(end); %%Last Point of the Positive Spectra i.e. 100kHz
N=find(Freq_kHz==Lastpoint);%%
Freq_kHz=Freq_kHz(I2:N);%%%Saving the Frequency from 0 to 100kHz in the Freq_kHz
Intensity=Intensity(I:N-37);%%%Saving the Intensity from 0 to 100kHz in the Intensity

figure(2)
plot(Freq_kHz, Intensity)
Mainarea1=trapz(Freq_kHz,Intensity) %%% Total Positive Area without the Basline Correction
using Trapz
% %
% % % %%
% % % %%% Part
B================================================================================
% %% Baseline Correction from cursor 5 and 6 (last two cursor)
```

```
Cursor5=1000;
Cursor6=1150;
Baslm=sum(Intensity(Cursor5:Cursor6));
Baslm=Baslm./(Cursor6-Cursor5); %%Baseline avaerage Y-value store in Baslm
Intensity(Cursor5:Cursor6)=Baslm;
BX=Freq_kHz(Cursor5:Cursor6-1); %%% Baseline Freq data point
Intensity(Cursor5:Cursor6-1)=Baslm ;%%% Average value of Y saved for the datapoint cursor5
and Cursor6
BY=Intensity(Cursor5:Cursor6-1);

%%% Integral Cut off Cursor 3 to Cursor 4
Cursor3=33;
Cursor4=1000;
CursorDiff=Cursor4-Cursor3;
CursorX=Freq_kHz(Cursor3:Cursor4-1);
CursorY=Intensity(Cursor3:Cursor4-1);
CRArea=trapz(CursorX*2*pi*1000,CursorY);%%% Integral Area from Cursor 3 and Cursor 4

BS1X=Freq_kHz(Cursor3:Cursor4-1);%%% Baseline X axis for cursor 3 to 4
BS1Y(1:CursorDiff)=Baslm;
BS1Area=trapz(BS1X*2*pi*1000,BS1Y);

RedArea1=CRArea-BS1Area %%% Reduced area = integral area - baseline area

%%Cursor Integral Cut off Cursor 2 to Cursor 3
Cursor2=27;
Cursor3=29;
CR2Diff=Cursor3-Cursor2;
CR2X=Freq_kHz(Cursor2:Cursor3-1);
CR2Y=Intensity(Cursor2:Cursor3-1);
CR2Area=trapz(CR2X*2.*pi*1000,CR2Y);%%% Integral Area from Cursor 2 and Cursor 3

BS2X=Freq_kHz(Cursor2:Cursor3-1);%%% Baseline X axis for cursor 2 to 3
BS2Y(1:CR2Diff)=Baslm;
BS2Area=trapz(BS2X*2*pi*1000,BS2Y);%%% Integral Area from Cursor 2 and Cursor 3

RedArea2=CR2Area-BS2Area %%% Reduced area = integral area - baseline area
%%%%%Main Area
TotArea=RedArea2+RedArea1


%%%%==========================================================================
========
%%% Part C Moment Calculation M1 and M2
Int1=Intensity(Cursor2:Cursor3);
Int1=Int1';
```

```
Int2=Intensity(Cursor3:Cursor4);
Int2=Int2';
Int=horzcat(Int1, Int2);
Int=Int';
Int=Int(:,1)-Balm;

Freq1=Freq_kHz(Cursor2:Cursor3);
Freq1=Freq1';
Freq2=Freq_kHz(Cursor3:Cursor4);
Freq2=Freq2';
Freq=horzcat(Freq1, Freq2);
Freq=Freq';
%%% M1
Gw11=Freq.*2*pi*1000; %%% Gw11: w=2*pi*frequency
Gw12=Int.*Gw11    ;  %%% Gw12=w*f(w)
Num1=trapz(Gw11,Gw12); %%% Integral(wf(w).dw)

%%% M2
Gw21=Freq.*Freq*4.*pi.*pi.*1000.*1000;
Gw22=Int.*Gw21;
Num2=trapz(Gw11,Gw22);

M1=Num1/TotArea
M2=Num2/TotArea

D2= M2/(1.35*M1*M1)-1

% % %
```

Appendix D

NMR Samples and SK number

NMR Sample No.	Experiment Name
SK-01	Bacillus Subtilis -Dr.Morrow's Instrument
SK-02	Bacillus Subtilis-Dr.Morrow's Instrument
SK-03	Bacillus subtilis- Dr.Morrow's Instrument
SK-04	Bacillus subtilis- Dr.Morrow's Instrument
SK-05	Bacillus subtilis- Dr.Morrow's Instrument
SK-06	DPPC-d62 - Dr.Morrow's Instrument
SK-07	DPPC-d62-salt-Dr.Morrow's Instrument
SK-08	JM-109-Dr.Morrow's Instrument
SK-09	JM-109- Dr.Morrow's Instrument
SK-10	JM-109- Dr.Morrow's Instrument
SK-11	PA-d31- Dr.Morrow's Instrument
SK-12	JM-109-Packing didn’t worked/ 600 MHz
SK-13	JM109- MAS Probe 600 MHz issue
SK-14	JM109- Flat coil probe
SK-15	JM109- Flat coil probe
SK-16	JM109-EDTA Treatment - Flat coil probe
SK-17	JM109- Flat coil probe/ Not a good rotor packing
SK-18	JM109- Flat coil probe
SK-19	JM109 -MAS Probe back -600 MHz

SK-20	DPPC -Static - MAS Probe -600 MHz
SK-21	DPPC-10 kHz Spinning rate-600 MHz
SK-22	JM109 - 5kHz spinning rate-600 MHz
SK-23	JM109- 2.5 kHz spinning rate-600 MHz
SK-24	JM109- 10 kHz spinning rate-600 MHz
SK-25	JM109 rotor packing -600 MHz
SK-26	JM109 pipette tips rotor packing technique
SK-27	JM109 rotor packing -600 MHz/ worked
SK-28	JM109 another rotor packing technique, spinning the sample to 5 kHz
SK-29	JM109- 5kHz spinning rate -600 MHz
SK-30	JM109 with 0.1 mM EDTA/ signal to noise bad
SK-31	JM109 with 0.1 mM EDTA/ 5 kHz MAS
SK-32	BSA experiment (NMR Course work)
SK-33	Lysozyme experiment (NMR Course work)
SK-34	JM109 Static/5 kHz spinning
SK-35	2.5 mM EDTA Treatment Static/5kHz
SK-36	9.0 mM EDTA Treatment Static/5kHz
SK-37	JM109 Static -new glycerol stock
SK-38	2.5 mM EDTA Treatment Static/5kHz
SK-39	9.0 mM EDTA Treatment Static/5kHz
SK-40	2.5 mM EDTA Treatment Static/5kHz
SK-41	9.0 mM EDTA Treatment Static/5kHz

SK-42	30% MSI-78 peptide was not desalted
SK-43	2.5 mM EDTA Treatment+Peptide (not desalted)
SK-44	9.0 mM EDTA Treatment+Peptide (not desalted)
SK-45	30% MSI-78 Peptide
SK-46	30% MSI-78 Desalted (peptide calculation needed to do for E. coli)
SK-47	30% MSI-78 Desalted
SK-48	2.5 mM EDTA+30%MSI-78 experiment didn't work
SK-49	2.5 mM EDTA+30%MSI-78
SK-50	9.0 mM EDTA+30%MSI-78
SK-51	JM109 Static didn't recorded instrument issue
SK-52	30%MSI-78 Peptide
SK-53	JM109 Static (new stock of JM109)
SK-54	2.5 mM EDTA+30%MSI-78
SK-55	9.0 mM EDTA+30%MSI-78
SK-56	2.5 mM EDTA+30%MSI-78 (forgot to do centrifuge after EDTA treatment
SK-57	30% MSI-78
SK-58	30% MSI-78 (new stock of peptide)
SK-59	JM109 Static
SK-60	9.0 mM EDTA+30%MSI-78 (New stock of peptide didn't work)
SK-61	New stock of MSI-78 with 40%
SK-62	9.0 mM EDTA+40%MSI-78

SK-63	New stock of MSI-78 with 50%
SK-64	New stock of MSI-78 with 60%
SK-65	New stock of MSI-78 with 60%
SK-66	9.0 mM EDTA
SK-67	9.0 mM EDTA+60%MSI-78 New stock
SK-68	JM109 Static
SK-69	JM109 Static
SK-70	JM109 5kHz/2.5 kHz/10 kHz: signal to noise bad
SK-71	30% CPP peptide
SK-72	9.0 mM EDTA+30% CPP peptide
SK-73	JM109 MAS 10 kHz signal to noise good
SK-74	JM109 MAS 10 kHz signal to noise bad
SK-75	30% CPP peptide
SK-76	E. coli +Ramos cells
SK-77	9.0 mM EDTA+30% CPP peptide
SK-78	30% MSI-78 10kHz MAS
SK-79	E. coli +Ramos cells+30% MSI-78
SK-80	JM109 for 24 hours experiment time 10 kHz
SK-81	First try to deuterated Ramos cell with PA

Permission to use Fig 4 and Fig 5

Santisteban, Nury Paula

to me

Hello Sarika,

As the author of those two images, I give you permission to use them on your thesis.

Regards,

Nury Paula Santisteban